

# **APSCO CubeSat Competition**

**“Conceptual and Preliminary Design Report”**

**(Sepehr)**

**(Iran)**

**Version 1**

**may 2024**

# **SPARCS**

## Mission

*Spacecrafts for Advanced Research and Cooperative Studies*

---





APSCO CubeSat Competition  
Conceptual and Preliminary Design Report – Ver. 1  
(IR-Sepehr)

## Team Introduction

### *Team general information*

<b>Team Title</b>	IR- Sepehr
<b>Mission (Project) Title</b>	SPARCS <sup>1</sup>
<b>Member State</b>	Iran
<b>Affiliating Entity</b>	Sharif University of Technology (SUT)
<b>Contact point of the team</b>	Mohammad Ali Torkaman Asadi, ali.torkaman@live.com, torkaman-asadi@ae.sharif.edu (+989128309568)

### *Team members list*

No.	Member full name (first middle surname)	Responsibility	Status
1	Mohammad Ali Torkaman Asadi	supervisor	supervisor
2	Amir Hossein Khodabakhsh	supervisor	supervisor
3	Danial Rezaei	Systems Engineering ADCS	Student
4	Ali Moradi	Payload	Student
5	Negar Rastin	Payload	Student
6	Mohammad Barzegar	Power	Student
7	Farzaneh MohammadiMajd	OBC	Student
8	Sina Safi	Communication	Student
9	Parsa Rahmani	Structure and Mechanism Thermal Control	Student
10	Seyyed Mohammad Mahdi Mosavati	Systems Engineering	Student

<sup>1</sup> Spacecrafts for Advanced Research and Cooperative Studies



APSCO CubeSat Competition  
Conceptual and Preliminary Design Report – Ver. 1  
(IR-Sepehr)

## Table of Contents

1.	Mission.....	6
1.1.	Mission Drivers .....	6
1.2.	Mission Statement.....	11
1.2.1.	Stakeholders .....	11
1.3.	Orbital Considerations.....	11
1.3.1.	Orbital Altitude .....	12
1.3.2.	Orbital Inclination .....	12
2.	Payload.....	14
2.1.	Tether .....	14
2.1.1.	Requirements .....	16
2.1.2.	Fundamentals & Physics of EDT.....	17
2.1.3.	Nonlinear pitch and roll motions of tethered satellites.....	18
2.1.4.	EMF .....	19
2.1.5.	Elastic oscillations of tethers .....	20
2.1.6.	Effect of aerodynamic forces.....	21
2.1.7.	Conclusion.....	22
2.1.8.	Configuration .....	23
2.1.9.	Components.....	23
2.1.10.	Deployment System .....	24
2.1.11.	Bias Control System .....	26
2.1.12.	Simulations & Verification .....	29
2.2.	ISL.....	31
2.3.	Dosimetry .....	31
3.	System.....	34
3.1.	Mission Requirements.....	34
3.2.	Mission Profile and Operational Modes.....	35
3.3.	Product Tree .....	37
3.4.	General Layout .....	38
3.5.	Budget Estimation .....	39
3.5.1.	Mass and Volume Budget Estimation .....	40
3.5.2.	Power Budget Estimation .....	40
3.5.3.	Cost Budget Estimation.....	41
3.6.	Model-Based System Engineering in SPARCS Mission .....	41
4.	OBC (Onboard computer).....	44
4.1.	Requirements .....	44
4.2.	Subsystem division .....	45
4.3.	OBC components.....	45
4.4.	Introducing the selected OBC board .....	49



APSCO CubeSat Competition  
Conceptual and Preliminary Design Report – Ver. 1  
(IR-Sepehr)

4.4.1.	Specifications .....	50
4.4.2.	Interfaces .....	51
4.4.3.	Software Info .....	51
4.5.	Operating system .....	53
4.6.	Frame work.....	53
4.7.	Telecommand and Telemetry Management.....	54
4.8.	Memory Management .....	56
4.9.	Time and Event Management .....	56
4.10.	Budget Estimation .....	56
5.	Communication.....	58
5.1.	Requirements .....	58
5.2.	Communication Architecture .....	58
5.2.1.	Block Diagram .....	58
5.3.	Product Tree .....	60
5.3.1.	ISIS UHF downlink / VHF uplink Full Duplex Transceiver (1 in each CubeSat) .....	60
5.3.2.	ISIS Deployable Antenna System (1 in each CubeSat) .....	60
5.3.3.	Frequency Down-Scaling System .....	60
5.4.	Operating features and parameters.....	60
5.4.1.	Operating Frequencies.....	61
5.4.2.	Antenna Types and Configuration .....	61
5.4.3.	Antenna Deployment and Placement.....	61
5.4.4.	Inter-Satellite Link (ISL) Configuration .....	61
5.4.5.	Radiation Patterns .....	62
5.4.6.	Communication Protocols and Data Handling.....	62
5.5.	Link budget .....	62
5.5.1.	Modulation Type and Bitrate.....	63
5.5.2.	Coding .....	63
5.5.3.	Link Budget Calculation for Uplink.....	63
5.5.4.	Link Budget Calculation for Downlink.....	63
5.6.	Budget estimation .....	64
5.6.1.	Mass and Dimension Estimation.....	64
5.6.2.	Power Estimation.....	64
5.6.3.	Cost Estimation .....	65
5.7.	Subsystem Summary .....	65
6.	ADCS.....	67
6.1.	Requirements .....	67
6.2.	Configuration Selection .....	67
6.3.	Component Sizing.....	70
6.3.1.	Component Sizing for SPARCS-B .....	70
6.3.2.	Component Sizing for SPARCS-A .....	74
6.4.	Operational Modes.....	76
6.5.	Architecture .....	78



APSCO CubeSat Competition  
Conceptual and Preliminary Design Report – Ver. 1  
(IR-Sepehr)

6.6.	Budget Estimation .....	79
7.	Power .....	80
7.1.	Requirements .....	80
7.2.	Component Configuration.....	81
7.2.1.	Solar Array Configuration .....	82
7.2.2.	Battery Configuration .....	83
7.2.3.	PCDU configuration and selection .....	83
7.3.	Power consumption estimation .....	85
7.4.	Cells selection and power generation estimation.....	88
7.5.	Battery sizing and selection.....	90
7.6.	Budget estimation .....	92
8.	Structure and mechanism.....	93
8.1.	Structure Materials.....	94
8.2.	Structural Subsystem Validation Plan .....	95
8.2.1.	Static loading design .....	95
8.2.2.	Modal analysis .....	99
8.3.	Budget Estimation .....	100
9.	Thermal control .....	102
9.1.	CubeSat Control Scenarios and Operational Modes .....	102
9.2.	CubeSat Orbital Conditions and Beta Angle .....	102
9.3.	Geometric Mathematical Modeling in Thermal Desktop Software .....	103
9.4.	Values of Parameters Used in Worst Case Hot and Cold Calculations.....	103
9.4.1.	Surface Heat Fluxes: .....	104
9.5.	Thermal Mathematical Model:.....	104
9.6.	CubeSat Model Meshing .....	105
9.7.	Applying Radiative Conditions to CubeSat Components:.....	106
9.8.	Results and Discussion:.....	106
9.9.	Summary:.....	107
10.	Ground station .....	108
10.1.	Requirements .....	108
10.2.	Communication Architecture .....	108
10.2.1.	Block Diagram and System Components .....	108
10.2.2.	Product Tree Breakdown .....	109
10.2.3.	Detailed Equipment Specifications .....	109
10.2.4.	Expected Performance Parameters .....	109
10.3.	Operating features and parameters.....	109
10.3.1.	Frequencies .....	109
10.3.2.	Antenna Types .....	110
10.3.3.	Antenna Gain .....	110
10.3.4.	Radiation Patterns.....	110
10.3.5.	General Radiation Characteristics.....	110



## List of Figures

Figure 1 - Increase in Operating Satellites [1].....	6
Figure 2 - Number of Payloads and rocket bodies in orbit by year [3].....	7
Figure 3 - Image of space debris in near-Earth orbits.....	7
Figure 4 - Process of de-orbit and re-entry of a spacecraft using the EDT module [5] .....	9
Figure 5- SPARCS Mission.....	11
Figure 6 Relation Between ILF and Orbital Inclination .....	12
Figure 7- Results of Criteria Rating in Expert Choice .....	13
Figure 8- Expert choice results for Orbital Inclination .....	13
Figure 9 - Medium close-up view, shows Tethered Satellite System deployment.....	14
Figure 10 - Tethered Formation Flying: by the MIT.....	14
Figure 11 - Momentum Exchange Tethers Example.....	15
Figure 12 - The HERTS is a spacecraft concept using an electric sail.....	15
Figure 13 - The types of tether stability constellations. [6] .....	17
Figure 14 - Geometry of the system. ....	18
Figure 15 - A schematic of the tether circuit. ....	19
Figure 16 - Electron density profile as a function of altitude.[8] .....	20
Figure 17 – Aerodynamic forces schematic. ....	21
Figure 18 - Magnitudes of perturbations, acting on the cable(20km). [16] .....	22
Figure 19 - The architecture of EDT .....	23
Figure 20 - The schematic of the tangling of the tether around satellites and the mission failure. ....	24
Figure 21 – A picture of the selected motor for deploying the tether. ....	24
Figure 22 – The schematic of monitoring the deployment of the tether using a camera.....	25
Figure 23 - Tether deployment system.....	25
Figure 24 - A Schematic of thermionic emitter.....	26
Figure 25 - An image of FEAC under a microscope.....	27
Figure 26 - Current Interaction with Plasma.....	27
Figure 27 – Tether bias system .....	28
Figure 28 - Tether cable (30AWG copper). .....	28
Figure 29 – Semi-major axis & <b>CD</b> Variation by Time (s).....	29
Figure 30- RadNano Dosimeter.....	32
Figure 31- RadNano Schematic of How its Work.....	33
Figure 32- Phase and Events timeline for SPARCS-A .....	35
Figure 33- Phase and Events timeline for SPARCS-B.....	35
Figure 34- Operational Modes in SPARCS Mission .....	36
Figure 35- Product Tree of SPARCS-A .....	37
Figure 36- Product Tree of SPARCS-B.....	38
Figure 37- 3D Views of SPARCS-A and SPARCS-B.....	39



APSCO CubeSat Competition  
Conceptual and Preliminary Design Report – Ver. 1  
(IR-Sepehr)

Figure 38- Location of subsystems in CubeSats, left: SPARCS-A, right: SPARCS-B.....	39
Figure 39- SPARCS Mission System Architecture.....	42
Figure 40- SPARCS-A System Architecture.....	42
Figure 41- SPARCS-B System Architecture .....	43
Figure 42- OBC schematic .....	45
Figure 43- Comparison of Overall Capacity .....	47
Figure 44- Comparison of NOR Flash and FRAM features .....	47
Figure 45- ISIS OBC & ISIS OBC Daughter board .....	50
Figure 46- Software Architecture based on SAVOIR standards .....	52
Figure 47- Board's architecture (ESA Standard).....	52
Figure 48- Kernel architecture .....	53
Figure 49- Telemetry & Telecommand framing based on CCSD standards.....	55
Figure 50- Categorizing the importance level of each part .....	55
Figure 51- Duplex Transceiver Block Diagram (source: PW-SAT) .....	59
Figure 52- Frequency Down-Scaling System.....	59
Figure 53- ISIS VHF uplink/UHF downlink Full Duplex Transceiver.....	60
Figure 54- ISIS Deployable Antenna System .....	60
Figure 55- Antenna System's Placing .....	61
Figure 56- General Antenna Pattern (source: PW-SAT).....	62
Figure 57- Feasible ADCS System options.....	68
Figure 58- selected configuration for sensors and actuators .....	69
Figure 59- ADCS Overall Configuration of SPARCS-A and SPARCS-B .....	70
Figure 60- ADCS-MTQ module .....	71
Figure 61- FSS-15 Sun Sensor.....	71
Figure 62- piNAV-NG GPS Receiver.....	72
Figure 63- ISIS GNSS Active Patch Antenna .....	73
Figure 64- ADIS16470 IMU .....	74
Figure 65- Compact Magnetorquer Dimensions.....	75
Figure 66- Compact Magnetorquers in SPARCS-A .....	76
Figure 67- HMR2300 Smart Digital Magnetometer .....	76
Figure 68- ADCS Operational Modes .....	77
Figure 69- Physical Architecture of SPARCS-A .....	78
Figure 70- Physical Architecture of SPARCS-B .....	78
Figure 71- SPARCS-B functional and component architecture (Similar to SPARCS-A, however, it doesn't have a DC to DC converter).....	82
Figure 72- Selected PCDU .....	85
Figure 73- Selected DC-to-DC converter component .....	85
Figure 74- Power consumption profile for some modes of SPARCS-A and SPARCS-B .....	87
Figure 75- Selected Solar cell general configuration .....	88
Figure 76- SPARCS-A and SPARCS-B power generation .....	89
Figure 77- Selected battery pack picture .....	92
Figure 78- Left: 2U Bus model of SPARCS-B; Right: 1U Bus model of SPARCS-A.....	93



APSCO CubeSat Competition  
Conceptual and Preliminary Design Report – Ver. 1  
(IR-Sepehr)

Figure 79- Dimensions of the main structure bodies (Left: SPARCS-B, Right: SPARCS-A) .....	94
Figure 80- Dimensions of the rib structures (dimensions in millimeters) .....	94
Figure 81- The contact conditions between the CubeSat and the payload in the rails.....	96
Figure 82- Payload-to-rail loading and boundary conditions for CubeSat in x and y directions .....	96
Figure 83- Boundary conditions simulated for the SEAM CubeSat .....	96
Figure 84- Sample mesh.....	97
Figure 85- Static analysis results .....	98
Figure 86- Lateral modes .....	99
Figure 87- Longitudinal modes .....	100
Figure 88- Orbit beta angle .....	103
Figure 89- CubeSat schematic in Thermal Desktop software for beta angles of 0 and 55 degrees..	103
Figure 90- Heat fluxes on CubeSat faces at .....	104
Figure 91- CubeSat Meshing and Grid Pattern .....	105
Figure 92- Temperature contour of equipment in WCH State .....	106
Figure 93- Ground Station Communication Schematic (source: PW-SAT) .....	108
Figure 94- Tonna 20818 Yagi antenna .....	111
Figure 95- ICOM IC-910H Transceiver.....	111



## List of Tables

Table 1- SPARCS Mission Orbit Parameters .....	13
Table 2- Components of the tether configuration along with budget allocations and general specifications. ....	23
Table 3 - Tether overall budget allocation.....	30
Table 4- Dosimeter Specifications.....	33
Table 5- SPARCS Mission Requirements .....	34
Table 6- SPARCS Mission Constraints .....	34
Table 7- Subsystem status during each mode in SPARCS-A.....	36
Table 8- Subsystem status during each mode in SPARCS-B.....	37
Table 9- Mass and Dimensions Budget for SPARCS Mission.....	40
Table 10- Power Budget for SPARCS Mission .....	40
Table 11- Cost Budget for SPARCS Mission.....	41
Table 12- I2C BUS and CAN BUS comparison.....	48
Table 13 - OBC Master & Slave Mode.....	48
Table 14- I2C Slave and Master Mode Comparison.....	49
Table 15 - Library peripherals & additional functionalities .....	51
Table 16- OBC Budgets for SPARCS-A, and B .....	57
Table 17- Communication Links.....	65
Table 18- Power Parameters and Budget .....	65
Table 19- Physical Parameters and Budget.....	66
Table 20- Cost Estimation .....	66
Table 21- ADCS-MTQ module Specifications .....	70
Table 22- FSS-15 Sun Sensor Specifications.....	71
Table 23- piNAV-NG GPS Receiver Specifications.....	72
Table 24- ISIS GAPA Specifications.....	73
Table 25- ADIS16470 IMU Specifications.....	74
Table 26- Compact magnetorquer Specifications.....	75
Table 27- HMR2300 Smart Digital Magnetometer Specifications .....	76
Table 28- ADCS Budgets for SPARCS-A .....	79
Table 29- ADCS Budgets for SPARCS-B.....	79
Table 30- PCDU General Features.....	84
Table 31- Product Information.....	84
Table 32- power consumption of SPARCS-A .....	86
Table 33- power consumption of SPARCS-B .....	86
Table 34- XTE-SF general features (post 1 MeV e-Retention) For Temperature coefficients (10°C to 70°C).....	88
Table 35- SPARCS-A and SPARCS-B Power generation .....	90



APSCO CubeSat Competition  
Conceptual and Preliminary Design Report – Ver. 1  
(IR-Sepehr)

Table 36- SPARCS-A and SPARCS-B average power generation and consumption .....	90
Table 37- Battery general specification .....	91
Table 38- Power subsystem budget estimation of SPARCS-A.....	92
Table 39- Power subsystem budget estimation of SPARCS-B.....	92
Table 40- Structure's main components for SPARCS-A and SPARCS-B.....	93
Table 41- Mechanical and thermal properties of the materials used in SPARCS-A, and B.....	94
Table 42- Quasi-static acceleration values .....	97
Table 43- Constraints on natural frequencies of Soyuz launch vehicle .....	99
Table 44- Structure mass and dimensions budget.....	100
Table 45- Values of parameters used in worst-case hot and cold calculations.....	104
Table 46- The applied thermal-optical coefficients used in the analysis.....	105
Table 47- Summary of the specifications of the thermal control subsystem considered .....	107

# 1. Mission

## 1.1. Mission Drivers

Since the dawn of the space age in the 1950s, humanity has launched thousands of rockets into space and deployed numerous satellites and spacecraft into Earth's orbits, with only a small fraction of them being operational, while many others remain inactive in orbit. According to statistics, currently out of approximately 8000 satellites placed in orbit, only about half of them are operational, and the rest have become space debris. This statistic is separate from the number of launchers and smaller particles that exist in space as space debris. This space debris can collide with active satellites and spacecraft, potentially causing their destruction. Moreover, such collisions generate thousands of smaller debris, increasing the likelihood of further collisions.

According to the Kessler syndrome proposed by Donald J. Kessler, a NASA scientist, in 1987, if the production of space debris in orbit continues to increase, it could lead to chain reactions of collisions among satellites and space debris, resulting in a significant increase in the amount of space debris to the extent that space becomes inaccessible for humanity. The primary reason for the increasing likelihood of the Kessler effect is the continuous rise in the number of satellite launches.

Nowadays, the demand for satellite launches into space is increasing significantly. Moreover, large companies such as SpaceX and Amazon are developing their mega-constellations for global satellite internet access coverage. To achieve this goal, over 50,000 additional satellites need to be deployed into Earth's orbit within the next few years. The graph below illustrates the trend of the number of satellites placed in orbit up to the year 2022, showing a notable growth in 2022 compared to 2021, which has been even higher in 2023.

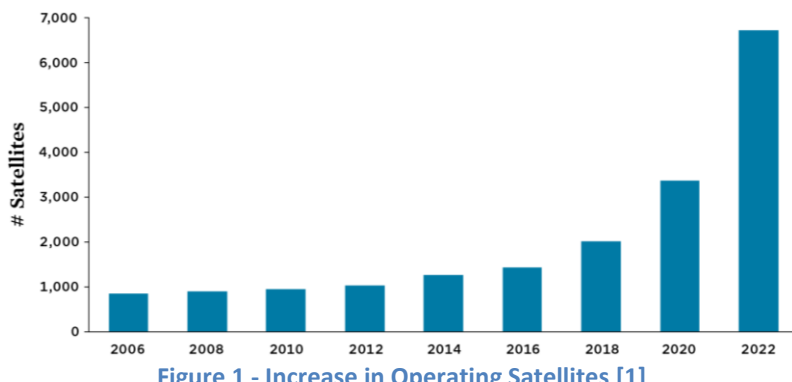


**Figure 1 - Increase in Operating Satellites [1]**

A significant portion of the satellites in space are in Low Earth Orbit (LEO). According to statistics, approximately 84% of satellites are in LEO (500-1000km), 12% are in Geostationary Orbit (GEO) at 36000km, and 3% are in Medium Earth Orbit (MEO) (5000-15000km).[2] Due to the applications of

LEO orbits, such as satellite internet, the number of satellites in this orbit is rapidly increasing. The graph below illustrates the number of payloads and launchers deployed in orbit over various years, indicating the upward trend of satellites in LEO.

Debris from launches or collisions is not counted. Objects are subtracted from the time series after they have reentered the Earth's atmosphere.

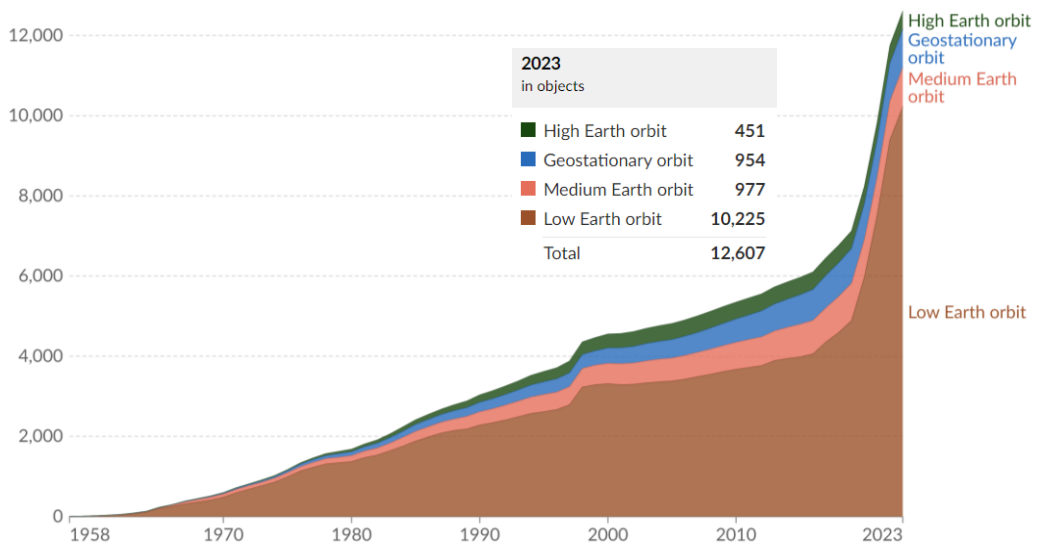


**Figure 2 - Number of Payloads and rocket bodies in orbit by year [3]**

Therefore, considering this trend, Earth's orbit will likely become increasingly cluttered with space debris in a relatively short period of time, and it is not far-fetched to expect the occurrence of the Kessler syndrome, rendering space unusable for human activities. One of the solutions being pursued today to prevent collisions between active objects and space debris involves the development of advanced tracking and collision avoidance systems.



**Figure 3 - Image of space debris in near-Earth orbits**

To prevent collisions between active objects and space debris, one of the solutions being pursued today is collision avoidance maneuvers. However, with the excessive increase in space debris, the



APSCO CubeSat Competition  
Conceptual and Preliminary Design Report – Ver. 1  
(IR-Sepehr)

need for an increased number of maneuvers arises, which is costly and complex to manage, and practically diminishes the effectiveness of these maneuvers. Therefore, it is necessary to devise a solution to either remove space debris or deorbit them from critical orbits.

According to guidelines, companies must remove their satellites from orbit within 25 years after the end of their mission. However, in 2022, the Federal Communications Commission (FCC) considered this timeframe too long and is seeking to reduce it to less than 5 years and even 1 year.[4] Given the importance of the space debris issue, the enforcement of these laws and even stricter regulations is highly probable.

Satellites with higher mass and orbits at higher altitudes generally have longer orbital lifetimes. Many satellites in orbits higher than 600 kilometers have orbital lifetimes exceeding 25 years at the end of their mission. Therefore, to comply with regulations regarding satellite deorbiting timeframes, active systems for satellite deorbiting must be utilized.

One of the best ways to remove space debris near Earth is through deorbiting, which ultimately leads to their burn-up in the Earth's atmosphere. Therefore, it's preferable for satellites to have active deorbiting systems. Several solutions exist for this purpose, and the SPARCS<sup>1</sup> mission is designed to research one of these methods, namely Electrodynamic Tether (EDT).

In EDT technology, a magnetic field interacting with an electric current, generated by solar energy absorbed through solar cells, creates a force that can change the orbital altitude. This force can be used to reduce the velocity, causing deorbiting, and the tether also increases the drag force that assists in this process.

Research on EDT technology is not only beneficial for space debris removal but also addresses a major human problem in space, which is the generation of propulsion required for orbital maneuvers. This force can be utilized endlessly and solely through the energy received from the sun, making it highly cost-effective.

The desire of the Sepehr Space Systems student initiative (iSSS) team is to develop lightweight plug-and-play modules with various functionalities using EDT technology that can be attached to satellites and other space objects in MEO and LEO orbits to accelerate their deorbiting. An advantage of these modules is that by increasing their number on each object, the deorbiting speed can be increased. Additionally, we intend to evaluate the capability of these modules to increase orbital altitude, orbital control, and electrical power generation, as well as compare their competitiveness with other technologies. The following images demonstrate the operation of these modules for deorbiting.

---

<sup>1</sup> Spacecrafts for Advanced Research and Cooperation Studies (SPARCS)



**Figure 4 - Process of de-orbit and re-entry of a spacecraft using the EDT module [5]**

In addition to the experimental EDT technology test mission, we intend to have another mission aimed at developing swarm technology. Nowadays, the concept of swarm for satellites has gained popularity as it offers various capabilities for human use of satellites. For example, with swarm technology, we can increase the data transmission time to the ground station. Also, remote sensing missions can be conducted, allowing us to use a number of smaller and simpler satellites for monitoring instead of relying on one expensive and complex satellite. Furthermore, nowadays numerous satellite constellations are emerging, including the Starlink constellation developed by SpaceX for providing global Internet service coverage. A prerequisite for achieving satellite constellation technology is the intercommunication capability for the satellites, i.e., Inter-Satellite Link (ISL). In general, swarms provide us with the ability to perform various missions at lower costs with high precision and enable simplification of satellites.

Despite the significant importance of satellite swarms, there are currently few swarm missions, and this technology has not yet become an accessible and affordable option for everyone. The



APSCO CubeSat Competition  
Conceptual and Preliminary Design Report – Ver. 1  
(IR-Sepehr)

development costs of swarm technology in satellites are still high and have not reached an optimal level. One of the main challenges for achieving swarms is their software challenges. In the SPARCS mission, we intend to conduct tests with our two CubeSats towards achieving software capables of managing space satellite swarm. Our goal is to test ISL (Inter-Satellite Link) and consequently strive to perform centralized control tests of one CubeSat by another CubeSat, relative navigation, and orbital monitoring.

Smaller satellites, due to their lower inertia, experience orbital decay in less time and have shorter orbital lifetimes. Therefore, measures should be taken to simplify and reduce the cost of these satellites with shorter lifespans. Swarms also serve this purpose and contribute to simplification and cost reduction. Thus, by developing this technology, instead of using large, expensive, and complex satellites, smaller swarm satellites can be used for the same mission with better performance, simplicity, and lower costs.

At first glance, the connection between the two missions, ISL and EDT, may not be apparent, but both missions aim to reduce the amount of space debris and the cost of using satellites. For larger satellites with longer orbital lifetimes, we use EDT to accelerate orbital decay after the mission ends. Additionally, with the help of ISL, we make satellites smaller and cheaper, resulting in reduced orbital lifetimes, allowing them to naturally de-orbit quickly after the mission ends.

Therefore, the Sepehr Space System student initiative team aims to carry out the SPARCS mission using two CubeSats to test EDT and ISL technologies with the goal of cost reduction in satellite construction and space debris cleanup in near-Earth orbits. In the ISL mission, due to volume constraints (aiming for smaller and simpler satellites), satellite components are moving towards miniaturization. One of these components is the compact magnetorquers, which by installing them behind the solar panels, can reduce the satellite's dead volume.

For both the ISL and EDT missions, a criterion is needed to assess their performance over time. Considering the physics of the space environment, we know that the amount of charged particles and radiation will impact the performance of EDT and ISL. Therefore, a third mission should be defined in line with the objectives of the previous two missions, aiming to measure radiation dose.

## 1.2. Mission Statement

Considering the issue of space debris and the trend towards satellite swarms, the Sepehr team intends to conduct a combined mission including EDT, ISL, and dosimetry. All of these missions are aimed at research and technology demonstrations. The EDT mission focuses on the issue of space debris and orbit correction. ISL is proposed for swarm satellites, and dosimetry will complement and provide additional data to better assess the performance of the payloads, measuring possible correlations between radiation dose and the payloads operation.

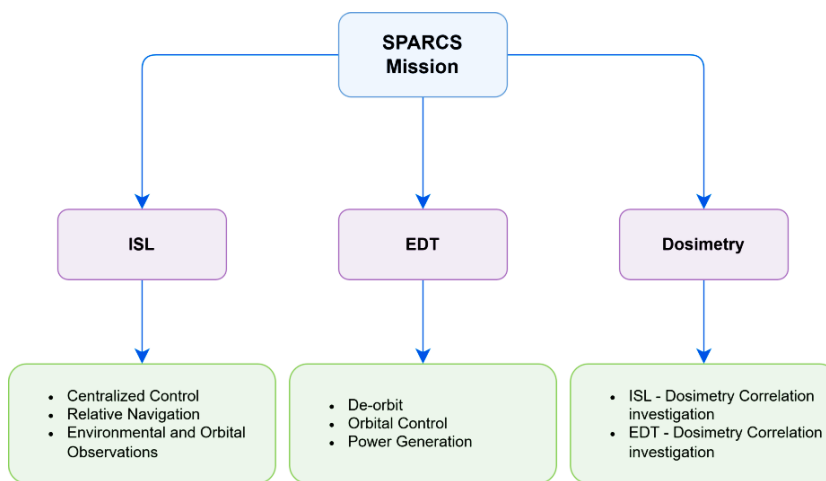


**Figure 5- SPARCS Mission**

### 1.2.1. Stakeholders

Multiple stakeholders can be defined and specified for this mission:

1. Stakeholders deriving from technology development: All owners and manufacturers of Low Earth Orbit (LEO) satellites can benefit significantly from the developed product in line with this mission, enhancing their company's offerings.
2. Stakeholders deriving from satellite data dissemination: Since the EDT mission is still under extensive research and development activities and shows great promise for future use-cases, disseminating the measured data by the satellite can better facilitate progress towards understanding physics phenomena (such as Alfvén wave and plasma physics).

## 1.3. Orbital Considerations

In the orbit design, we aim to determine the appropriate orbital inclination and altitude for the SPARCS<sup>1</sup> mission. To implement the mission proposed earlier, we intend to develop two modular CubeSats, namely SPARCS-A, a 1U CubeSat and SPARCS-B, a 2U CubeSat. The SPARCS-A and SPARCS-B will be deployed from a single 3U P-PO, so initially, they will have approximately the same orbit.

---

<sup>1</sup> Spacecrafts for Advanced Research and Cooperation Studies (SPARCS)

### 1.3.1. Orbital Altitude

Based on the requirements, SPARCS-A and SPARCS-B will be placed in LEO, and their orbital altitude must be at least 500km. Considering mission lifetime and launch constraints, we have chosen an orbital altitude of 550 km(TBC). Simulations conducted in STK indicate that the satellites' orbital lifetime at this altitude exceeds 1 year, making it suitable for SPARCS mission duration and launch constraints.

### 1.3.2. Orbital Inclination

To select an appropriate orbital inclination for the SPARCS mission, the following criteria are considered:

**EDT Performance:** The induced Lorentz force in EDT is dependent on the orbital inclination angle because the magnetic field orientation relative to the tether changes with inclination. Lower inclination angles result in higher ILF<sup>1</sup> values, as depicted in simulations. Therefore, the orbital inclination affects the performance of the EDT system. (Figure 6)

**Electrical Power Generation:** The orbital inclination affects the duration of sunlight exposure and, consequently, the electrical power generation from solar cells. Generally, higher orbital inclinations lead to greater power generation, especially in sun-synchronous orbits where this maximum value aligns.

**Launch Frequency:** CubeSats are typically secondary payloads launched into space, and their orbital inclinations depend on the primary payload. Some inclinations are more frequently used for launches than others. For example, launches into a 55-degree orbit may be more common than into a 73-degree orbit. This criterion is considered in selecting the orbital inclination.

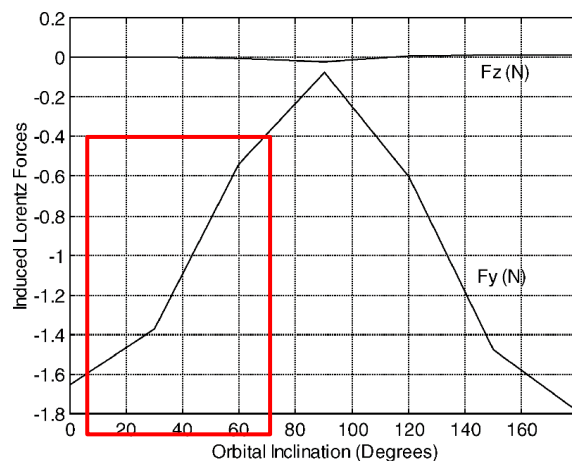


**Figure 6 Relation Between ILF and Orbital Inclination**

For selecting the orbital inclination angle, we utilized decision-making software called "Decision Making Expert Choice". Initially, we assigned weights to the considered criteria based on Figure 7, and then proceeded with binary decision-making to select the inclination based on these criteria.

<sup>1</sup> Induced Lorenz Force



APSCO CubeSat Competition  
Conceptual and Preliminary Design Report – Ver. 1  
(IR-Sepehr)

Figure 8 presents the results of this decision process, indicating that an inclination angle of 55 degrees is suitable for the SPARCS mission.



Figure 7- Results of Criteria Rating in Expert Choice



Figure 8- Expert choice results for Orbital Inclination

Thus, the orbital parameters considered are provided in Table 1.

Table 1- SPARCS Mission Orbit Parameters

Type	Circular
Inclination	55 deg
Altitude	550km

According to simulations conducted in STK, during the initial approximately two months of the mission, SPARCS-A and SPARCS-B are positioned at an appropriate distance (more than 10 km) to conduct ISL-related tests.

## 2. Payload

In this chapter, we will discuss the design and description of the mission payloads for SPARCS. Below are the details for each of the three payloads: EDT, ISL, and dosimetry.

### 2.1. Tether

Tethers are used for various purposes in engineering; but how is the idea of a space tether? A space tether is a long cable that connects spacecraft as they orbit the central body (i.e., Earth). Tethers are usually made of thin strands of high-strength fibers such as Spectra or Kevlar. Any space-tethered system, due to inducing gravity gradient, is intimately connected to the gravitational force field.



Figure 9 - Medium close-up view, shows Tethered Satellite System deployment.

In addition to their primary functions, conducting tethers present further benefits within space missions. Leveraging magnetic and electric force fields facilitates the generation of electric currents, enabling functionalities such as orbital correction maneuvers. These versatile tethers offer enhanced capabilities, contributing to efficient spacecraft operations and mission success.

In the case of a non-conductive tether, only mechanical forces are present and the resistance of the materials will be very important. In this case, several missions can be defined; like tethered formation flying (Figure 10), momentum exchange tethers (Figure 11), etc.



Figure 10 - Tethered Formation Flying: by the MIT.

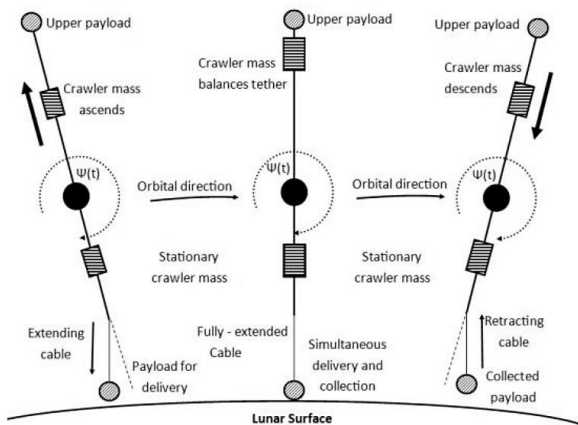


**Figure 11 - Momentum Exchange Tethers Example.**

In the case of a conductive tether, other forces and conditions are added, which will make the physics of the problem more complicated depending on the structure of the cable. In this case, electromagnetic forces, Lorentz's law, and Lenz's law govern the situation, depending on the conditions, we can either produce electrical power or electromagnetic force (EMF). In this case also, several missions can be defined; like electrodynamic tethers (EDT), electric sail (Figure 12), etc.



**Figure 12 - The HERTS is a spacecraft concept using an electric sail.**

The payload aboard the SPARCS-B mission encompasses a scientific payload specifically dedicated to EDT research. This payload necessitates a comprehensive investigation into the intricate physics and governing laws underlying EDT operations. Such an endeavor entails a meticulous exploration of electromagnetic interactions, tether dynamics, and associated phenomena, ultimately contributing to a deeper understanding and advancement of EDT technology and its applications in space exploration and satellite operations.

In most satellite missions, one crucial element will be the Earth's magnetic field. Despite its minimal strength, which diminishes with increased altitude from the Earth's surface, over time, it can generate electric power or EMF for us. This power and force are computable through the laws of Lorentz and Lenz. According to the Lorentz law, if we place a wire within a magnetic field and pass an electric current through it, a force will be exerted on the wire, which can be calculated using the Eq. 2-1.

$$\mathbf{F} = I \int d\mathbf{l} \times \mathbf{B} \quad (2-1)$$



Where  $\mathbf{I}$  is a vector, whose magnitude is the length of the wire, and whose direction is along the wire, aligned with the direction of the conventional current  $I$  and  $\mathbf{B}$  is magnetic field. Since the Earth's magnetic field is weak, the force exerted on the wire will be very small. However, in satellites, this force can continuously act on the wire over time. Integrating this force over time will be effective for us. Additionally, we experience fewer disruptive forces compared to those on the Earth's surface. Therefore, we can utilize this force for various orbital maneuvers. This method, unlike others such as solid fuel thrusters or ion thrusters, will not have material limitations (such as fuel depletion) and can be utilized for much longer durations in space.

Also, according to Lenz's law, if we move a conducting wire in a magnetic field, a current will be induced in the wire. The amount of induced voltage  $V$  can be calculated from the [Eq. \(2-2\)](#). Where  $\mathbf{L}$  is a vector, whose magnitude is the length of the wire, and whose direction is along the wire, aligned with the direction of the conventional current  $I$ ,  $\mathbf{B}$  is magnetic field and  $\mathbf{v}$  is wire speed in space orbit.

$$V = (\mathbf{v} \times \mathbf{B}) \cdot \mathbf{L} \quad (2-2)$$

A satellite in Earth's orbit has velocity and is also influenced by the Earth's magnetic field. Consequently, we will observe the generation of electric current within a conductive wire. The induced voltage is low, but similar to before, due to its continuous presence over time, it will be significant and effective.

### 2.1.1. Requirements

For design of the tether payload, requirements have been considered based on research and studies conducted on tethers:

- The tether shall be deployed as an end-body in SPARCS-B.
- The tether wire's length shall be 12 meters or less.
- SPARCS-B shall be able to de-orbit.
- The tether deployment process shall take a maximum of 1 month.
- The tether shall provide a mean to measure Lorentz force.
- The tether shall have the ability to measure induced voltage.
- SPARCS-B shall be equipped with a monitoring camera & processor capable of image processing.
- The tether should not generate excessive and uncontrollable tensile force controlled by ADCS.
- The tether shall have separate processor and memory from the main satellite computer.
- The tether wire's density should be low.
- The tether wire shall have high electrical conductivity.
- The tether motor must be capable of deploying and retracting the tether cable.
- The tether's coating and thickness should protect the conductive material from space environmental conditions.
- The tether cable should not experience bending during deployment.

- The power subsystem shall provide a voltage of 200 volts for the tether bias system.
- The roll and pitch rate of SPARCS-B during tether deployment should be less than two (2) degrees per minute (TBC).
- SPARCS-B shall provide nadir pointing with accuracy better than ten (10) degrees (RMS) towards the Earth during tether deployment.
- Magnetorquers shall be off as much as possible during payload operation.
- The OBC computer shall be able to establish serial communication with the tether processor.
- The tether deployment mechanism shall have a reset mode.
- The tether shall have appropriate thermal resistance to space radiation.
- The tether shall withstand all the forces exerted on it and does not tear apart.
- The tether MCU shall autonomously (TBC) validate the tether's deployment.
- In case of tether deployment failure, the deployment process shall be halted, and a report shall be issued to the ground station.

### 2.1.2. Fundamentals & Physics of EDT

The tether experiences various forces and conditions, impacting the overall dynamics of the entire space system. Therefore, initially, the impact of each term should be examined separately and in combination. Tethers can be stabilized using various methods. The two primary methods of satellite stabilization are static and dynamic. Static stabilization relies on environmental forces like electromagnetism and aerodynamics, aiming for very low pitch and roll rates. Dynamic stabilization, on the other hand, utilizes centrifugal force and satellite motion, sometimes supplemented by gravity gradient force, to maintain stability. In the SPARCS-B mission, we have opted for static stabilization and have chosen to utilize gravitational gradient for this purpose. This stability method necessitates the design of a CubeSat with differential weight distribution at both ends of the tether; thus, we will have an End-Body at the end of SPARCS-B. The different types of constellations for tether stability can be observed in Figure 13.

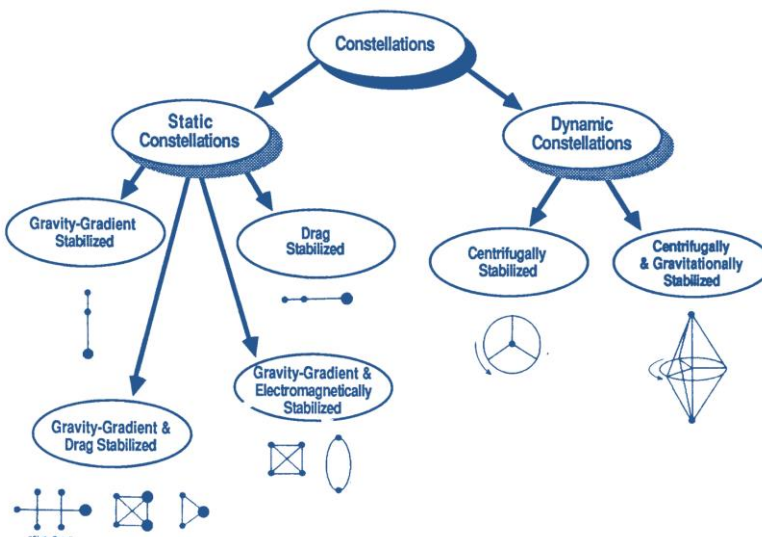
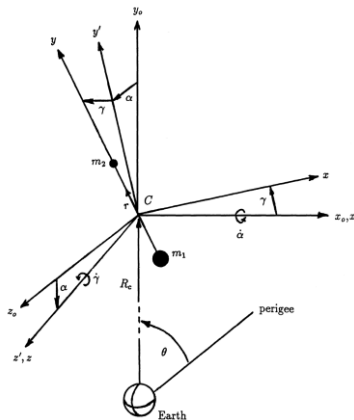


Figure 13 - The types of tether stability constellations. [6]

Tether can be stabilized to some extent using gravitational gradient force; however, due to certain perturbations, complete stability cannot be achieved. The most influential factors are as follows:

### 2.1.3. Nonlinear pitch and roll motions of tethered satellites

The equations governing the dynamics of tethered satellites are highly nonlinear. Hence the dynamical behavior is very rich and, in some cases, can be chaotic. The general dynamics of such systems involves pitch and roll motions of the tether, longitudinal and transverse elastic oscillations of the tether and three-dimensional attitude dynamics of the end-bodies. Pitch and roll motions of the tether are only marginally affected by the elastic oscillations of the tether and the rigid body dynamics of the end-bodies. Therefore, these two rotational motions can be investigated by modeling the system as one that consists of two-point end-masses,  $m_1$  and  $m_2$ , connected by a straight, rigid tether of length  $l$  and mass  $m_t$  (Figure 14). The equations governing the pitch angle  $\alpha$  in the orbital plane (y-z plane) and roll angle  $\gamma$



**Figure 14 - Geometry of the system.**

out-of-the orbital plane are then given by nonlinear pitch and roll angle as follows [7]

$$\cos^2 \gamma \left[ (\ddot{\alpha} + \dot{\theta}) + \left\{ 2r \left( \frac{l}{l} \right) - 2\dot{\gamma} \tan \gamma \right\} (\dot{\alpha} + \dot{\theta}) + 3 \left( \frac{\mu}{R_c^3} \right) \sin \alpha \cos \alpha \right] = \frac{Q_\alpha}{m_e l^2} \quad (2-3)$$

$$\ddot{\gamma} + 2r \left( \frac{i}{l} \right) \dot{\gamma} + \left[ (\dot{\alpha} + \dot{\theta})^2 + 3 \left( \frac{\mu}{R_c^3} \right) \cos^2 \alpha \right] \sin \gamma \cos \gamma = \frac{Q_\gamma}{m_e l^2} \quad (2-4)$$

Where  $Q_\alpha$  and  $Q_\gamma$  are the generalized forces corresponding to  $\alpha$  and  $\gamma$ , respectively,  $R_c$  and  $\theta$  are radial distance of the center of mass and true anomaly, respectively, while  $m_e$  and  $r$  are the equivalent mass of the system and a mass ratio, given by

$$m_e = \frac{[m_1 m_2 + (1/3) m_t (m_1 + m_2) + (1/12) m_t^2]}{(m_1 + m_2 + m_t)} \quad (2-5)$$

$$r = \frac{[m_1 (m_2 + (1/2) m_t)]}{[m_1 m_2 + (1/3) m_t (m_1 + m_2) + (1/12) m_t^2]} \quad (2-6)$$

It is assumed here that the sequence of rotations is pitch angle  $\alpha$  about the local vertical, followed by out-of-plane roll angle  $\gamma$ . It may be noted that, if the tether mass is small compared to the two end-masses,

$$m_e = m_1 m_2 / (m_1 + m_2), \quad r = 1 \quad (2-7)$$

The term  $i$  appears only during deployment. Otherwise,  $\dot{i} = 0$ . For small pitch and roll motions, in the absence of generalized forces and for a circular orbit,

$$\begin{aligned} \ddot{\alpha} + 3n^2\alpha &= 0 \\ \ddot{\gamma} + 4n^2\gamma &= 0 \end{aligned} \quad (2-8)$$

- Pitch frequency is  $\sqrt{3}$  times the orbital frequency.
- Roll frequency is 2 times the orbital frequency.
- Coupled pitch and roll motions are quasi-periodic in the general case.
- Under certain conditions, motion can become chaotic.

#### 2.1.4. EMF

There are two kinds of conductive tether: insulated and bare wires. In our case of insulated wires, the only trade of electron happens at cathode and anode at the end the wire which is fully discussed in section 2.1.11. Considering this aspect, the Lorentz force on the tether can be simplified and turn into as Eq. (2-9).

$$\mathbf{F}_{mag} = \int_0^l I(d\mathbf{l} \times \mathbf{B}) \rightarrow \mathbf{F}_{mag} = I \int_0^l d\mathbf{l} \times \mathbf{B} \quad (2-9)$$

Because current remains constant across the length of insulated tether, the system can be modeled with electrical circuits:

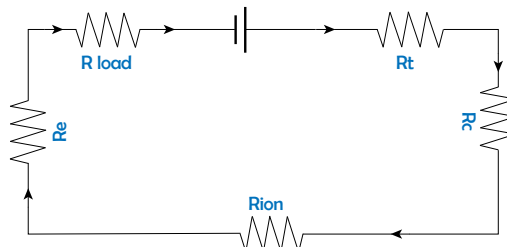
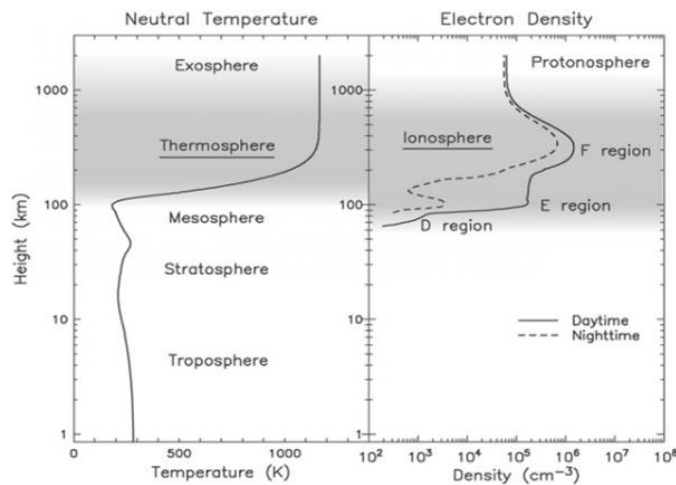


Figure 15 - A schematic of the tether circuit.

$R_t$ ,  $R_c$ ,  $R_e$ ,  $R_{ion}$  and  $R_{load}$  denote the tether, collector, emitter, ionosphere and load resistances. Also, for analyses it's important to calculate maximum current by ignoring the resistance of the load. Eq. (2-10) also includes the effect of variable  $n_e$ , ionospheric electron density, which varies up to two orders depending on whether it's day or night.

$$I_{max} = K n_e \sqrt{T} \left[ \frac{1}{2} + \left( \frac{\gamma}{\gamma_0} \right)^{0.528} \right] \quad (2-10)$$



**Figure 16 - Electron density profile as a function of altitude.[8]**

$K$  is experimental constant,  $T$  is ionospheric plasma temperature,  $\gamma$  is the electrical potential calculated with Eq. (2-10) and  $\gamma_0$  is given in Eq. (2-11).

$$\gamma_0 = A \cdot \frac{B^2 e^-}{8\pi m_e} \quad (2-11)$$

Now we have an important conclusion: total surface area of the collecting body,  $A$  is now involved in the output current. The rest of the notations are constants,  $B$  is the magnitude of the magnetic field,  $e^-$  represents the elementary electron charge and  $m_e$  is the electron mass.

### 2.1.5. Elastic oscillations of tethers

The tethers in tethered satellite systems are likely to undergo both longitudinal and transverse elastic oscillations. These oscillations are somewhat different from the standard string oscillations because the tether is subjected to a non-uniform axial tension generated due to the gravity-gradient and centrifugal force-gradient. In general, the longitudinal and transverse oscillations are coupled, but the coupling is weak in most cases. The equation governing longitudinal oscillations of a tether, deployed from a large orbiter in a circular orbit, is given by

$$EA \frac{\partial^2 u}{\partial s^2} - \rho \frac{\partial^2 u}{\partial t^2} + 3\rho\Omega^2(s+u) = 0 \quad (2-12)$$

with the boundary conditions

$$u(0, t) = 0, \\ -EA \frac{\partial u}{\partial s}(l_o, t) - m_2 \frac{\partial^2 u}{\partial t^2}(l_o, t) + 3m_2\Omega^2[l_o + u(l_o, t)] = 0. \quad (2-13)$$

Here  $l_o$ ,  $A$ ,  $E$  and  $\rho$  stand for the nominal length, area of cross-section, Young's modulus and mass per unit length of the tether, while  $u(s, t)$  is the longitudinal displacement of an element of the tether located at a distance  $s$  from the orbiter.  $\Omega$  is the angular velocity of the orbiter in the circular orbit. Eq. (2-12), with boundary conditions Eq. (2-13), can be solved analytically [9].

### 2.1.6. Effect of aerodynamic forces

As is well-known, aerodynamic forces can be nondimensionalized using Eq. (2-14). We will also utilize this equation to extract the aerodynamic force on the tether, considering the aerodynamic force term dependent on another set of parameters.

$$C_x = \frac{F_x}{\frac{1}{2} \rho V^2 S} \quad (2-14)$$

Atmospheric lift and drag drastically modify the trajectory of satellites in LEO. Their most dramatic effect is the decay of the semi-major axis. The decay rate increases more or less exponentially as the altitude decreases. This phenomenon becomes a true concern for altitudes below 500 km. Although they considered the effects of aerodynamic drag [10, 11], most of the previous analyses of tether dynamics have not considered aerodynamic lift. Nonetheless, studies [12, 13] have shown that lift has a significant effect on the attitude dynamics of tethered systems. The present formulation accounts for the combined effect of both air lift and drag.

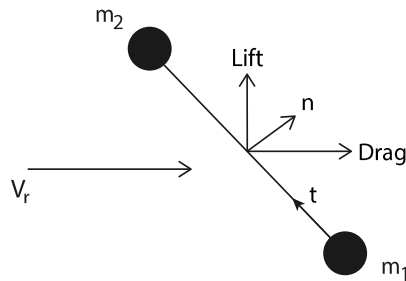


Figure 17 – Aerodynamic forces schematic.

Hughes [14] presents a particularly detailed derivation of the air lift and drag force acting on a spacecraft (Figure 17). He bases his analysis on the free-molecular flow model. This model assumes that the mean free path of the air molecules is much larger than the size of the spacecraft. As a result, the effect of collisions between air molecules and the spacecraft is greater than the effect of collisions among air molecules. This situation applies in rarefied density environments like LEO. Hughes states that in such cases, the combined lift and drag force on a surface due to its interaction with the atmosphere is given by aerodynamic force as

$$\mathbf{F}_{air} = \rho_{air} V_r^2 \left[ \sigma_r A_p^D v_r + \sigma_n \left( \frac{V_b}{V_r} \right) A_p^D + (2 - \sigma_n - \sigma_t) A_{pp}^D \right] \quad (2-15)$$

where  $\rho_{air}$  is the atmospheric density,  $v_r$  is a unit vector in the direction of the velocity of the local atmosphere relative to the surface and  $V_r$  is the speed of the atmosphere with respect to the surface.  $A_p^D$ ,  $A_p^D$  and  $A_{pp}^D$  are called shape factors. These parameters depend on the shape and size of the spacecraft surface.  $\sigma_n$  and  $\sigma_t$  are the accommodation coefficients in the normal and tangential direction respectively. The value of the two accommodations coefficients usually varies between 0.85 and 0.95. The limiting cases of specular and diffuse reflection correspond to

$\sigma_n = \sigma_t = 0$  and  $\sigma_n = \sigma_t = 1$ , respectively.  $V_b$  is the speed of the air molecules at the temperature of the tether  $T$ . In other words,

$$V_b = \sqrt{\frac{\pi R_u T}{2m_m}} \quad (2-16)$$

where  $R_u$  is the universal gas constant and  $m_m$  is the molecular mass of the air. The method for calculating the shape factor values involves lengthy equations that are beyond the scope of this text. Detailed information can be found in reference [15].

### 2.1.7. Conclusion

Even though the formulation and mathematics seem too complicated and the modeling has a lot of room to improve, these relations clarify why some requirements need to be satisfied and show us key points that we need to reconsider in our design process. For example, by studying the aerodynamic forces in Eq. (2-15), we understand that tether needs to have resistance to temperature change, as it increases air speed and the resultant disruptive aerodynamic forces. Or by using Eq. (2-9), we can take the effect of the environment into account and study the behavior of the ionosphere in different circumstances. Also, evaluating the vibrations of the tether gives us a hint about which material to use.

It can be confidently stated that this project can amend this set of formulations and help future attempts to be as accurate as they can be, or expand the field for scientific experiments. So, we need the ability to measure voltage, current, ionizing radiation, etc. to fully calculate and study all parameters involved. Also, the magnitude of various forces acting on the tether can be observed and analyzed in Figure 18.

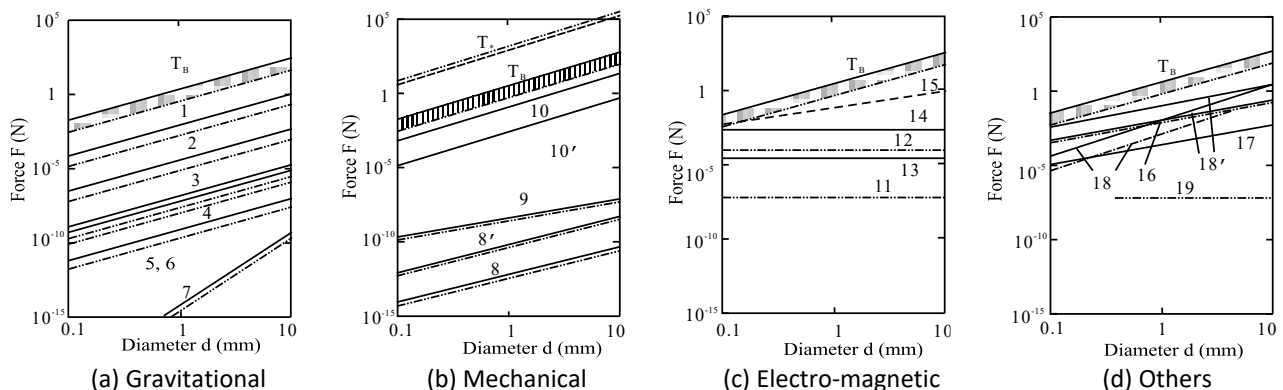


**Figure 18 - Magnitudes of perturbations, acting on the cable(20km). [16]**

The original SPARCS-B design used a 2U CubeSat physical package. The result of combining the analyses of the various models showed that, for a 2U CubeSat:

- To make up for atmospheric drag caused by the satellite, tether, and end mass, we need at least  $0.1 \mu\text{N}$  of thrust.
- The tether shall be approximately 12 meters long or less.
- The tether current shall be at least 2 mA.
- Voltage applied to the tether shall be approximately 200 volts.
- The net thrust will be approximately  $0.2 \mu\text{N}$ .
- The power consumed by operating the tether for thrust generation will be approximately 1.6 W.
- The tether should operate on at least a 40% duty cycle to overcome drag.

### 2.1.8. Configuration

The EDT is still under extensive research and development activities and shows great promise for future use-cases, and many institutions such as NASA and JAXA are actively working on it. It lacks a specific and defined configuration. Additionally, many of its components cannot be readily assembled together and require design work. We have identified the parts that are available as COTS elements and have proceeded to design the remaining components. Also, the interface of EDT with other subsystems and the architecture of EDT can be shown in Figure 19.

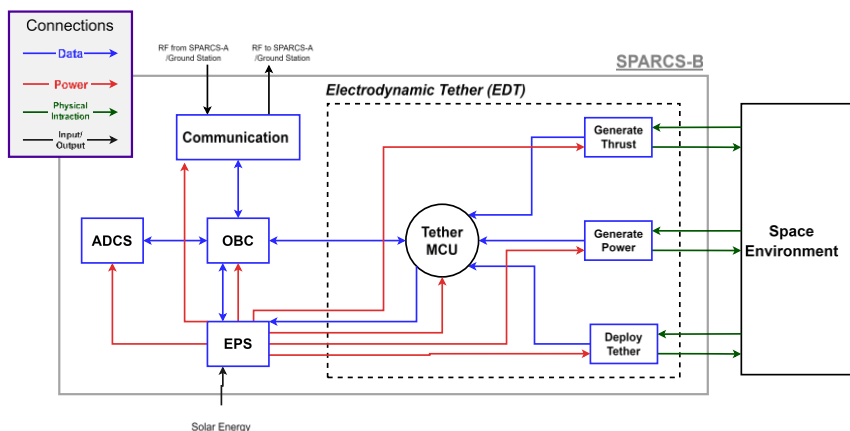


**Figure 19 - The architecture of EDT**

### 2.1.9. Components

**Table 2- Components of the tether configuration along with budget allocations and general specifications.**

Type	Component	Number
COTS	Servo Motor	1
	Camera	1
	Wire	1
	MCU	1
Design	Emitter	6
	Collector	2
	PCB Board	2
	End-body Plate	1
	Supporter	2
	Reel	3

### 2.1.10. Deployment System

Upon reviewing previous EDT projects, it became evident that one of the main reasons for their failure was the problem with tether deployment. When the tether is deployed, the wire wraps around the satellite, causing mission disruption and, in the worst-case scenario, loss of satellite communication. Therefore, one of the challenges is always the deployment of the tether.

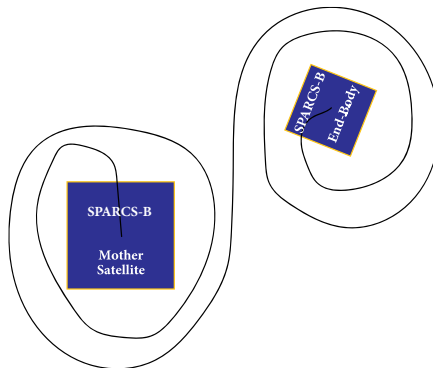


**Figure 20 - The schematic of the tangling of the tether around satellites and the mission failure.**

To solve EDT deployment problem, it was decided to slow down and elongate the deployment process. By doing so, we give the satellite the opportunity to make necessary corrections in case of any issues and settle to its steady-state dynamics. Additionally, by reducing the deployment speed of the EDT wire, we allow the gravitational gradient to affect the satellite system, causing the mother and daughter satellites to start separating.

The gravitational gradient force acting on the two ends of the wire will create a force to facilitate the opening of the wire. Due to the gravitational gradient equations, selected configuration and orbit, a force of  $5.5 \mu N$  will be exerted on both ends of the tether. However, due to the low stiffness of the wire and the extended duration of force application, the tether will be released from the canister.

Additionally, we will implement a monitoring mechanism to control the deployment speed. This mechanism will consist of a 360-degree servo motor capable of continuous rotation. This motor will unroll the cable at an approximate speed of 1 centimeter per minute.



**Figure 21 – A picture of the selected motor for deploying the tether.**

When the mother satellite and the end-body are connected to each other, due to their close proximity, the gravitational gradient force will be very weak. Therefore, an initial force needs to be generated to separate them. This can be achieved by using separation springs positioned between

the mother satellite and the end-body. These springs are very small and fit between the ribs of the satellite structure. They also have a low stiffness coefficient.

A camera is also designed to be installed to automatically monitor the EDT wire deployment process using image processing. This camera is precisely positioned along the axis of the EDT wire deployment to provide a clear and perpendicular view of the daughter satellite. By placing several LED on the End-Body plane, the angle and distance between the two satellites can be determined relative to each other.

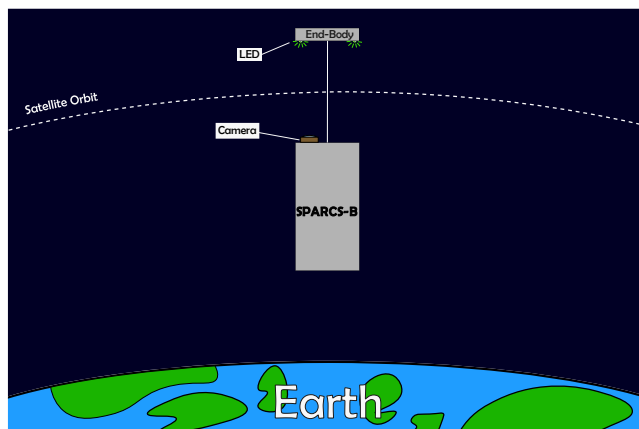


**Figure 22 – The schematic of monitoring the deployment of the tether using a camera.**

To ensure that the EDT wire remains straight during deployment and does not become kinked or bent, we need to compel it to open smoothly. For this purpose, we will utilize the inherent stiffness of the wire and implement a creative design.

In normal circumstances, if a minimal force is applied to a material, its deformation will be small. Similarly, in the space environment, disturbances are minimal, and due to the gravitational gradient force, the EDT wire will experience tension and remain straight.

However, since we will no longer have physical access to the satellite after launch, we must exercise caution and consider redundancy. The mechanism is designed in such a way that two sturdy reels hold the EDT wire between them, and by rotating one of the reels using a servo motor, the EDT wire starts to become free. The tether shall be equipped with its own dedicated MCU to control and manage deployment operations and voltage generation.

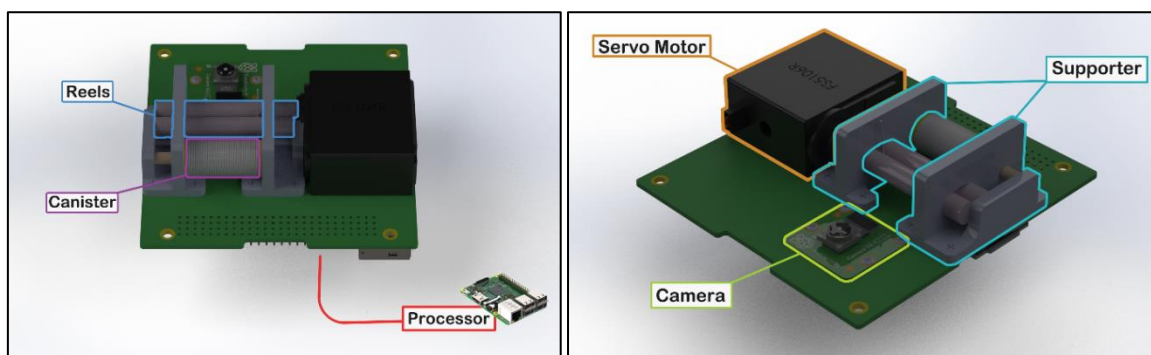


**Figure 23 - Tether deployment system.**

### 2.1.11. Bias Control System

There's still a fundamental problem. The EDT operates similarly to magnetorquers, but Due to the arrangement of the EDT wire, its configuration will be significantly different and more complex. In magnetorquers, it is easy to create a voltage difference between two wire ends and generate an electric current. However, in EDT, the ends of the wire are located at a considerable distance. This challenge can be addressed with the assistance of the Earth's plasma layer (Ionosphere). In high-altitude regions of the atmosphere, due to solar radiation, we will have positively charged ion particles and electron perfect environment for a bias system. This sea of electrons acts similarly to conductive materials (metals, water, etc.) for EDT. By utilizing plasma, it is possible to complete the electrical circuit of EDT wire, thus a voltage difference that creates an electric current.

To communicate with the atmospheric plasma, a set of components is required. An electron emitter (cathode), similar to electron guns, which propels and emits electrons into the atmosphere, and an electron collector (anode), which collects electrons.

As mentioned, the electron emitter comes in various types, which have been attempted to be downsized and utilized in this project. One example is thermionic emitter that its process is also used in converting thermal energy into electrical energy. According to Richardson's law if a metallic substance is heated to sufficiently high temperatures, excited electrons leave the cathode.

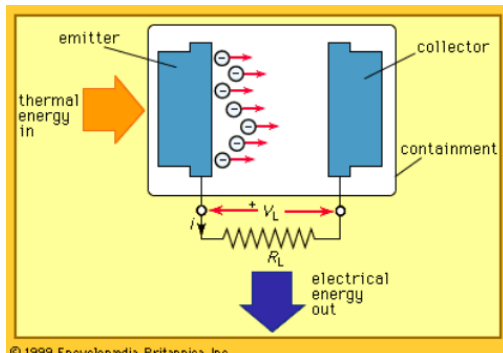


**Figure 24 - A Schematic of thermionic emitter.**

$$J = A_G T^2 e^{-\frac{W}{kT}} \quad (2-17)$$

Where  $J$  is the emission current density,  $T$  is the temperature of the metal,  $W$  is the work function of the metal,  $k$  is the Boltzmann constant and  $A_G$  is a parameter described in Eq. (2-18).

$$A_G = \lambda_R A_0 \quad (2-18)$$

where  $A_0$  is a universal constant and  $\lambda_R$  is a material-specific corrosion factor. So, it's important to choose the right substance; usually tungsten. Thoriated tungsten, and oxide coated metals are considered for the task.

The other variant is field emission array cathodes (FEACs) that are called cold cathodes. Emission is induced by an electrostatic field that makes electrons escape the surface (covered in sharp tips) and pass through apertures. Despite the advantage of reducing the required resilience to heat, the

efficiency is lower; a large percent of the electrons is absorbed by the gates and only a fraction of the current leaves the FEAC.

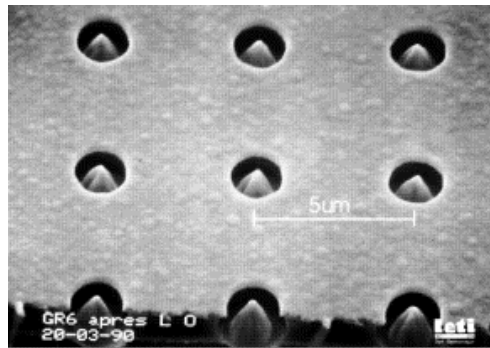


**Figure 25 - An image of FEAC under a microscope.**

In order for the electrodynamics tether to generate force in two opposing directions, we need to generate an electric current towards the end-body and another towards the mother satellite. As mentioned regarding the emitter and collector functions, it is necessary for both emitter and collector to be present in both the end-body and the mother satellite. This structure and design are visible in the illustration. The preliminary version of the electron emitter and collector has been designed based on existing versions in the market and their functionality.

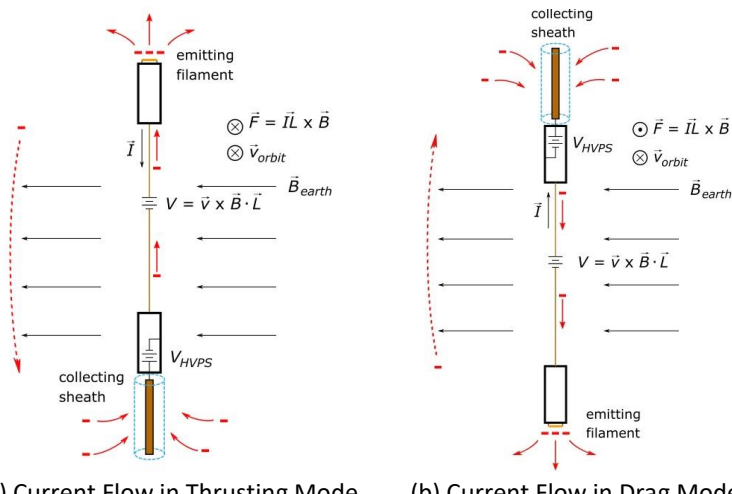
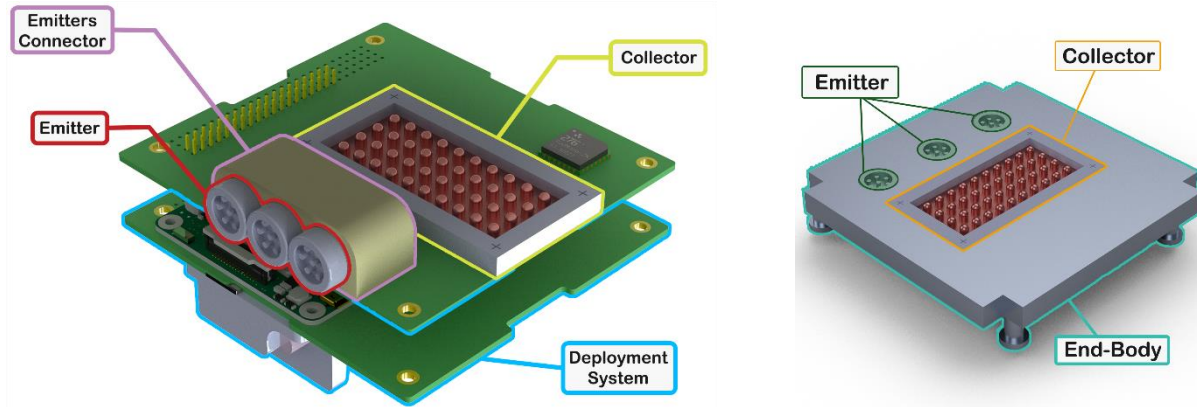


**Figure 26 - Current Interaction with Plasma.**

For commercial and completed products, existing market components can be used for the electron emitter, but for the SPARCS mission, it is desirable to design and develop them. Therefore, with consideration of mission requirements, the detailed design of these components will be completed in the detailed design phase.

In the preliminary design, a statistical design has been performed based on similar versions. According to this design, the weight of each emitter is 12 grams and the weight of each collector is 60 grams. The collector plates are made of copper and have a very large cross-sectional area to maximize plasma contact. Due to the challenges associated with designing and manufacturing a

single-pin thermionic emitter and its negative impact on the satellite platform, we are turning to FEAC. This model is made of silicon and is cost-effective to manufacture.



a) Emitter & Collector in SPARCS-B

Figure 27 – Tether bias system.

b) Emitter & Collector in End-Body

According to the requirements of the tether, it should have low electrical resistance and enhanced electromagnetic properties. Additionally, the tether wire should be thin enough to be easily coiled or uncoiled. For this purpose, a 30AWG copper wire is suitable. This wire not only has low electrical resistance but also exhibits high thermal resistance against radiation and heat, allowing it to operate effectively up to 80 degrees Celsius.

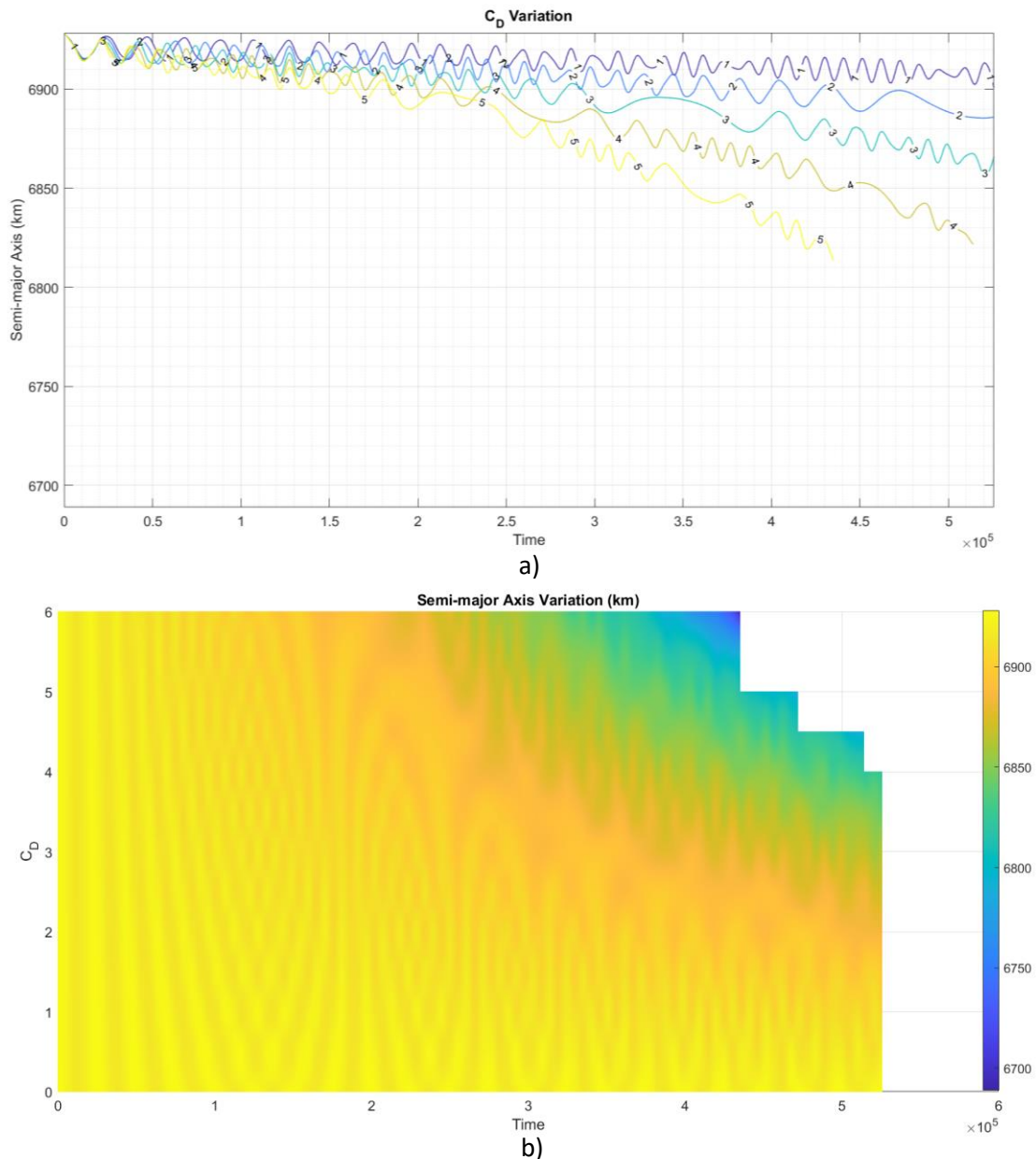


Figure 28 - Tether cable (30AWG copper).

In the End-Body section, it is not feasible to place a battery and processor for controlling and switching the tether (to change its direction of current flow) due to budget constraints. Therefore, the direction and current switching will be performed in the mother satellite. Hence, two tether wires are required for this task, each wire independently connected to an emitter collection and a collector. These wires will be connected to the power subsystem board, and commands from the tether control processor section will be sent to the power subsystem board, turning on the tether.

### 2.1.12. Simulations & Verification

Based on the equations in section 2.1.6, the drag coefficient has a direct relationship with the applied force on the tether. Both electromagnetic and aerodynamic forces extensively affect the tether. Therefore, by adjusting the  $C_D$  value in STK<sup>1</sup> software, the impact of the tether on orbital decay can be examined. Since the payload is scientific, it's not possible to precisely calculate the tether force over time, and only estimates of it are available. The Figure 29 illustrates the changes in the semi-major axis over time for different  $C_D$  values. With the help of this graph, the effect of tether activation time can be investigated.



**Figure 29 – Semi-major axis &  $C_D$  Variation by Time (s).**

---

<sup>1</sup> System Tool Kit



APSCO CubeSat Competition  
Conceptual and Preliminary Design Report – Ver. 1  
(IR-Sepehr)

Considering the design and COTS components, the overall budget allocation for the tether payload will be as follows:

**Table 3 - Tether overall budget allocation.**

Component	Model	Num.	Mass	Dimensions (cm)	Temp. (°C)	Voltage Supply (V)	Nominal Power Consumption	Maximum Power Consumption	Duty Cycle	Price (\$)
Servo Motor	FS5106R	1	40 g	4.08×2.01×3.8	-15 to 70	4.8 – 6	954 mW	6.6 W	%1	230 (TBC)
Camera	Raspberry Pi Cam	1	3 g	2.386×2.5×0.9	-20 to 60	3.3	900 mW	1.4 W	%1	380 (TBC)
Emitter	Must be ordered	6	12 g (TBC)	7.0×7.0×1.0	TBD					5000 (TBC)
Collector	Must be ordered	2	60 g (TBC)	7.1×7.0×1.0	TBD	200	1600 mW (TBC)	4 W	%30	5000 (TBC)
Cable	30AWG Copper	2	10 g	L:1000, D:0.04	-65 to 150					100 (TBC)
Tether MCU	Raspberry Pi (Opt)	1	150 g	7.32×4.5×3.5	-10 to 50	5.1	2.6 W	---	%10	6900 (TBC)
PCB Board	Standard (FR-4)	2	25 g	9.017×9.589×0.175	---	---	---	---	---	200 (TBC)
End-Body Plate	Designed	1	170 g	9.84×9.84×1.8	---	---	---	---	---	300 (TBC)
Supporter	Designed	2	Total: 30 g	---	---	---	---	---	---	120 (TBC)
Reel	Designed	3	Total: 9.5 g	---	---	---	---	---	---	60 (TBC)



## 2.2. ISL

The inter-satellite link (ISL) system is a crucial technology our team intends to evaluate during the mission. It is particularly relevant for swarm systems, an area that aligns with our team's research interests and promises significant benefits. Development of this system is necessary to achieve satisfactory data rates and processing capabilities without substantially altering the telemetry, tracking, and control (TT&C<sup>1</sup>) subsystem. This will require the creation of a frequency down-converter to enable the use of our existing TT&C antenna systems.

Utilizing the same components across systems reduces the risk of reliability issues within the communication subsystem. It is important to recognize that incorporating the ISL inherently enhances our system's reliability. A common issue in satellite communication systems is the inability of a CubeSat to establish a link with a ground station. The ISL addresses this problem by allowing a nearby satellite to temporarily connect with and support the affected CubeSat using its operational TT&C system.

A more comprehensive explanation of the ISL is provided in the communication subsystem report. Even under the most conservative estimates discussed therein, the combined requirements of the ISL and TT&C systems do not exceed 15% of any given budget, while offering greater bandwidth than necessary for our mission objectives.

## 2.3. Dosimetry

A CubeSat dosimeter is a radiation monitoring device designed to measure and monitor the radiation environment in space. Dosimeters used in CubeSats serve several purposes and have various applications:

- **Radiation Monitoring:** One of the primary functions of a CubeSat dosimeter is to monitor the radiation levels in the space environment. This includes measurements of cosmic rays, solar energetic particles, and trapped radiation in the Van Allen belts. Understanding these radiation levels is crucial for assessing the risks to both satellite electronics and human spaceflight missions.
- **Space Weather Research:** CubeSat dosimeters contribute to the study of space weather phenomena. By collecting data on radiation levels, scientists can better understand the impact of solar storms and geomagnetic disturbances on satellites, spacecraft, and even ground-based infrastructure such as power grids and communication networks.
- **Spacecraft Health Monitoring:** Monitoring radiation exposure is essential for assessing the health and longevity of spacecraft components. Dosimeters can help spacecraft operators understand the cumulative radiation dose experienced by critical systems and electronics, allowing them to predict potential degradation or failure over time.

---

<sup>1</sup> Communication

- Risk Mitigation for Human Spaceflight: For future human missions beyond Earth orbit, such as to the Moon or Mars, understanding the radiation environment is critical for ensuring the safety of astronauts. CubeSat dosimeters can provide valuable data for assessing the radiation risks to crew members during these missions and for developing strategies to mitigate those risks.
- Educational and Outreach Activities: CubeSats, including those equipped with dosimeters, often serve as platforms for educational and outreach activities. Students and researchers can participate in designing, building, and operating CubeSats, gaining hands-on experience in space science and engineering.

In the current mission we utilize Dosimeter for three main applications:

- **To measure the radiation levels :**Since two CubeSats, after being placed in orbit, experience altitude differences over time due to orbital decay, we can use dosimeters on each of the CubeSats to measure the radiation levels at different altitudes and store and use that data.
- **Correlation between EDT and Dosimeter investigate:** Since there are alpha particle radiations present, it affects the EDT. Therefore, we need to investigate the correlation between EDT and Dosimeter.
- **Measuring the alpha particles effect on ISL**

The Dosimeter Chosen for the current mission is RadNano Dosimeter. RadNano is a tiny electronic dosimeter module, optimized for small size and power consumption. These instruments use semiconductor-based technology to sense and measure the ionizing radiation that reached the electronics, including gamma, X-ray and high-energy proton radiations.



Figure 30- RadNano Dosimeter

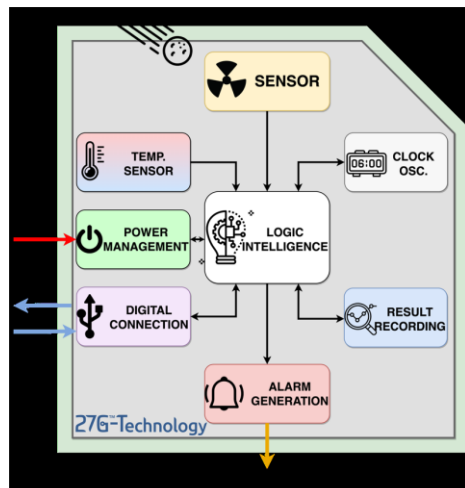


**Figure 31- RadNano Schematic of How its Work**

**Table 4- Dosimeter Specifications**

Dimensions	12.7×12.7×2.5 mm
Mass	< 1.0 g
Sensitivity	1mGy to 20/100/400 Gy
Power usage	< 10 µW standby < 10 mW active
Supply Voltage	3.3 V or 5V ± 10 %10
Communication	UART and other protocols
Reliability	MTTF > 1.1 M hours (50°C, MIL-HB-217F)



## 3. System

SPARCS mission requirements are presented in this section as follows

### 3.1. Mission Requirements

Table 5- SPARCS Mission Requirements

Mission	<ul style="list-style-type: none"><li>The mission duration shall be at least 1 year</li><li>Communications shall be conducted in the UHF and VHF bands</li><li>SPARCS-A and SPARCS-B shall establish communication with the ground station at least 4 times per day</li><li>SPARCS-A and SPARCS-B shall have pointing errors of less than 10 degrees</li><li>During the deployment of the tether, a daily image of the tether's deployment status shall be transmitted via downlink to the ground station</li><li>In the ADCS subsystem, neither of the two CubeSats shall use a separate microcontroller, and the OBC shall be used for this purpose</li><li>Both CubeSats shall have fail-safe capabilities</li></ul>
Payload	<ul style="list-style-type: none"><li>The deployment process for Tether shall be gradual and completed within less than 1 month</li><li>The tether deployment shall be executed as an end-body deployment and implemented on SPARCS-B</li><li>The tether length shall be a minimum of 10m(TBC) and a maximum of 20 m (TBC)</li><li>The power consumption and duty cycle of using the tether shall be within the capacity of the power system to supply</li><li>The input voltage to the tether wire shall be boosted</li><li>SPARCS-A and SPARCS-B shall have dosimeters</li></ul>
Orbit	<ul style="list-style-type: none"><li>The orbital altitude shall be at least 500km</li><li>For optimal payload (tether) operation, the minimum possible orbital inclination angle shall be selected.</li></ul>
Environment	<ul style="list-style-type: none"><li>Both CubeSats shall be capable of withstanding the space conditions in LEO</li></ul>

Table 6- SPARCS Mission Constraints

Dimensions	The total dimensions of the CubeSats shall not exceed 3U
Cost	The maximum engineering model cost shall be \$100,000
Regulations	For management, product assurance and system engineering proceedings we will act according to ECSS standards
Development Constraints	The spacecraft development has to be done according to the CubeSat specifications and is restricted in mass, size and power consumption

### 3.2. Mission Profile and Operational Modes

The duration of the SPARCS mission is one year. Figure 32 and Figure 33 respectively illustrate the phase and events of the SPARCS-A and SPARCS-B missions.



**Figure 32- Phase and Events timeline for SPARCS-A**

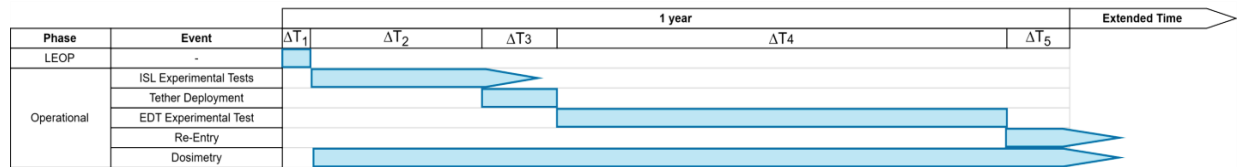


**Figure 33- Phase and Events timeline for SPARCS-B**

According to the figures above, each SPARCS-A, and B CubeSat mission consists of two phases; LEOP and Operational. In the Operational phase of SPARCS-B, ISL tests will be conducted for more than 2 months until communication is established between SPARCS-A and SPARCS-B. After 2 months from the start of the mission (TBC), the tether deployment process begins and will continue for 1 month (TBC). Following tether deployment, EDT tests will commence and will continue for a duration of  $\Delta T_4$ . After that, the re-entry process for SPARCS-B will be initiated using EDT. This process will continue as long as communication with SPARCS-B is maintained. After a prolonged loss of communication, the SPARCS-B mission will conclude. For both SPARCS-A and SPARCS-B CubeSats, dosimetry will begin from the start of the Operational phase and will continue until the end of their operational life. The end of SPARCS-A's life will occur either when it loses communication with the ground station or by command from the ground station to terminate its mission.

The main modes of the SPARCS mission are as follows:

- **Nominal Mode:** is the standard mode for SPARCS-A, B during normal mission activities and is also known as the default mode. Both SPARCS-A and SPARCS-B communicate with the ground station in this mode, and transitions to other modes are initiated from this mode.
- **Health Monitoring mode:** This mode continuously monitors the SPARCS-A, and B systems and components to detect any anomalies or issues promptly. for checking the health of the EDT payload components, SPARCS-B enters this mode at specific intervals.
- **Safe Mode:** This mode is engaged during critical or standby periods to ensure the safety and integrity of the spacecraft. In Safe Mode, the spacecraft operates with minimal functionality to conserve resources and protect against potential hazards.
- **ISL Experimental Mode:** In this mode, ISL tests will include data relay, centralized control, relative navigation, and orbit monitoring.

In addition to the common modes in SPARCS-A and SPARCS-B, the following modes are defined specifically for the SPARCS-B payload concerning the EDT payload:

- **Tether Deployment Mode:** SPARCS-B will enter this mode daily over a one-month period (TBC), during which the tether will be deployed slowly and using the designated mechanism.
- **EDT Experimental Mode:** In this mode, planned tests for the EDT payload will be conducted, and the data will be transmitted to the ground station.
- **Re-entry Mode:** Most subsystems will operate in a low-power consumption state, with the majority of power generated being used to produce force through the EDT to facilitate noticeable orbital decay for space debris mitigation. Necessary data will be transmitted to Earth via beacon.

The figure below illustrates the operational modes of SPARCS-A and SPARCS-B along with their transitions.

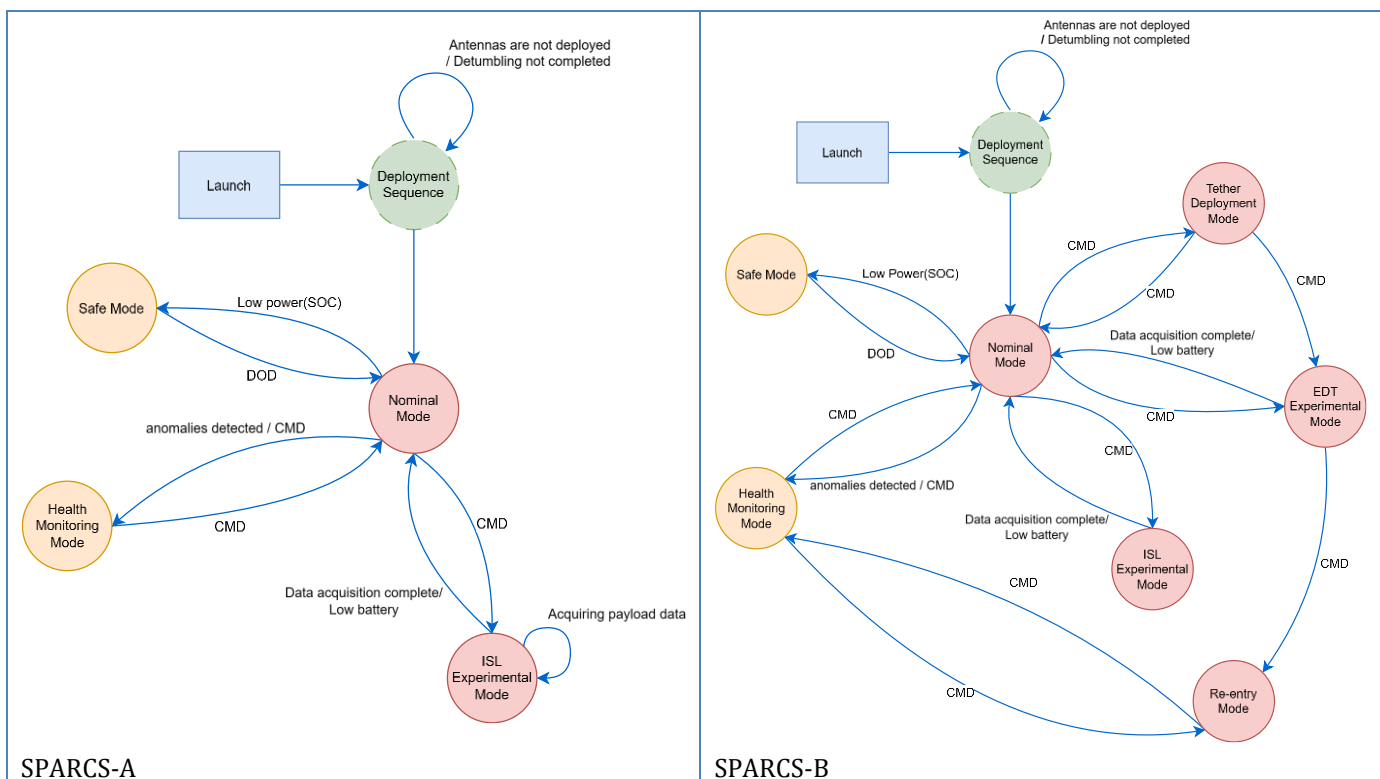


**Figure 34- Operational Modes in SPARCS Mission<sup>1</sup>**

The operating details of each mode are presented in Table 7 and Table 8.

**Table 7- Subsystem status during each mode in SPARCS-A**

	Nominal Mode	ISL experimental Mode	Safe Mode	Health Monitoring Mode
OBC	On	On	On	On
EPS	On	On	On	On
TTC	On/Idle	On/Idle	Beacon	Beacon
ADCS	On/Idle	On/Idle	Off	Idle
Payload(EDT)	Off	Off	Off	Idle
Payload(ISL)	Off	On	Off	Idle
Payload(Dosimeter)	On	On/Idle	Off	Idle

<sup>1</sup> CMD: Command, SOC: State Of Charge, DOD: Depth Of Discharge

**Table 8- Subsystem status during each mode in SPARCS-B**

	Nominal Mode	ISL experimental Mode	Tether Deployment Mode	EDT Experimental Mode	Re-entry Mode	Safe Mode	Health Monitoring Mode
<b>OBC</b>	On	On	On	On	On	On	On
<b>EPS</b>	On	On	On	On	On	On	On
<b>Comms</b>	On/Idle	On/Idle	Idle	Idle	Beacon	Beacon	Beacon
<b>ADCS</b>	Idle/On	On/Idle	On/Idle	Idle/On	Off	Off	Idle
<b>Payload (EDT)</b>	Off	Off	Off	On	On	Off	Idle
<b>Payload (ISL)</b>	Off	On	Idle	Idle/On	Off	Off	Idle
<b>Payload (Dosimeter)</b>	On/Idle	On/Idle	On/Idle	On/Idle	On/Idle	Off	Idle

### 3.3. Product Tree

The product tree for SPARCS-A and SPARCS-B is depicted in Figure 35 and Figure 36. The key components of each subsystem, along with their quantities, are listed in the product tree. Further details of each component are provided in the report for each subsystem.

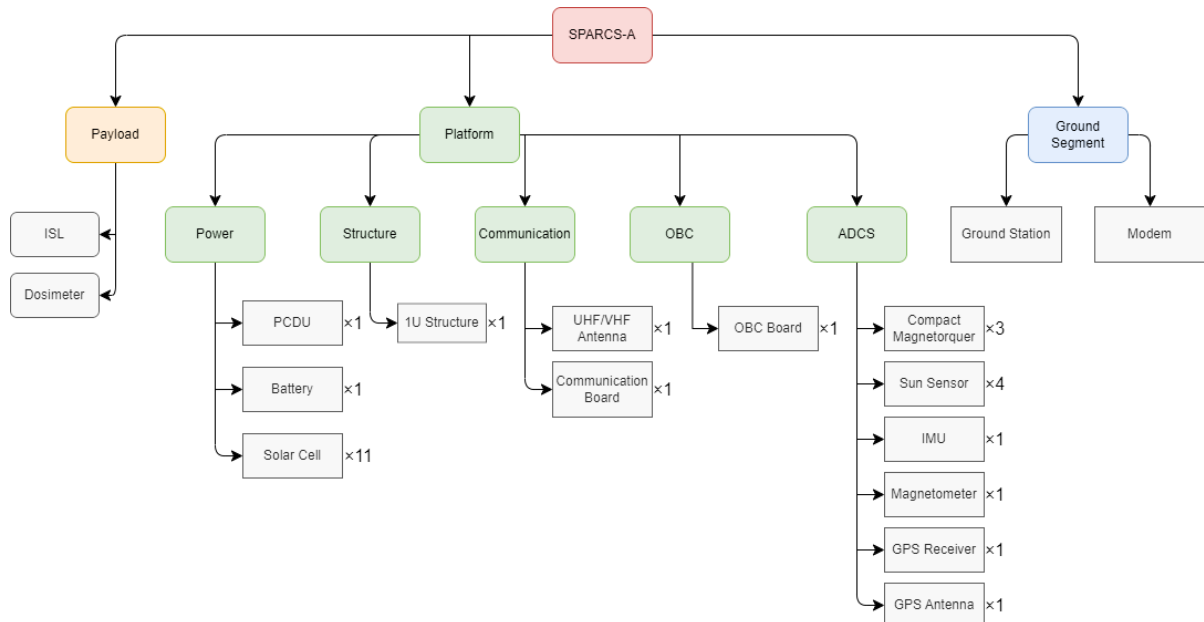


**Figure 35- Product Tree of SPARCS-A**

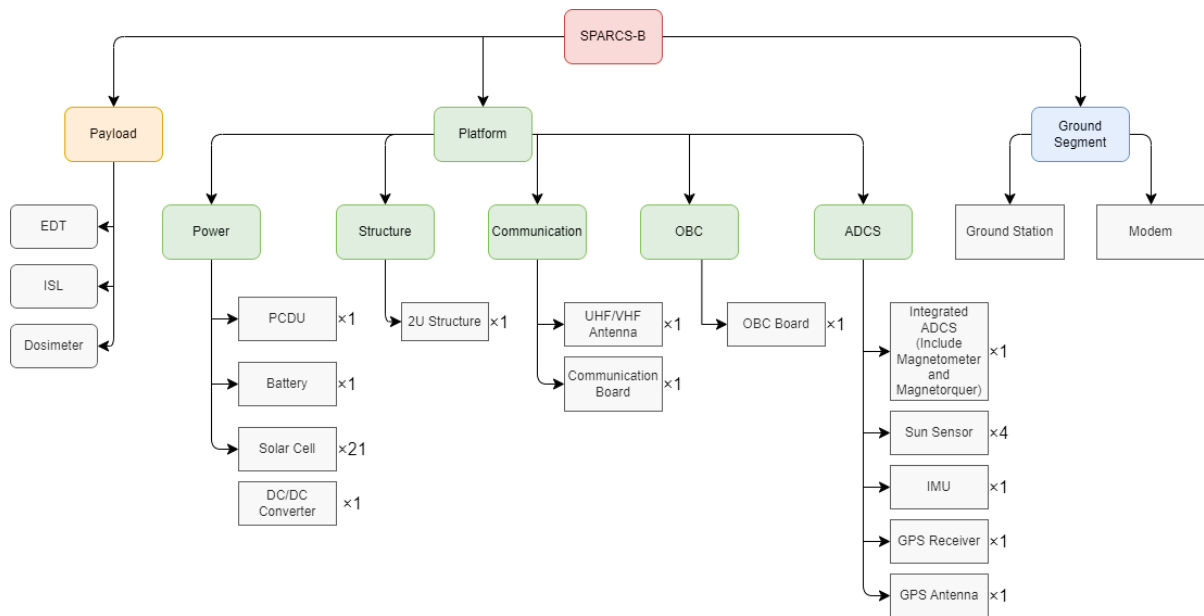


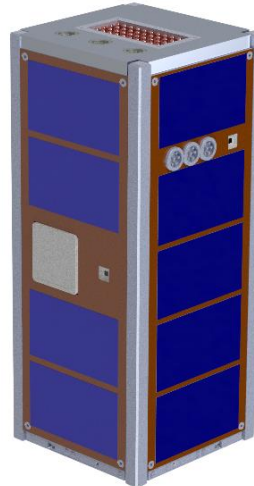
**Figure 36- Product Tree of SPARCS-B<sup>1</sup>**

### 3.4. General Layout

The 3D view of SPARCS-A and SPARCS-B is presented in the following figures. Additionally, the primary locations of each subsystem are indicated in Figure 38.



(a) Outside view of SPARCS-A



b) Outside view of SPARCS-B

<sup>1</sup> PCDU: power control and distribution unit



c) Outside view of SPARCS-B

d) Interior view of SPARCS-B

**Figure 37- 3D Views of SPARCS-A and SPARCS-B**

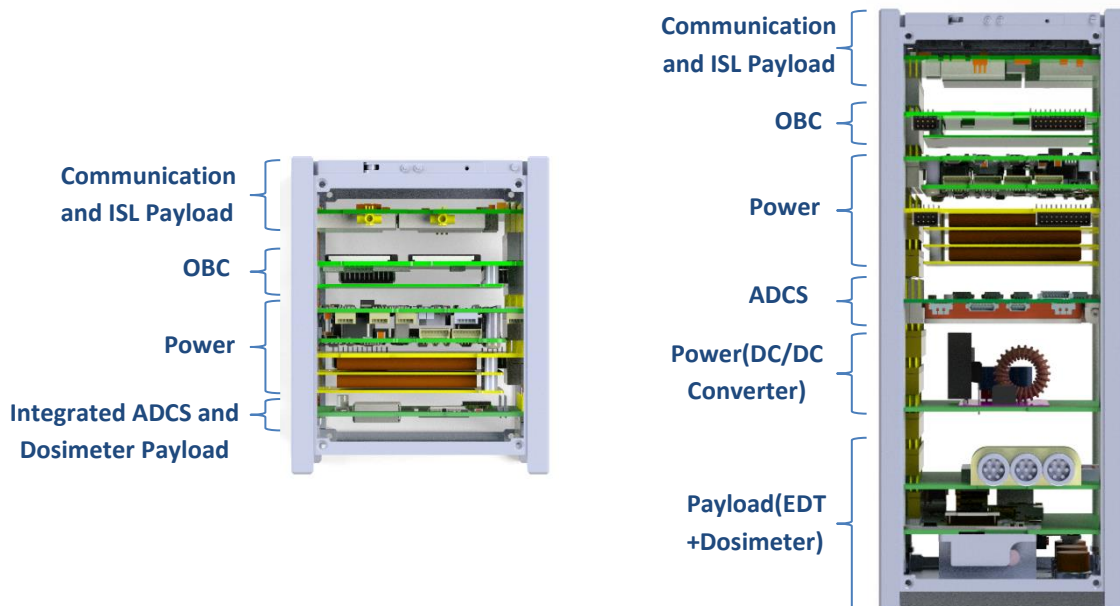


**Figure 38- Location of subsystems in CubeSats, left: SPARCS-A, right: SPARCS-B**

### 3.5. Budget Estimation

In this section, mass, volume, electrical power consumption, and cost budgets down to the subsystem level are provided. To estimate mass, volume, and electrical power budgets, we utilized datasheets for COTS components or performed regression analysis using available CubeSats datasets for components where this information was not available or needed to component be designed. Additionally, for estimating the cost budget, we employed regression analysis using the CubeSats dataset and considered the mission concept of SPARCS. Initially, this budget was broken down as a percentage of the total among the subsystems, and then each subsystem was responsible for



APSCO CubeSat Competition  
Conceptual and Preliminary Design Report – Ver. 1  
(IR-Sepehr)

managing its costs up to this percentage limit. Further details on how these budgets were estimated are provided along with these budgets down to the subsystem level.

All subsystems must design their components in a way that their budgets do not exceed the allocated amounts. Below are the mass, volume, power consumption, and cost budgets for the SPARCS mission based on subsystem designs.

### 3.5.1. Mass and Volume Budget Estimation

Table 9 presents the mass and volume budgets for SPARCS-A and SPARCS-B, as well as their summation. In estimating the volume budget, it was assumed that the main components of each subsystem housed within the structure are contained within a rectangular prism with an internal cross-section equivalent to a 1U CubeSat and a height that represents the volume of that subsystem as a multiple of U. In this manner, components like sun sensors, solar panels, and certain other components are not included in the volume budget. It's worth noting that the mass of components with uniform density, such as structures, was extracted from CAD models based on material definitions. To reduce volume, some components have been integrated onto a single PC104 board, including:

- Dosimeter with GPS receiver and magnetometer in SPARCS-A.
- Dosimeter on the tether board in SPARCS-B.

**Table 9- Mass and Dimensions Budget for SPARCS Mission**

Subsystem	Mass(g)			Dimensions(U)		
	SPARCS-A	SPARCS-B	Sum	SPARCS-A	SPARCS-B	Sum
Payload	10(TBC)	640	660	-	0.54	0.54
OBC	100	100	200	0.17	0.17	0.34
ADCS	158	210	368	0.09	0.15	0.24
Power	316	511	827	0.33	0.73	1.06
Communication	175	175	350	0.27	0.27	0.54
Structure	191	294	485	-	-	-
etc.	40(TBC)	50(TBC)	90(TBC)	-	-	-
Reserve				0.14	0.14	0.28
SUM	1000	1980	2980	1	2	3

### 3.5.2. Power Budget Estimation

The estimated power consumption budget for the SPARCS mission, broken down by subsystem level, is presented in the table below. The approach used to estimate power budget is similar to that used for estimating mass budget.

**Table 10- Power Budget for SPARCS Mission**

Subsystem	Power Consumption(Wh)		
	SPARCS-A	SPARCS-B	Sum
Payload	10 $\mu$	0.76	0.76
OBC	0.4	0.4	0.8
ADCS	0.81	0.68	1.49
Power	0.2	2	2.2
Communication	0.45	0.45	0.9



APSCO CubeSat Competition  
Conceptual and Preliminary Design Report – Ver. 1  
(IR-Sepehr)

Structure	0	0	0
SUM	1.86	4.29	6.15

### 3.5.3. Cost Budget Estimation

In estimating the cost budget, we initially divided the cost budget among subsystems as a percentage, using regression analysis of the CubeSats datasets and considering the SPARCS mission concept.

The budget estimate for expenditure takes into account statistical data, where approximately 50% of the procurement and manufacturing costs relate to engineering model components. Negotiating with component vendors can potentially reduce this by about 30%.

Considering a budget of \$100,000 allocated for the mission, it is estimated that the cost of manufacturing the flight model will exceed \$200,000. This budget allocation, as outlined in the budget breakdown shown in Table 11 across subsystems, has not been exceeded by any subsystem in its estimated cost projection. Based on available data, all estimated values are below this threshold. Therefore, the SPARCS mission meets the cost constraints as specified. The cost budgets presented for the subsystems are related to the flight model.

**Table 11- Cost Budget for SPARCS Mission**

Subsystem	Cost Budget (%)	Flight model Cost (USD)	Engineering model Cost (USD)
Payload	30	60000	30000
OBC	15	30000	15000
ADCS	15	30000	15000
Power	15	30000	15000
Communication	15	30000	15000
Structure	5	10000	15000
Etc.	5	10000	15000
SUM	100	100000	15000

### 3.6. Model-Based System Engineering in SPARCS Mission

Model-Based Systems Engineering (MBSE) is an approach to system design and development that uses models as the main basis for understanding, analyzing, and communicating system requirements and design decisions. MBSE employs visual and textual models to represent various aspects of a system, facilitating a comprehensive and integrated understanding of the system's requirements, behavior, and architecture. Some key features of MBSE include:

- Early Error Identification
- Improved Collaboration
- minimizing unnecessary work and rework
- Traceability and Consistency

In the SPARCS mission, we used Simulink System Composer for implementing MBSE, which emphasizes the creation and utilization of digital models to conceptualize, analyze, and manage

system requirements, architecture, and behavior throughout the lifecycle of the SPARCS-A, and B. The figures below provide a view of System Architecture down to the subsystem level in System Composer.

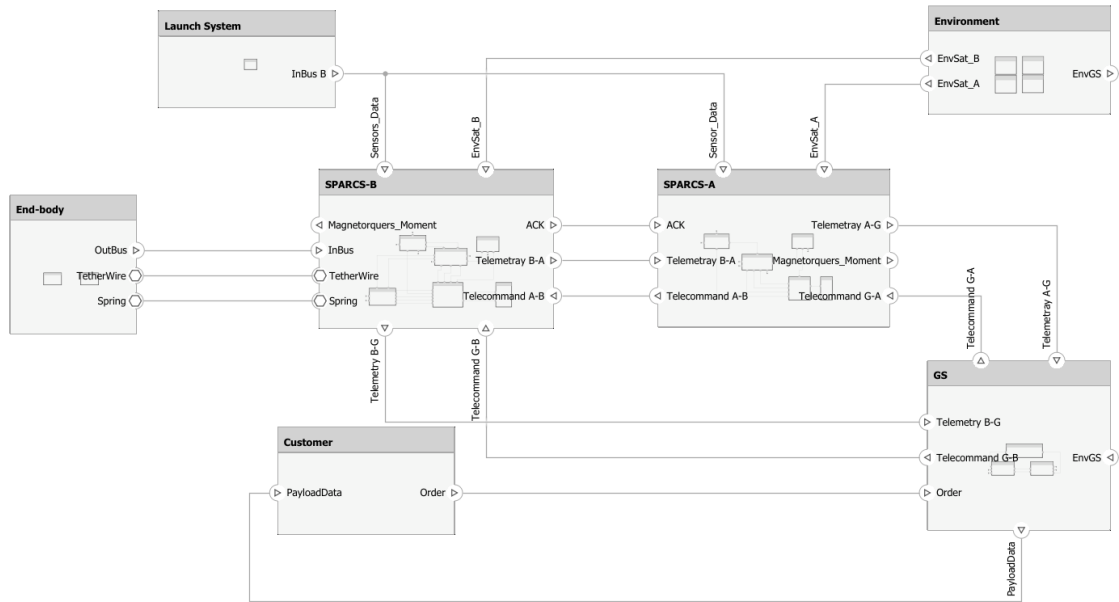


**Figure 39- SPARCS Mission System Architecture**

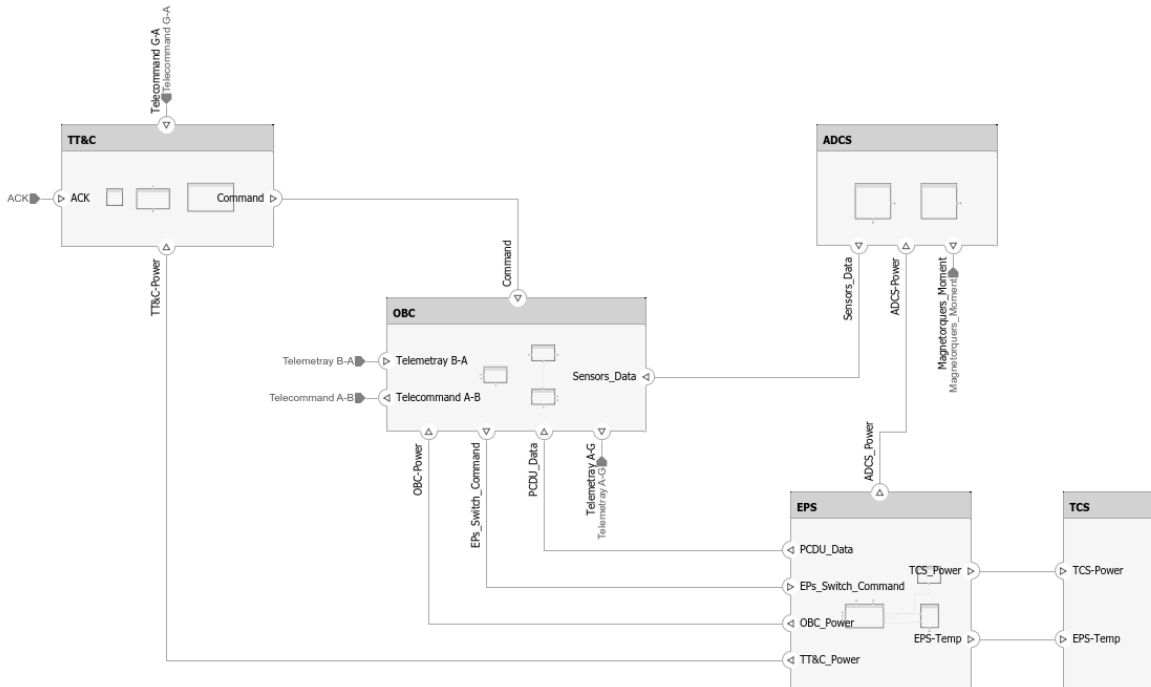


**Figure 40- SPARCS-A System Architecture**

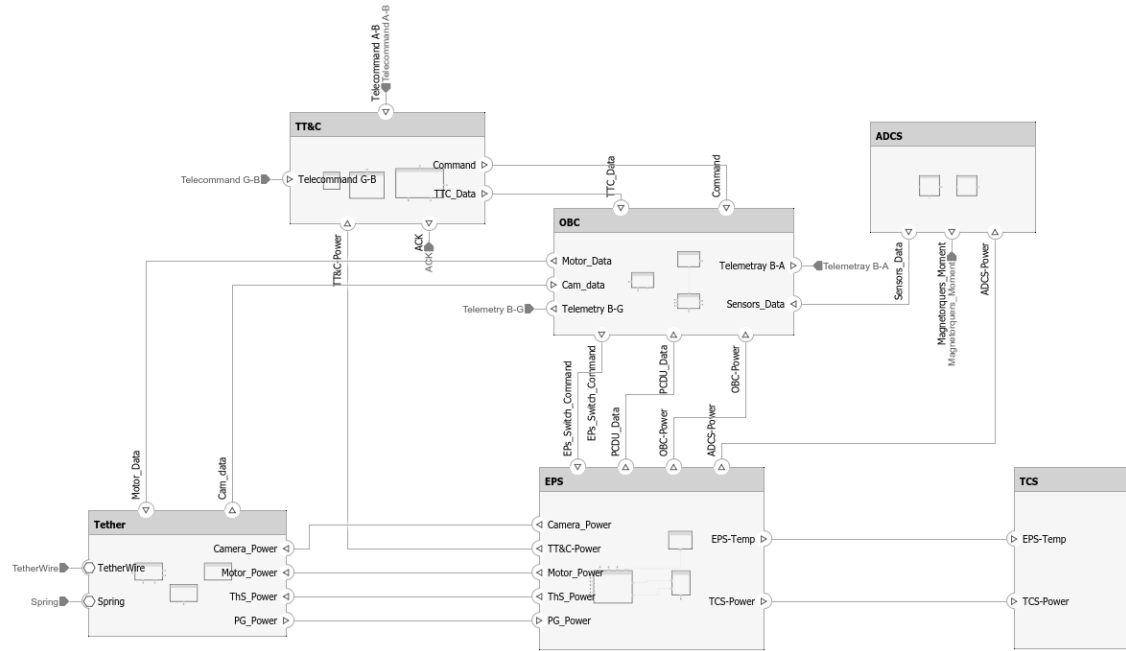


**Figure 41- SPARCS-B System Architecture**



## 4. OBC (Onboard computer)

The On Board Computer also known as OBC, is the brain of the satellite which is responsible for the tasks such as coordination of all the actions, sending orders to the different modules, the reception and storage of information of the CubeSat, sending this information back to Earth via the TCS error handling within the CubeSat.

The OBC section must contain the following content:

- General architecture and specification of the hardware (in the form of block diagram including the inputs and outputs)
- General architecture and specification of the software (in the form of block diagram including the inputs and outputs)
- Processing power estimation
- Memory space estimation
- Budget estimation

### 4.1. Requirements

- SPARCS-B must be able to control SPARCS-B and vice versa.
- Link A-B must transfer data at a rate between 1200 to 9600 bits per second daily.
- Link A-G must transfer data at a rate between 1200 to 9600 bits per second daily.
- The telemetry data rate from A-G must be between 1200 to 9600 bits per second.
- The telemetry data rate from A-B must be within the range of 1200 to 9600 bits per second.
- It must have the capability to establish serial communication with a processor.
- Software development deployment should be established for opening and closing the tether.
- The OBC must have the capability to process control data for SPARCS-B.
- Processor: At least 400MHz 32-bit
- Volatile Memory: Between 32-64 MB
- Critical Data storage: 512kb FRAM
- The system must establish communication with the ground station for 4 to 7 minutes during the day.
- The OBC must have one memory card.
- The OBC must have I2C chip and the ability to switch between Master and Slave modes in both Cube A and B.
- All inputs and outputs on the board must be specified.
- The software on the board must support all mission stages and requirements.

- If communication with the ground station is not established for any of these two CubeSats after 30 days, it must enter beacon mode.
- The OBC must have a GYRO for ADCS use.

## 4.2. Subsystem division

The OBC is divided into three subsystems which are Microcontroller, Interfaces and Electronics.

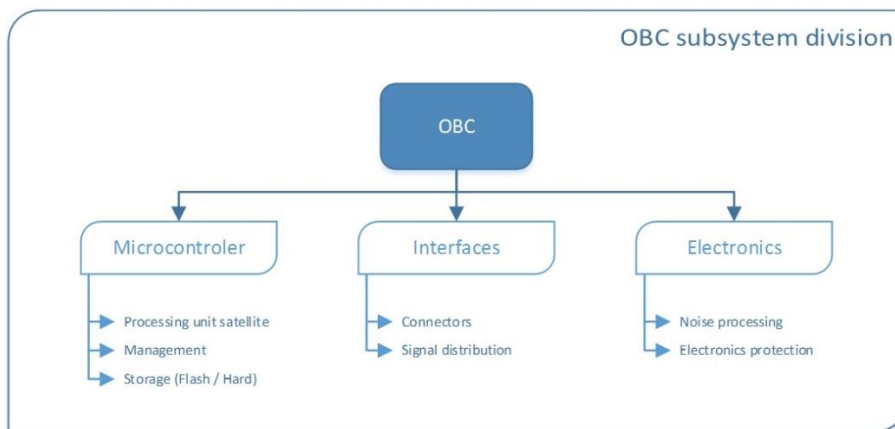


**Figure 42- OBC schematic<sup>1</sup>**

- **Microcontroller:** The microcontroller will run around 3.3 V to save power consumption and to fit with other CubeSats experiments.
- **Interface:** The Interface of an OBC facilitates communication between the OBC and other subsystems/payloads using standard protocols, ensuring reliable data transfer and system integration within the satellite.
- **electronics:** OBC electronics comprise the central processing unit (CPU), memory modules, communication interfaces, and sensors, enabling autonomous operation, data handling, and communication with ground stations for mission control and telemetry retrieval.

## 4.3. OBC components

**Processor:** The most essential part of any board is the processor. They usually vary from 8 bit to 32 bit.

The number of bits of the processor will have an impact on the power consumption and the efficiency for the calculation. An 8-bit processor will consume less while a 32-bit processor will have a better efficiency. Nevertheless, the new generations of 32-bit processors are low power consumption and could be used in CubeSat's architecture.

As for this mission since there is no complicated algorithm applied a 32-bit with 200 MIPS processing power is chosen.

<sup>1</sup> <http://www.ece3sat.com/cubesatmodules/obc>



To measure MIPS (Million Instructions Per Second), we need to determine how many operations our program requires per second, summing these operations, then selecting a processor capable of offering more processing power per second than the calculated amount.

For the CubeSat flight software, a cautious estimate for the Attitude Determination and Control System (ADCS) is typically around 42 MIPS. Assuming we have four other application software programs besides the ADCS, each requiring approximately 14 MIPS, and the operating system needing around 10 MIPS, we cautiously estimate a total processing power requirement of 108 MIPS.

The selected MIPS value for satellite operations is significantly higher. Here, it's beneficial to present the computational budget of each section in terms of MIPS. We then prioritize operations, allocating computational resources based on the real-time constraints and importance. Operations that are not real-time critical or less important are given lower priority, while algorithms with real-time computational constraints are prioritized. A significant portion of this process is planned through scheduling with the selected operating system's scheduler.

**RAM:** Volatile memory also known as RAM (Random Access Memory), serves as the OBC's workhorse for active data processing. It provides high-speed temporary storage for the operating system, program instructions, and real-time data manipulations. However, unlike non-volatile memory, RAM requires constant power to maintain its contents. Upon power loss, all data stored in volatile memory is irretrievably lost. This characteristic makes it unsuitable for long-term data storage but ideal for fast and efficient program execution within the CubeSat OBC. About the current mission for the least RAM memory needed which will be able to handle multiple packets of data will be less than 1 MB.

To calculate the RAM requirement: For this task, we've currently assumed a working frequency of one Hertz. Additionally, we've assumed that in each executable program on the On-Board Computer (OBC), except for ADCS, we have approximately 20 floating-point variables. Before writing to the main memory, these variables must remain in RAM for up to an hour. Therefore, considering that each float occupies four bytes, we need 15 kilobytes or 2 kilobytes per variable. Our upper estimate for parameters is around 50 variables, which we double to account for a margin, considering 100 variables. Thus, for data, we require around 200 kilobytes of memory.

Moreover, with a significantly high margin, we consider the same amount of memory for algorithm parameters (parameters are constant over time, but variables change over time). Hence, with a more conservative approach, our maximum memory requirement would be around 400 kilobytes. Again, since we are in the initial design phase, we consider a system-level confidence factor of two, meaning it would be 800 kilobytes, implying that we can confidently choose a one-megabyte RAM.

The second type of memory is Non-volatile memory, which unlike RAM, remembers stored information even when the power is off. This makes it ideal for permanently storing important data like program code and critical mission information on your CubeSat.

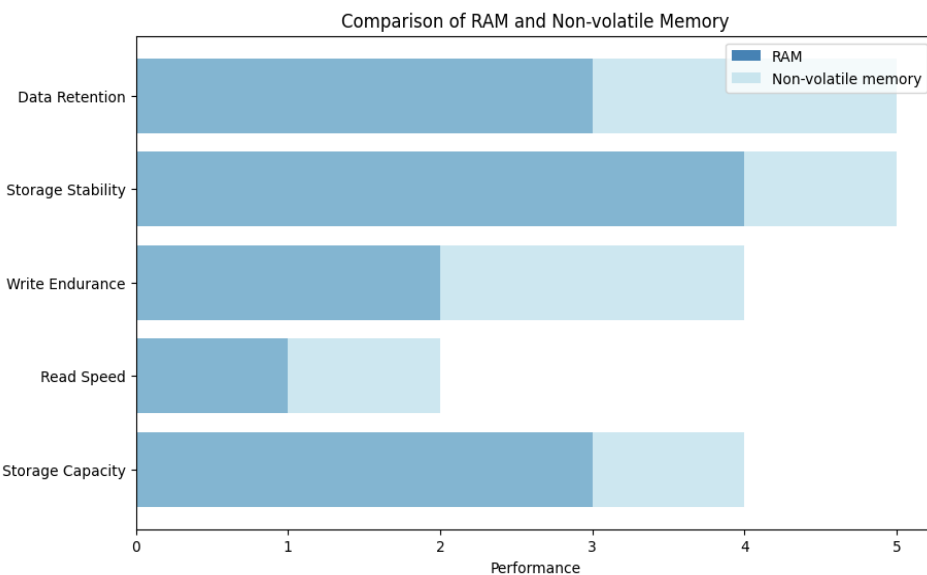


**Figure 43- Comparison of Overall Capacity**

There are two types of non-volatile memory:

1. NOR Flash
2. FRAM

NOR Flash is ideal for frequently accessed code due to its fast read speeds and rewratability, but offers lower storage capacity. FRAM prioritizes reliable data storage with high endurance for frequent updates, but has similar density limitations.

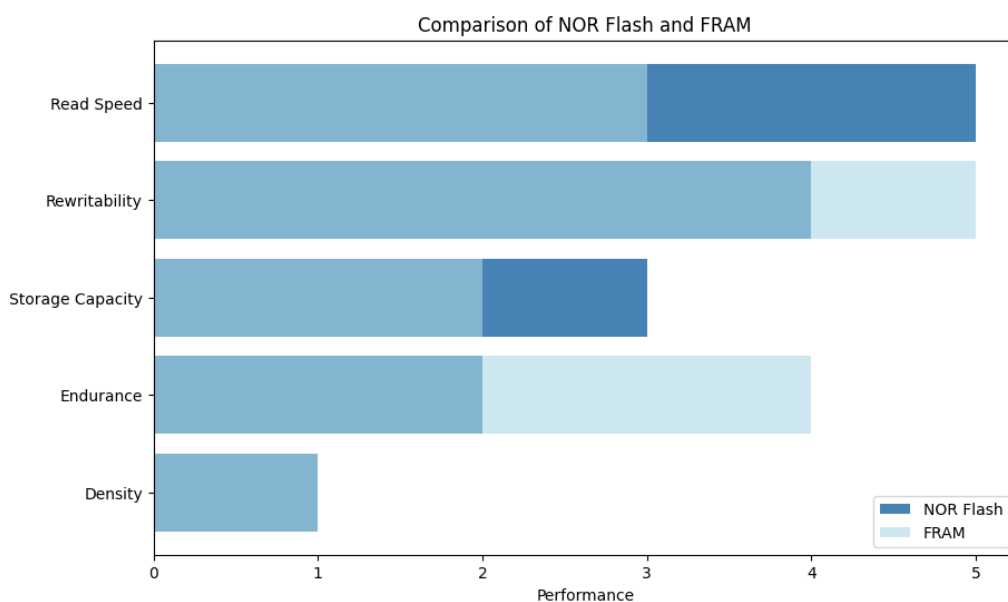


**Figure 44- Comparison of NOR Flash and FRAM features**



APSCO CubeSat Competition  
Conceptual and Preliminary Design Report – Ver. 1  
(IR-Sepehr)

For the current mission we expect the CubeSat to support up to 2,000 Terminals. Each Terminal stores 4 kilobytes (KB) of data, and for redundancy purposes, four copies of this data need to be maintained per Terminal. By calculating the total data per Terminal with all versions (4 KB/Terminal\*4 versions/terminal = 16 KB/terminal), and multiplying it by the total number of terminals (2,000 Terminals), we arrive at a total memory requirement of 32 megabytes (MB) or 256 megabits (Mb).

**Satellite Data Bus:** Within a satellite, various subsystems need a secure and reliable method to exchange data for coordinated operation. This critical role is fulfilled by the **satellite data bus**, which acts as a central communication channel enabling seamless data flow between different onboard electronics. To enhance overall system reliability and prevent communication bottlenecks, many satellite designs implement **redundant data buses**. This means subsystems connect to each other through more than one data bus, ensuring continued communication even if one bus experiences a malfunction. The choice of data bus protocol depends on the satellite's size and complexity. Larger satellites often utilize the Controller Area Network (CAN) protocol, known for its robust error detection and message prioritization features. Smaller satellites, due to their power and size constraints, might opt for CAN as well, or employ alternative protocols like the Inter-Integrated Circuit (I2C) bus, which offers simpler communication for a limited number of devices which has been chosen for the current mission.

**Table 12- I2C BUS and CAN BUS comparison**

features	I2C BUS	CAN BUS
Topology	Master/Slave (One master device can control multiple slaves)	Peer-to-Peer (all devices can communicate with each other)
Data Rate	Low (100 kbps-400 kbps)	Medium
Cable Length	Short (Limited a few meters)	Medium (Up to 1 Mbps)
Complexity	Simpler implementation	More complex protocol
Error Detection	Limited Error detection (Checksum)	Robust Error detection (CRC)
Addressing	Fixed 7-bit or 10-bit slave addresses	Flexible identifier-based addressing
Broadcast	Limited broadcast capability	Supports message broadcasting
Power Consumption	Lower power consumption	Higher power consumption

In the context of communication interfaces like I2C and SPI, master and slave modes define the roles devices play in data exchange:

**Table 13 - OBC Master & Slave Mode**

**Master Mode**

The master device initiates communication on the bus (I2C) or clock signal (SPI).

It controls the data flow by specifying which slave device it wants to communicate with and the type of data transfer (read or write).

The master generates the necessary clock signals for data synchronization on the bus.

It typically has more processing power and control logic compared to slave devices.



Slave Mode
The slave device waits for the master to initiate communication.
It responds to the master's commands, either sending data (read operation) or receiving data (write operation) on the bus or clock signal.
Slave devices typically have simpler designs and lower processing power requirements compared to the master.

**Table 14- I2C Slave and Master Mode Comparison**

Feature	Master	Slave
Role	Initiate communication	Responds to communication
Data flow control	Controls data direction	Follows master's direction
Clock signal generation	Generate clock signal	Synchronizes with clock
Processing power	Typically, higher	Typically, lower

Benefits of Master Mode:

- Centralized control over data transfer on the bus.
- Can communicate with multiple slave devices.
- Suitable for scenarios where the OBC needs to collect data from various sensors or control multiple actuators.

Benefits of Slave Mode:

- Simpler design and lower power consumption.
- Can be used for multiple slave devices on the same bus, allowing efficient communication with the master.
- Suitable for devices with a specific function, like a sensor sending data to the OBC upon request.

Choosing Between Master and Slave Mode:

The choice between master and slave mode depends on the specific application and the role of the OBC within the CubeSat system:

- If the OBC needs to collect data from multiple sensors or control various actuators, it will likely operate in master mode on the communication interfaces like I2C and SPI.
- Devices like sensors or simple actuators will typically be configured as slaves on the bus, responding to the master's commands.

For the current mission we are able to switch between two modes whenever it was needed.

#### 4.4. Introducing the selected OBC board

The ISIS On Board computer (IOBC) is a flight-proven, high-performance processing unit based around an ARM9 processor with a speed of 400 MHz, making it one of the most capable on-board computers for CubeSats, currently available on the market within the same price range. Its pluggable

daughter board offers additional flexibility and customizability by providing a wide range of extra interfaces for payloads, sensors or actuators in a compact form factor.



**Figure 45- ISIS OBC & ISIS OBC Daughter board**

The Mass94g mainboard is a compact and versatile On-Board Computer (OBC) well-suited for CubeSat applications. This lightweight option, weighing only 100 grams with the EM daughterboard attached, boasts a low average power consumption of 400mW, making it ideal for power-constrained CubeSat designs. At its core lies a powerful 400MHz 32-bit ARM9 processor, providing ample processing capability for various onboard tasks.

The OBC comes equipped with 64MB of SDRAM for volatile data storage, along with 1MB of NOR flash for program storage and 512kb of FRAM for critical data storage, offering reliability even in case of power loss. For mass data storage, the Mass94g features two high-reliability 2GB SD card slots, expandable to 32GB upon request, or it can accommodate standard SD cards of any size.

#### **4.4.1. Specifications**

Mass	94g mainboard only, 100g with EM daughter board
Dimensions:	9.6 x 9.0 x 1.24 [cm] (including FM daughter board)
Power Consumption:	400mW average
Power Supply:	3.3V
Operating Temperature:	-25 °C to +65 °C
Processor:	400MHz 32-bit ARM9 processor
Volatile Memory:	64MB SDRAM
Code Storage:	1MB NOR Flash
Critical Data Storage:	512kb FRAM
Mass Data Storage:	2 x 2GB high reliability SD cards for fail safe data storage



#### 4.4.2. Interfaces

- I<sup>2</sup>C master or slave mode
- SPI master mode up to 8 slaves
- 2x UART (RS232 + RS232 / RS485 / RS422)
- General Purpose Input / Output pins (GPIO)
- ADC: 8 channels, 10-bit
- PWM: 6 channels
- JTAG for programming and debugging
- Dedicated debug LEDs and UART
- USB host and device
- Image sensor interface

#### 4.4.3. Software Info

##### Hardware Abstraction Layer Library

This library supports the following peripherals and offers the following additional functionalities:

Table 15 - Library peripherals & additional functionalities

Peripherals	Additional functionalities
I <sup>2</sup> C master mode	Check summing (CRC-8, CRC-16, CRC-32)
I <sup>2</sup> C slave mode	Interface to iOBC Supervisor
Pulse Width Modulation (PWM)	Watchdog kicking
UART (RS232, RS422, RS485)	Timekeeping
SPI master mode	FreeRTOS operating system
FRAM read and write	AT91 library from Atmel
SD card using failsafe FAT journaling filesystem	
Real-Time Clock (RTC) and OBC internal timer (RTT)	

The chosen architecture for the software is a modern microservices architecture. In this architecture, the core execution unit will be the operating system, and all software components will run as separate software on separate computational threads. In the proposed software architecture, access to hardware is limited to the operating system, and software, or user space, will not have direct access to any hardware elements. This architecture enables the decoupling of software from the operating system through the definition of APIs, significantly facilitating software development on the board regardless of the chosen operating system.

In this architecture, due to the execution of different software on independent computational threads, these software components must be implemented as independently as possible, avoiding unsafe data sharing methods such as memory sharing. Based on this, in the proposed architecture,

all software components will be connected to each other via a Data Pipe. Placing data on the Data Pipe will result in an interruption in the computational threads, and with the help of this interruption and sender-receiver addressing in the message header, data transmission and reception management between programs will be performed. The concept of the Data Pipe essentially represents a chosen architecture for the software in the form of a modern microservices architecture. The following Diagram represents SAVOIR standard:

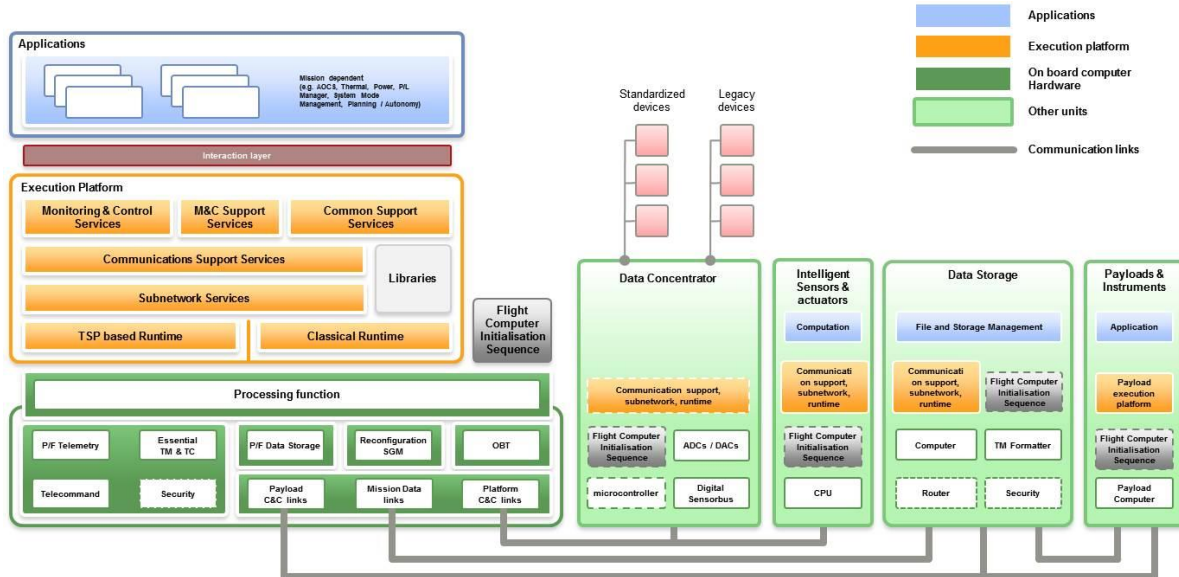


**Figure 46- Software Architecture based on SAVOIR standards**

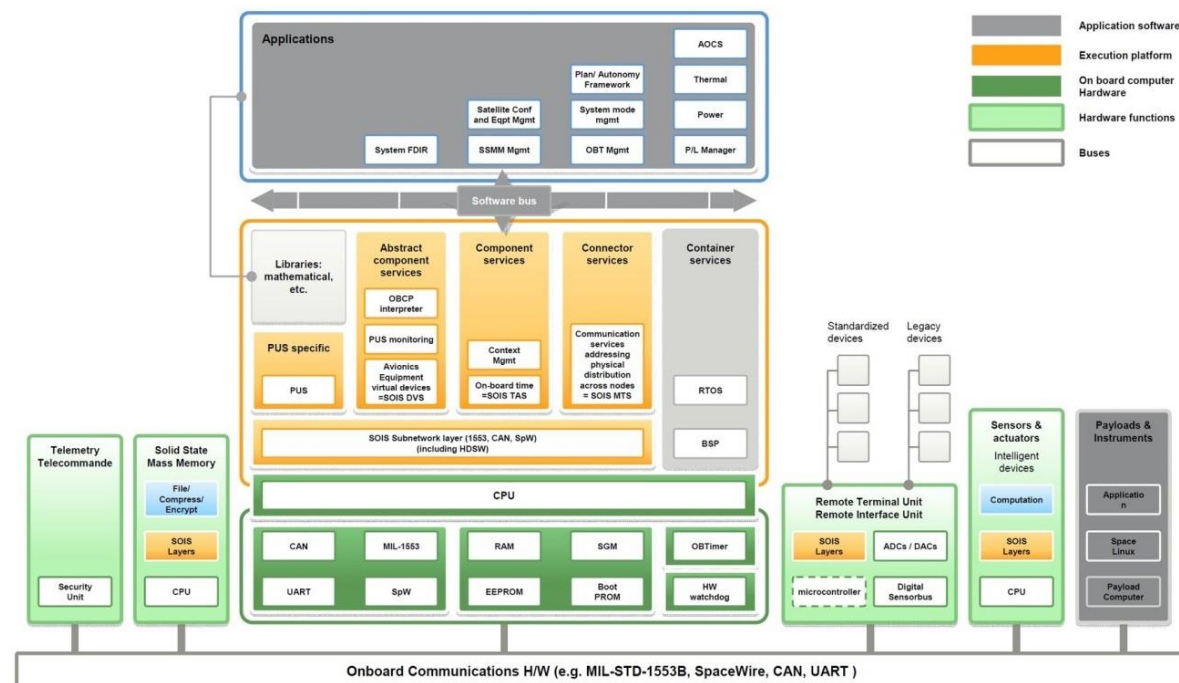


**Figure 47- Board's architecture (ESA Standard)**

Considering the proposed structure, expected functionalities will be implemented as microservices. Payload will be stored directly in memory via the bus and will only be accessible under the supervision of the central processor. Therefore, all computations related to the payload will be modularly implemented on the respective board. Without adopting a standard communication method, examining the software structure will be challenging.

Given the ease of access and compatibility with the proposed hardware communication layer (internal command and control bus), implementation will be done using the I2C protocol. Communications at the application level will be ensured through software bus. ZephyrOS kernel will be used for implementation. With its monolithic kernel structure, this system enables the implementation of single address space, time division, and modular design while maintaining a small footprint and providing protection for memory and both synchronous and asynchronous processing. Memory management will also utilize FAT-FS.

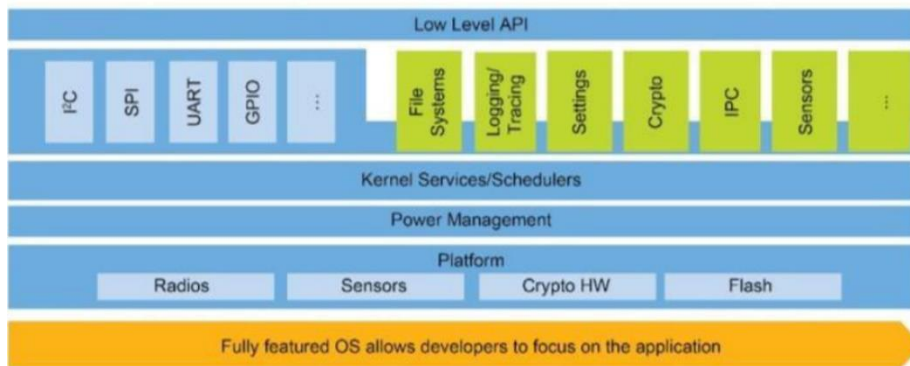


**Figure 48- Kernel architecture**

#### **4.5. Operating system**

The Zephyr customized operating system has been chosen for implementation on the satellite. This operating system has a rich development history and review by the renowned and experienced company, Wind River, the creator of the VxWorks operating system. By transferring it to the Linux Foundation and open-sourcing it, it is now recognized as one of the most prominent real-time operating systems available. Utilizing this operating system provides highly practical features such as memory management, thread management, interrupt management, and reliable communication solutions like I2C. The development language under this operating system is C. Moreover, this operating system conforms to the POSIX standard.

#### **4.6. Frame work**

The OS is the part of the OBC software that trades data with the hardware components. To use the application of the board a Frame Work is needed. For the current mission, F' is chosen.

F' (or F Prime) is a software framework for the rapid development and deployment of embedded systems and spaceflight applications. Originally developed at NASA's Jet Propulsion Laboratory, F' is open-source software that has been successfully deployed for several space applications. It has been used for but is not limited to, CubeSats, Small Satellites, instruments, and deployable.



F' has the following features:

- Component architecture with well-defined interfaces
- C++ framework providing core capabilities like queues, threads, and operating-system abstraction
- Tools for designing systems and automatically generating code from systems design
- A standard library of flight-worthy components
- Testing tools for unit and system-level testing

These key features make this framework easy to use and apply. In software In loop level of modeling the OBC F prime is tested via Qemu simulator and tested on the virtual environment provided by that and is ready to run on the actual board.

#### 4.7. Telecommand and Telemetry Management

The data framing for telecommand and telemetry data is fully aligned with CCSDS recommendations. Utilizing these proposals and standards will satisfy a wide range of space communication requirements and significantly enhance communication reliability and data management. All transmitted commands to the satellite will include a timing flag. This flag will be evaluated relative to both reception time and absolute (UTC) time standards. Besides the timing flag, commands will consist of two main sections.

The first section, Command-ID, will address the command's allocation, while the second section, Command Argument, will contain the necessary data for executing the command. In the telecommand section, all data will be stored and transmitted in timed packets. Telecommand packets may contain a single data sample or multiple samples. Each sample's data will begin with a unique timestamp, and after presenting the Primary Time (UTC), subsequent sample times within the packet will be relative. In storing telecommand data in satellite memory, each packet will be saved in a separate file named after the primary time tag, and file names will be kept in a queue. Management of the file queue will be accomplished using a combination of FILO (First In, Last Out) and FIFO (First In, First Out) methods, executable from the ground station.

The satellite software will include two applications: Telecommand Parser and Telemetry Manager. The Telecommand Parser program will interpret commands sent from the ground station, check for potential conflicts, ensure acknowledgment, and upon validation of performance in all preceding sections, generate one or more command messages for one or more onboard programs and place them on the Data Pipe. Conversely, the Telemetry Manager will be responsible for retrieving telecommand data from the Data Pipe, forming telecommand packets, writing files to memory, and ultimately preparing them for transmission to the ground station.

packet primary header							packet data field	
packet version number	packet ID			packet sequence control		packet data length	packet secondary header	user data field
	packet type	secondary header flag	application process ID	sequence flags	packet sequence count or packet name			
3 bits	1 bit	1 bit	11 bits	2 bits	14 bits	16 bits	variable	variable
2 octets				2 octets		2 octets	1 to 65536 octets	

**Figure 49- Telemetry & Telecommand framing based on CCSD standards**

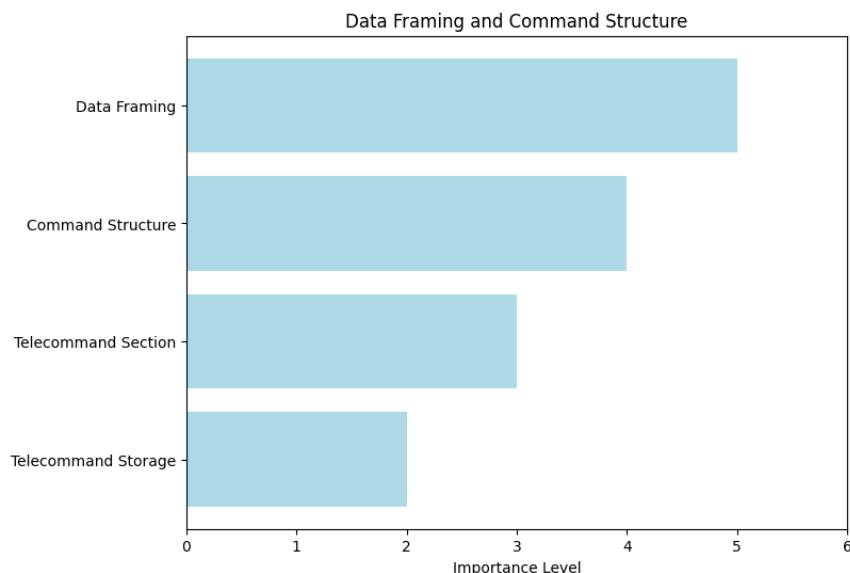


**Figure 50- Categorizing the importance level of each part**

Subsystem Management and Satellite Monitoring (Housekeeping) and User Interface Software Data Management will generally be divided into five types of general services:

- Execution Management Services
- Time Management Services
- Event Management Services
- Data Pipe Management Services
- Large Data Management Services (Tables)

Each subsystem software will consist of one or more of the specified services. Each software will be responsible for managing its own services. By utilizing the command structure, each program will retrieve its relevant commands from the Data Pipe and adjust its parameters accordingly. Additionally, each program will be obliged to form its own telecommand packet and place it onto the Data Pipe.



## 4.8. Memory Management

The File-System will be used for memory management. Despite having significant overhead, considering the advancement of storage components, this overhead can be overlooked. One of the microservices, Telemetry Manager, registers on memory. Given the relatively lengthy time for registering data on permanent memory, the Telemetry Manager program is obligated to form a memory mapping queue. The registering microservice is obliged to name files based on the Primary Time Tag. Consequently, the File System table will also be utilized as a reference for interpreting the queued files mapped onto memory.

## 4.9. Time and Event Management

Time management on the satellite is facilitated by the Time Manager program, which consists of a time management service. This program synchronizes the satellite's time periodically with the GNSS time signal, if available. In the absence of access to GNSS time, Time Manager will only update the time upon receiving a time packet from the telecommand Parser ground station command. Otherwise, it will publish the last synchronized time. Time on the satellite is maintained in UTC standard, not GPS Time. The time reference is the zero hour (equivalent to 00:00:00-01-01-2023 for the satellite, counted in seconds). Event detection and management vary depending on the programs. Hardware events detection is managed by the operating system, while software events are generated and managed within the programs. The transfer of events between computational threads is handled by the operating system.

## 4.10. Budget Estimation

### Processing Power

We mentioned predicting that a MIPS 200 processing power could be adequate for such a satellite mission. However, the presence of 320 DMIPS processing power in the proposed product leaves no doubt about its sufficiency and provides a considerable margin for this phase.

### Memory

It was stated that the product includes 12 Mbyte temporary data memory, 2 Mbyte permanent code memory, and 4 Mbit permanent data memory alongside up to 24 Gbyte flash memory. It's worth noting that for the current application, 1 Mbyte RAM for code memory and Mbyte data memory are sufficient, all of which are abundantly available in the current product.

### TT&C Data Communication

Two I2C communication buses are provided for exchanging telemetry data and commands among subsystems of the satellite. Additionally, besides the capability of collecting real-time Housekeeping data during communication, sufficient permanent memory on the OBC allows storing such data during the mission.



APSCO CubeSat Competition  
Conceptual and Preliminary Design Report – Ver. 1  
(IR-Sepehr)

### Communication with Sensors and ADCS Operators

The variety of serial interfaces introduced in the OBC allows for the effective management of all ADCS operators and sensors, including GPS, in addition to the subsystems connected via the CAN bus, without the need for intermediary management.

**Table 16- OBC Budgets for SPARCS-A, and B**

Parameter	Value	Comment
Power Supply	3.3V	Alongside with 400mW average power consumption.
Dimension	96 x 90 x 12.4 (mm <sup>3</sup> )	Including FM daughter board
Mass	100 g	94g mainboard only, 100g with EM daughter board
Cost estimation	15000\$-20000\$	By reviewing the prices of similar OBC boards and calculating the mean price based on the features each OBC had the cost was calculated as following: The cost of the first product sample, which is largely similar to the flight model in terms of hardware and software, along with a complete software package, is approximately \$15000. The flight model, along with a complete software package, costs around \$20000. With one OBC on each Cube the total cost will be around 30000\$.



## 5. Communication

The communication subsystem has been carefully designed to fulfill the specified criteria outlined in the mission and payload directives. Its paramount objective is to establish a dependable connection between each CubeSat and the ground station, while additionally facilitating Inter-Satellite Link (ISL) communication between the SPARCS-A and SPARCS-B satellites.

### 5.1. Requirements

- The communication system must be able to link the satellite to the ground station with minimum effort and link SPARCS-A and SPARCS-B in an ISL communication.
- The design must correspond to the parameters of the purchased boards.
- Different budget estimations (including mass, cost, and power) must be less than 15% of the total budget of the whole system.
- The designed boards must fit in the communication system and link perfectly with the purchased boards.
- The system must be able to transmit and receive more than the maximum data rate required in our system.
- For reliability purposes, the antennas must be able to transmit the required output power to ensure a safe margin. Also, each CubeSat must be able to communicate with the ground station to further increase the reliability of the system.

### 5.2. Communication Architecture

#### 5.2.1. Block Diagram

- **ISIS UHF Downlink / VHF Uplink Full Duplex Transceiver**

The cornerstone of the satellite's communication subsystem, this transceiver enables simultaneous receiving (uplink) and transmitting (downlink) capabilities, critical for ongoing communication with the ground station. For both the SPARCS-A and SPARCS-B satellites, this transceiver operates with:

- UHF downlink frequency: 435.020 MHz
- VHF uplink frequency: 145.900 MHz

The transceiver supports uplink bitrates of 1200 bps using AFSK modulation and downlink bitrates of 9600 bps using BPSK modulation, both utilizing the AX.25 protocol. This setup ensures robust communication links under the mission's operational parameters.

- **ISIS Deployable Antenna System**

An essential component for the transmission and reception of RF signals. Given the size constraints of SPARCS-A and SPARCS-B satellites, this system employs a compact and efficient deployable mechanism to maximize communication range and clarity. The antenna system is designed for automatic deployment once in orbit, enhancing the satellite's operational readiness and signal reach.

- **Frequency Down-Scaling System (For ISL)**

- This board, which must be designed and manufactured by us, will play an essential role in ISL communication. As each system is only capable of receiving the uplink frequency, this board will convert the downlink signal the uplink so that the same communication architecture applies to the ISL application.
- Two general techniques for this down-conversion are mixing and PLL's. The design is to be determined at the next phase.

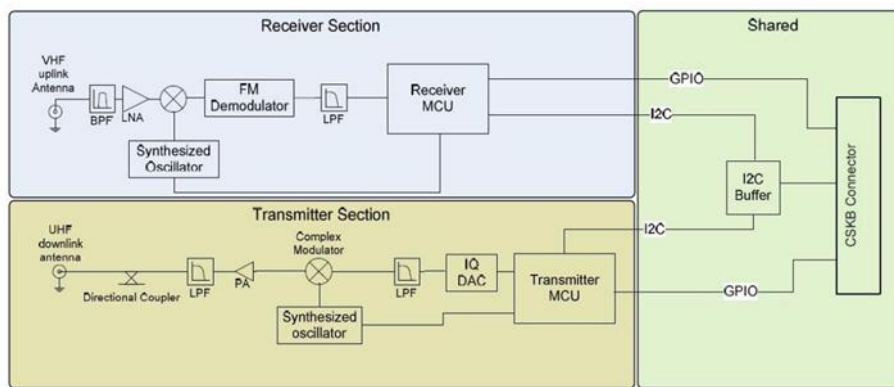


**Figure 51- Duplex Transceiver Block Diagram (source: PW-SAT)**

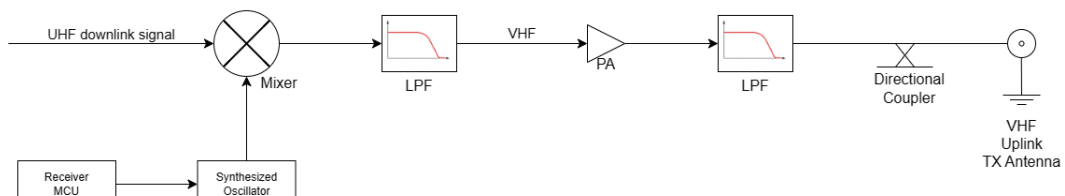


**Figure 52- Frequency Down-Scaling System**

### 5.3. Product Tree

#### 5.3.1. ISIS UHF downlink / VHF uplink Full Duplex Transceiver (1 in each CubeSat)



**Figure 53- ISIS VHF uplink/UHF downlink Full Duplex Transceiver**

- 
- |   |   |
|---|---|
| <ul style="list-style-type: none"> <li>• UHF Transmitter                     <ul style="list-style-type: none"> <li>○ RF Output Power: 500 mW</li> <li>○ Bitrate: 9600 bps</li> <li>○ Modulation: BPSK</li> </ul> </li> </ul> | <ul style="list-style-type: none"> <li>• VHF Receiver                     <ul style="list-style-type: none"> <li>○ Sensitivity: -98 dBm</li> <li>○ Bitrate: 1200 bps</li> <li>○ Modulation: AFSK</li> </ul> </li> </ul> |
|---|---|
- 

#### 5.3.2. ISIS Deployable Antenna System (1 in each CubeSat)

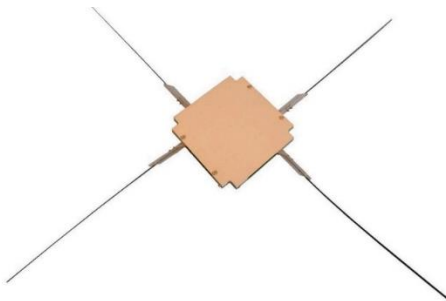


**Figure 54- ISIS Deployable Antenna System**

- Deployment Mechanism: Engineered to fit the compact dimensions of SPARCS-A and SPARCS-B satellites, this mechanism ensures reliable antenna deployment post-launch.
- Antenna Gain: 0 dBi, optimized for the satellite's operational needs.
- Interfaces: Dual Bus (I2C) for seamless control and telemetry data exchange, ensuring efficient subsystem integration and operation within the satellite's architecture.

#### 5.3.3. Frequency Down-Scaling System

- Electric Board Components including mixer and oscillators: Can vary according to design challenges (TBC)

### 5.4. Operating features and parameters

The communication subsystem of the satellite, centering around the ISIS UHF downlink / VHF uplink Full Duplex Transceiver and the ISIS Deployable Antenna System, operates under specific parameters

designed to ensure optimal performance and reliable communication between the satellite and the ground station. This analysis covers the general operating parameters, including frequencies, antenna types, estimated location of the antennas, and their general radiation pattern.

#### **5.4.1. Operating Frequencies**

- Uplink Frequency (VHF Band): 145.900 MHz. This frequency is primarily used for commands sent from the ground station to the SPARCS-A, and B. It will also be used for ISL.
- Downlink Frequency (UHF Band): 435.020 MHz. This frequency is utilized for the SPARCS-A, and B to send back telemetry and mission data to the ground station.

#### **5.4.2. Antenna Types and Configuration**

- VHF Antenna for Uplink: Efficiently operates at the VHF uplink frequency, ensuring high clarity in receiving commands from the ground station.
- UHF Antenna for Downlink: Optimized for the UHF downlink frequency, this antenna is crucial for transmitting data back to Earth.

#### **5.4.3. Antenna Deployment and Placement**

- The antennas are deployable, designed to stow compactly during launch and deploy once in orbit. This feature maximizes the effective use of space and signal strength.
- Placement: Antennas are strategically placed on the SPARCS-A, and B with deployable booms to ensure minimal interference and optimal function. We used our previous experience and use the following placement strategy:

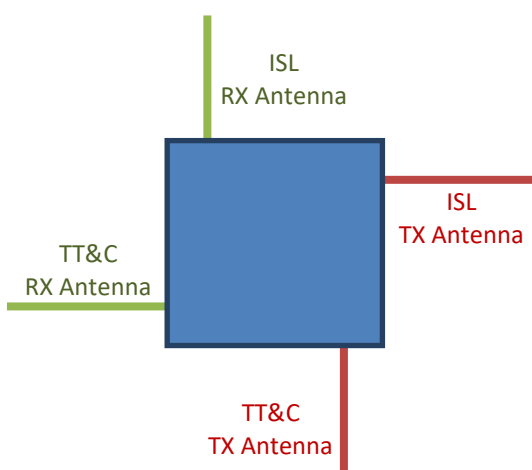


**Figure 55- Antenna System's Placing**

#### **5.4.4. Inter-Satellite Link (ISL) Configuration**

- ISL Functionality: Our system establishes a dedicated link between the SPARCS-A, and B to share data and coordinate operations while in orbit. The trick is to work in uplink frequency so that the same components do the job.

- Technologies Considered: The overall technology in this part is a Phase Locked Loop and a mixer. According to design challenges, we might need some filters and encoders.

#### 5.4.5. Radiation Patterns

- The radiation patterns are designed to be generally omnidirectional, ensuring broad coverage which is critical for maintaining communication irrespective of the satellites' orientations relative to each other and the ground station.
- Simulation Results: It is obvious that the overall architecture of the CubeSat only influences the near-field of the antenna system's pattern.

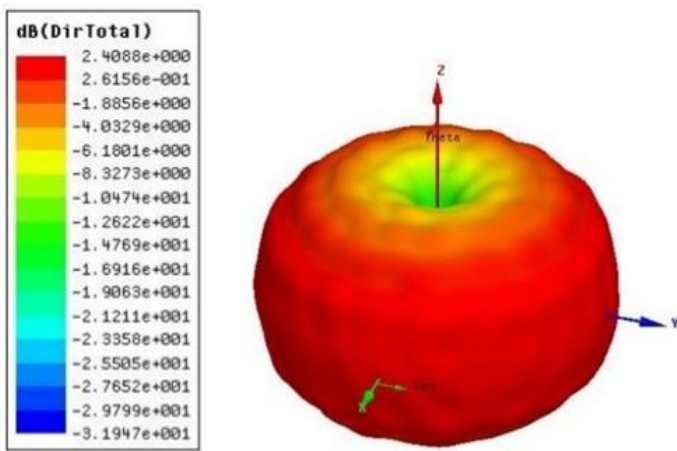


**Figure 56- General Antenna Pattern (source: PW-SAT)**

As we know, both ISL and downlink communication are in the km-order distance. So, it is a fair deduction that the far-field of a similar system gives us enough information to analyze the overall capability of the antenna system to transmit data.

#### 5.4.6. Communication Protocols and Data Handling

- Modulation Techniques: BPSK for downlink and AFSK for uplink to optimize clarity and minimize interference.
- Data Link Layer Protocol: AX.25, facilitating error checking and frame management.

### 5.5. Link budget

The link budget calculation is an essential aspect of the communication subsystem design, providing a comprehensive analysis of the satellite's ability to maintain a reliable communication link with the ground station. This calculation takes into account various factors including modulation type, bitrate, coding, transmitter power, receiver sensitivity, and the antennas' characteristics. Here, we present a detailed link budget analysis for both the uplink (from the ground station to the satellite) and the downlink (from the satellite to the ground station).



### 5.5.1. Modulation Type and Bitrate

- Uplink: The modulation type for the uplink is AFSK (Audio Frequency Shift Keying) with a bitrate of 1200 bps. AFSK is chosen for its simplicity and robustness in the VHF frequency band.
- Downlink: For the downlink, BPSK (Binary Phase Shift Keying) modulation is utilized, offering a higher bitrate of 9600 bps. BPSK is selected for its efficiency and ability to maintain signal integrity over long distances.

### 5.5.2. Coding

- AX.25 Protocol: Both the uplink and downlink utilize the AX.25 protocol, a data link layer protocol derived from the X.25 protocol suite and adapted for amateur radio use. It is particularly well-suited for error detection and correction, which is critical for reliable satellite communication.

### 5.5.3. Link Budget Calculation for Uplink

- Transmit Power (PTx): 50 dBm (100 W), as typically used by ground stations for satellite communication.
- Transmitter Antenna Gain (GTx): 14.8 dBi, achieved using directional Yagi antennas.
- Path Loss (Lpath): Calculated based on the free-space path loss formula, considering the frequency of 145.900 MHz and the maximum satellite-ground distance.
- Receiver Antenna Gain (GRx): 0 dBi, assuming an omnidirectional antenna pattern for the satellite's VHF uplink antenna.
- Receiver Sensitivity (PRx): -98 dBm, indicating the minimum signal strength at which the satellite's receiver can reliably decode signals.

The link margin is calculated by considering the gains and losses in the signal path, including atmospheric losses and polarization mismatch. A positive link margin indicates a reliable communication link under nominal conditions.

### 5.5.4. Link Budget Calculation for Downlink

- Transmit Power (PTx): 27 dBm (500 mW), as provided by the ISIS UHF downlink / VHF uplink Full Duplex Transceiver.
- Transmitter Antenna Gain (GTx): 0 dBi, considering the omnidirectional radiation pattern of the deployable UHF antenna.
- Path Loss (Lpath): Computed based on the free-space path loss formula, given the frequency of 435.020 MHz and the typical satellite-ground distance.
- Receiver Antenna Gain (GRx): 14.8 dBi, achieved using directional Yagi antennas at the ground station.
- Receiver Sensitivity (PRx): Based on the ground station receiver's capabilities, typically around -126 dBm for SSB receivers in the UHF band.



Again, the link margin is assessed by aggregating all gains and subtracting losses, ensuring that the signal received at the ground station exceeds the receiver's sensitivity threshold.

## 5.6. Budget estimation

The mass, dimension, power, and cost estimations for the satellite communication subsystem, comprising the ISIS UHF downlink / VHF uplink Full Duplex Transceiver and the ISIS Deployable Antenna System, are crucial for ensuring the subsystem aligns with the satellite's overall design parameters and mission budget. These estimations facilitate the integration process, ensuring the subsystem does not exceed the satellite's mass, volume, power, and cost constraints. Here, we detail these estimations based on the subsystem's components.

### 5.6.1. Mass and Dimension Estimation

- **ISIS UHF downlink / VHF uplink Full Duplex Transceiver**
  - Mass: The transceiver unit typically weighs around 0.12 kg. This includes the weight of the printed circuit board (PCB), components, and housing.
  - Dimensions: The standard dimensions for the transceiver are approximately 96 mm x 90 mm x 12 mm. This compact size ensures that the transceiver can be easily accommodated within the limited space available in most CubeSat structures, adhering to the CubeSat Design Specification (CDS).
- **ISIS Deployable Antenna System**
  - Mass: The deployable antenna system, including the mechanism and antennas, weighs about 0.15 kg. This mass includes all components necessary for deployment and stable operation in orbit.
  - Dimensions: When stowed, the antenna system's dimensions are designed to fit within a small volume on the satellite's exterior, typically not exceeding a few cubic centimeters. Deployed, the antennas extend several tens of centimeters from the satellite body to ensure effective signal transmission and reception.

### 5.6.2. Power Estimation

- **Operational Power Consumption**
  - Receiving Mode: When operating in receiving mode, the transceiver's power consumption is typically around 0.6 W. This mode is active when the satellite is listening for commands from the ground station.
  - Transmitting Mode: In transmitting mode, when the satellite is sending data to the ground station or the other CubeSat, the power consumption increases to approximately 6 W, due to the higher energy required for signal transmission over long distances.
- **Power Budgeting**

The satellite's power system must account for these consumption rates, ensuring that sufficient energy is available for the communication subsystem's operation alongside other satellite functions.



APSCO CubeSat Competition  
Conceptual and Preliminary Design Report – Ver. 1  
(IR-Sepehr)

This is typically achieved through a combination of solar panels and rechargeable batteries, designed to meet the satellite's total power demand.

### 5.6.3. Cost Estimation

- **Subsystem Cost**
  - ISIS UHF downlink / VHF uplink Full Duplex Transceiver: The cost of the transceiver is a significant portion of the communication subsystem's budget. Prices for such transceivers typically range from \$3,000 to \$5,000, depending on the specific model and the volume of purchase.
  - ISIS Deployable Antenna System: The deployable antenna system, another critical component, usually costs between \$2,000 and \$4,000. This price includes the deployment mechanism and the antennas themselves.
  - Frequency Down-Scaling System: The estimated budget for designing and manufacturing of this board is around \$500.
- **Overall Subsystem Cost**
  - Combining the costs of the transceiver and the deployable antenna system, the total estimated cost for the communication subsystem ranges from \$6,000 to \$10,000. This estimation considers the procurement of individual components at retail prices; volume discounts or institutional partnerships may significantly reduce these costs.

## 5.7. Subsystem Summary

A comprehensive overview of the whole subsystem can be found in the following tables:

**Table 17- Communication Links**

ISIS UHF Parameters (Downlink)		
Parameter/Link	Comment	Value
RF Output Power		500 mW (27 dBm)
Bitrate		9600 bps (max)
Modulation		BPSK
Link Layer Protocol		AX.25

ISIS VHF Parameters (Uplink + ISL)		
Parameter/Link	Comment	Value
Sensitivity		-98 dBm (@BER = 1e-5)
Data Rate		1200 bit/s
Modulation		AFSK
Link Layer Protocol		AX.25
Frequency Deviation		3.5 kHz
Transmitter Antenna Gain	Omnidirectional.	0 dBi
Receiver Antenna Gain		14.8 dBi

**Table 18- Power Parameters and Budget**

Parameter/Link	Comment	Value
----------------	---------	-------



APSCO CubeSat Competition  
Conceptual and Preliminary Design Report – Ver. 1  
(IR-Sepehr)

Power consumption (While transmitting and receiving with $V_{sup} = 8V$ , including a 25% margin for ISL board)	Less than 15% of the total satellite system's budget.	Max. 6000 mW
Power consumption (While receiving with $V_{sup} = 8V$ , including a 25% margin for ISL board)	Less than 15% of the total satellite system's budget.	Max. 600 mW
Supply Voltage	6-20 VDC	

**Table 19- Physical Parameters and Budget**

Mass	Less than 15% of the total satellite system's budget.	Transceiver: 0.12 kg ISL Board: TBD Antenna System: 0.15 kg
Size	Less than 15% of the total satellite system's budget.	Transceiver: 96 mm × 90 mm× 12 mm ISL Board: TBD Antenna System: Varying - Outside

**Table 20- Cost Estimation**

Component	Cost
Transceiver	\$3,000 to \$5,000
ISL Board	TBD (estimated around \$500)
Antenna System	\$2,000 to \$4,000
Total	\$5,500 to \$9,500 (Less than 15% of the total satellite system's budget.)



## 6. ADCS

In this chapter, we aim to investigate and design an appropriate configuration for the ADCS subsystem for SPARCS-A and B, this design procedure includes sizing the required actuators and sensors, as well as presenting the physical architecture of the ADCS. Finally, an estimation of mass, dimensions, required electrical power, and cost budgets are provided.

### 6.1. Requirements

The starting point of the configuration selection and designing the system, as well as each of its subsystems, is to consider the mission objectives and meet the design requirements. The design requirements for the ADCS subsystem include:

- The ADCS shall autonomously detumble SPARCS-A and SPARCS-B within fewer than 5 orbits after deployment into orbit
- The ADCS shall be designed to be as simple, compact, and lightweight as possible
- The ADCS shall exhibit low power consumption, particularly for SPARCS-B
- To the extent possible, COTS components shall be used in the design of the ADCS
- SPARCS-A and SPARCS-B shall maintain a pointing error of less than 10 degrees
- To optimize the size of the ADCS within SPARCS-A, compact magnetorquers integrated with solar panels and sun sensors shall be considered
- The ADCS subsystem of SPARCS-B shall be capable of detumbling upon deployment and activation of the tether
- The dimensions, mass, and cost allocations for the ADCS in both SPARCS-A and SPARCS-B shall not exceed 15% of the total budget
- The ADCS reliability in SPARCS-B shall be better than 0.7

### 6.2. Configuration Selection

To select the overall configuration of the ADCS subsystem, we first need to choose suitable configurations of sensors and actuators, which are the main components of the ADCS. We will use existing CubeSats datasets, our policy for utilizing algorithms, and the provided requirements for our selection. Figure 57 illustrates our feasible options for selecting a suitable configuration of sensors and actuators based on frequentist statistical data of existing CubeSats.

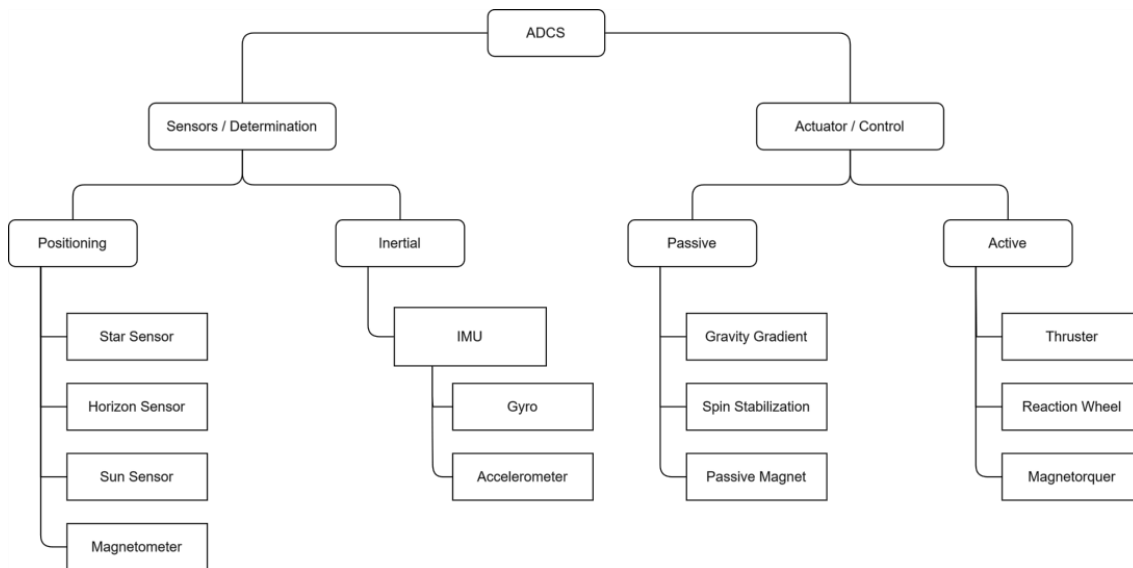


**Figure 57- Feasible ADCS System options**

**Actuator/Control Configuration Selection:** Considering the requirements, the reaction wheel is not suitable for SPARCS mission because it occupies too much space and is not suitable in terms of cost, mass, and power budget. Moreover, for the <10deg pointing error, a three-axis magnetorquer is suitable, and there is no need for a reaction wheel. The thruster is also eliminated for the same reasons and is not a suitable actuator. Therefore, the only suitable active actuator for the SPARCS mission is magnetorquer.

For SPARCS-B, after separating the end body from the main body an additional stabilizing moment is also exerted on the CubeSat through gravity gradient, though the moment is very small. Since SPARCS-B pointing requirements are also very similar to the SPARCS-A, we chose a similar strategy with magnetorquers for SPARCS-B, as well.

**Sensor Configuration Selection:** Considering the requirement for minimal pointing error, cost-effectiveness, and low power consumption and dimensions for the ADCS subsystem, the star sensor is deemed unsuitable for the SPARCS mission due to its high cost, power consumption, and dimensions. Similarly, the Horizon sensor also exhibits high power consumption, cost, and dimensions, making it unsuitable for our requirements.

We have decided to use B-Dot controllers for detumbling and LQR controllers (TBC) for modes requiring precise pointing. These controllers are among the most commonly used for CubeSats based on frequentist statistical data.

In detumbling mode, the magnetometer is used to get information about the CubeSat's rotation. B-Dot algorithm refers to the change of the Earth's magnetic field as a source of information about a satellite's rotation. Indication from the onboard magnetometers is used to track the rotation vector magnitude in the detumbling mode and the gyroscope data will be used to assess and verify the detumbling algorithm performance. When the overall magnitude of the angular rate vector drops below a defined threshold(1 deg/s - TBC), the detumbling mode is turned off. Therefore, for

implementing the B-Dot algorithm, we require a three-axis magnetometer and a triaxial Gyro. Given the very small dimensions of modern MEMS IMUs, we prefer to use this type of sensor instead of gyroscopes alone so that we can also measure rotational accelerations. However, for our mission's sizing requirements, using a gyroscope alone is sufficient.

Therefore, to implement the LQR algorithm for pointing, we need to have the attitude of the SPARCS CubeSats at each moment in time. Determining the attitude requires at least two orthogonal vectors. One of these vectors is considered the magnetic field vector, obtained through the three-axis magnetometer. Given the remaining feasible sensor options, choosing the sun sensor is appropriate, which allows us to use the sun vector as the second vector for state determination.

The figure below illustrates the selected sensors and actuators among the feasible options.

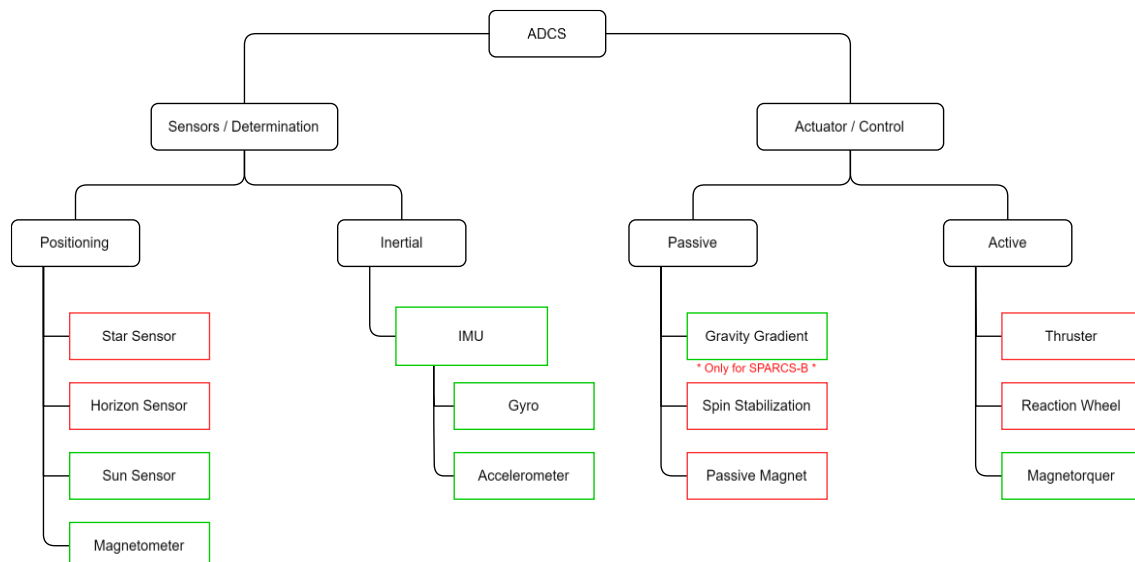


**Figure 58- selected configuration for sensors and actuators**

Given the selected sensors, the optimized TRIAD algorithm can be used to determine and estimate the initial attitude of both CubeSats, followed by attitude propagation and estimation using the Extended Kalman Filter (EKF). The reason for choosing this algorithm over other methods is its higher reliability in providing attitude data within a short period of time and its low computational complexity. Moreover, by combining TRIAD with the developed Kalman filter, the multi-sensor update feature will also be utilized. Thus, the TRIAD algorithm will serve as the algorithm providing initial conditions for the Kalman filter.

Considering the use of the TRIAD algorithm for attitude determination, we require the precise position of the CubeSats in space over time. Therefore, it's necessary to consider a GNSS module for each CubeSat.

Therefore, the configuration of the ADCS subsystem has been specified. The diagram below illustrates the configuration of SPARCS-A and SPARCS-B. It's worth mentioning that, due to constraints related to component placement on panels, for now, we have considered a total of 4 sun

sensors for the side panels of each CubeSat. In subsequent phases, if feasible, we can increase the number of these sensors to 6.

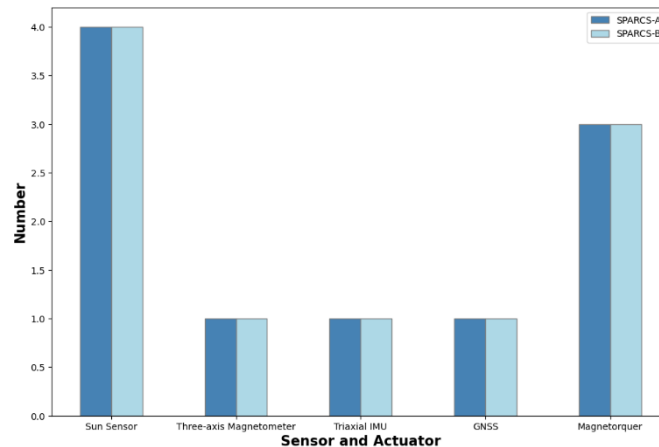


**Figure 59- ADCS Overall Configuration of SPARCS-A and SPARCS-B**

### 6.3. Component Sizing

Based on the overall configuration of the ADCS, the mission concept, and requirements, we are conducting the sizing of components for this subsystem. Next, we will begin with sizing the components for SPARCS-B followed by SPARCS-A.

#### 6.3.1. Component Sizing for SPARCS-B

- **Magnetometer and Magnetorquer**

The MTQ Integrated ADCS from Tensor Tech company is being utilized. The board comprises 2 rods and 1 air core. It includes temperature sensors and a magnetometer, along with a control module that applies PWM signals to the coils. These components are fabricated on a single PCB and support the I2C bus. This board has space heritage and is at TRL 9, making it a highly reliable option. Moreover, multiple components have been integrated onto a single board, minimizing space requirements and meeting mission requirements in terms of power consumption, cost, and mass.

**Table 21- ADCS-MTQ module Specifications**

Parameter	Value
Magnetic dipole moment	< 0.2 Am <sup>2</sup> for 2-axis and < 0.1 Am <sup>2</sup> for 1-axis
pointing accuracy	< 10deg
Power consumption	< 1W(@ 3.3V and 5V bus)
Interface	I2C
mass	140g
volume	0.2U
Operational temperature range	-40°C to 70°C

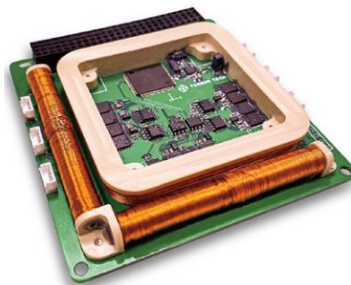


**Figure 60- ADCS-MTQ module**

- **Sun Sensor**

The FSS-15 digital Sun sensor from Tensor Tech company is being utilized. FSS-15 is a minimized fine sun sensor that features a microcontroller to produce a pre-calibrated error table for a tabulated correction, which enables it to achieve a higher precision. This sun sensor, alongside the MTQ module, provides excellent capabilities and ensures pointing accuracy <10deg for SPARCS-B. With space heritage and TRL 8, this sensor guarantees reliability.

Key features of FSS-15 sun sensor:

- Digital-type Fine Sun Sensor
- Embedded firmware for radiation-caused transient error detection and recovery
- 2-axes digital sun sensor embedded with calibration error table and micro-controller



**Figure 61- FSS-15 Sun Sensor**

The table below shows the overall specification of FSS-15.

**Table 22- FSS-15 Sun Sensor Specifications**

<b>Parameter</b>	<b>Value</b>
field of view	±60 deg (±45 deg for optimal performances)
field of view accuracy	±0.1 deg within ±45 deg FOV (1-sigma) ±0.5 deg within ±60 deg FOV (1-sigma)
power consumption	< 2 mA (sampling) < 0.5 mA (idle)
sample frequency	2 Hz/4 Hz/8 Hz/16 Hz
data interface	I2C
mass	<4g

- **GPS receiver**

The PiNAV-NG GPS receiver board from SkyFox Labs is being utilized. The primary reason for selecting this board is its significantly low power consumption compared to other GPS receivers, allowing it to meet mission power consumption requirements. Key features of this board include:

- Ultra Low Power Consumption: Consumes only 10% of the power compared to conventional space-grade GPS receivers.
- Continuous Accurate Position Determination
- Ultra-Low Mass and Dimensions
- Easy-to-Use Serial Data Interface: Outputs standardized NMEA sentences via a serial data interface, making it compatible with various space-grade projects requiring precise position, time, date, and velocity information.
- Housekeeping Measurements
- Engineering Models (EM) Available



**Figure 62- piNAV-NG GPS Receiver**

Table below shows the overall specification of piNAV-NG Receiver.

**Table 23- piNAV-NG GPS Receiver Specifications**

<b>Parameter</b>	<b>Value</b>
Operating Power Consumption with Passive GPS Antenna	125mW
Operating Power Consumption with Active GPS Antenna	324mW 540mW
Valid Position Pulse Accuracy ( $2\sigma$ )	100ns
Horizontal Position Accuracy ( $2\sigma$ )	10m
Operating Velocity	Up to 9km/s(Flight model) up to 0.5 km/s (Engineering model)
power supply Voltage	2.7 to 3.6V
Position update rate	1Hz
Protocols	NMEA 0183 (standard GPS sentences) piNAV (NMEA sentences extension)
temperature range	-40°C to +85°C
mass	24g

- **GNSS Patch Antenna**

The GNSS Active Patch Antenna from ISIS company is being utilized. The GNSS Patch Antenna is a compact, low-mass active antenna.

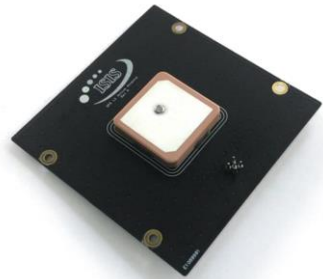


**Figure 63- ISIS GNSS Active Patch Antenna**

Table below shows the overall specification of ISIS GNSS Active Patch Antenna (GAPA).

**Table 24- ISIS GAPA Specifications**

Parameter	Value
Frequency Range	1572 – 1578MHz
Signal gain (active circuitry)	34.5dB
Antenna peak gain	5.2dBi (1575 MHz)
Axial ratio	< 3dB
Return Loss	> 15dB
Bandwidth	6 MHz
Supply voltage	3 – 5V
Current consumption	< 10 mA
Mass	18g

- Micro-controller

We will implement the ADCS algorithm in the OBC MCU and will not consider a dedicated MCU for the ADCS, and we will not consider a separate board for it. The attitude of the spacecraft is determined with the help of certain attitude sensors and this attitude information is sent to the ADCS algorithm with the current and target attitude. The ADCS algorithm then sends torque commands to actuate compact magnetorquers after calculations of desired torque for desired attitude attainment. The new attitude is fed back to the ADCS algorithm and the loop continues.

- IMU

When choosing an IMU, key factors include noise, bias instability, and temperature sensitivity. ADXRS453 MEMS IMU from Analog Devices company appears to be a highly suitable option for us, considering these factors. ADIS16470 is a miniature MEMS IMU that includes a triaxial gyroscope and a triaxial accelerometer. Considering the small dimensions of this IMU, we plan to integrate it onto the OBC daughterboard (TBC). Additionally, besides this IMU, we may also consider using a MEMS gyro provided by the manufacturer (ISIS) for the OBC motherboard, but for now, we are selecting this IMU.



**Figure 64- ADIS16470 IMU**

Table below shows the specifications of the digital ADIS16470 IMU.

**Table 25- ADIS16470 IMU Specifications**

<b>Parameter</b>	<b>Value</b>
Measurement range	$\pm 2000^\circ/\text{sec}$
	$\pm 40 \text{ g}$
Noise density	$0.008^\circ/\text{sec}/\text{VHz}$
Supply voltage	3.0 V to 3.6 V
Power Supply Current	42mA @ 3.3V
Operating temperature range	-25°C to +85°C
Dimensions	1.1 cm x 1.5 cm x 1.1 cm
Mass	<10g

### 6.3.2. Component Sizing for SPARCS-A

All ADCS components in SPARCS-A have been selected similarly to SPARCS-B, except for the magnetorquers and magnetometers. Next, we will proceed with sizing these two components for SPARCS-A.

- Magnetorquer

Based on mission requirements, we are using compact magnetorquers as actuators in SPARCS-A. Compact magnetorquers have the following key features:

- Compact magnetorquers occupy less volume than rod magnetorquers, allowing us to utilize the empty space behind panels and allocate the internal space of the CubeSat to other subsystems
- Considering their shape and dimensions, compact magnetorquers can be integrated with sun sensors, magnetometers, and solar cells on a panel, reducing the utilized space
- The torque generated by compact magnetorquers can be increased by either increasing the number of turns in their coils or increasing the number of coils for control in each axis. However, this increase in the number of turns or coils, while boosting the generated torque, also leads to higher power consumption. Therefore, for sizing a compromise must be made between the generated torque and power consumption
- Compact magnetorquers have a suitable power consumption compared to rod magnetorquers, especially for a 1U CubeSat, due to their small size

Considering the requirement for minimal power consumption, we use three Compact Magnetorquers for three-axis control, adjusting only the dimensions and number of turns for each coil. In this design phase, we use statistical data for sizing compact magnetorquers to meet the requirement for pointing error of <10deg and also to adhere to budget requirements. We further utilize detailed design data from the COMPASS-1<sup>1</sup> CubeSat mission for sizing the compact magnetorquers. In COMPASS-1, compact magnetorquers with the dimensions shown in Figure 65 are used to achieve a pointing error of <8deg for a 1U CubeSat. Considering the differences in configuration and algorithms between SPARCS-A and COMPASS-1, using these dimensions for SPARCS-A is appropriate. The accuracy of these dimensions will be confirmed in the detailed design phase, and if necessary, these Dimensions will be adjusted considering constraints and requirements.

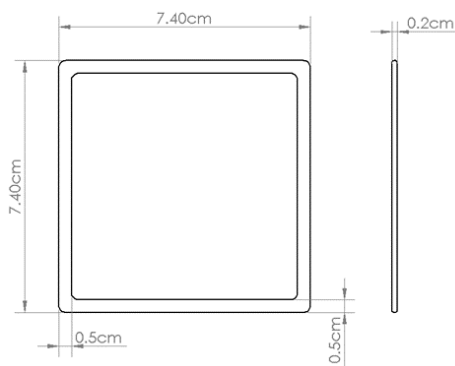


**Figure 65- Compact Magnetorquer Dimensions**

For estimating mass budget and power consumption, we also rely on data from COMPASS-1. Additionally, based on statistical data and considering a factor of 3 for product development, we estimate the cost of each compact magnetorquer to be 1500 USD for flight model. Table 26 presents the specifications of the designed compact magnetorquer, and Figure 66 illustrates the placement of compact magnetorquers in SPARCS-A.

**Table 26- Compact magnetorquer Specifications**

Parameter	Value
Maximum Power Consumption	0.25W(TBC)
Maximum Coil Voltage	4.8V(TBC)
Mass	20g(TBC)
Dimension	7.4cm×7.4cm×0.2cm(TBC)
Cost	1500USD(TBC)

<sup>1</sup> <https://www.raumfahrt.fh-aachen.de/compass-1/home.htm>

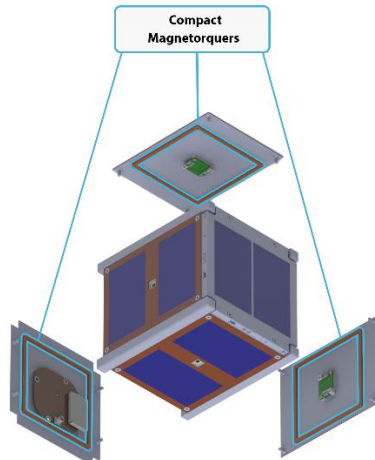


**Figure 66- Compact Magnetorquers in SPARCS-A**

- Magnetometer

We select the HMR2300 magnetometer from Honeywell company. The HMR2300 is a high-precision digital magnetometer with a suitable measurement range. Additionally, this magnetometer has power consumption, mass, and dimensions that meet the requirements. The HMR2300, along with a dosimeter and a GNSS receiver board, will be integrated onto a single board.



**Figure 67- HMR2300 Smart Digital Magnetometer**

Table below shows the overall specification of HMR2300 Smart Digital Magnetometer.

**Table 27- HMR2300 Smart Digital Magnetometer Specifications**

Parameter	Value
Measuring Range	$\pm 2\text{Gauss}$
Resolution	$67\mu\text{Gauss}$
Data Interface	RS-232/RS458
Supply Voltage	6.5 - 15V
Supply Current(@15V)	30mA
mass	28g

#### 6.4. Operational Modes

In both CubeSats, we have considered the following operational modes for the ADCS subsystem:

**Detumbling Mode:** This mode activates after first turn-on of the power supply and initial attitude determination in the initial phase of the mission (LEOP). In the subsequent phases of the mission,

Autonomous transition to this mode has to be done after exceeding predetermined threshold of the angular velocity vector's magnitude. We consider this critical value to be equal to 10 deg/s(TBC). Detumbling mode requires magnetometer and at least two actuators working properly.

**Normal Mode (Nadir Pointing - idle):** After detumbling the controller is going to be switched into the normal mode. This mode is selected as the “Park mode” or “default mode”, and transitions from this mode to other modes are executed. Here the complete ADCS will try to keep the satellite fixed onto nadir pointing. In this mode, only limited power will be consumed. The generated torques will be small compared to the detumbling torques since the motion/attitude of the spacecraft will not be altered significantly. The ADCS will only actively compensate disturbance torques. Communication with the ground station will be established in this mode. Therefore, pointing in this mode will be performed with less precision compared to the control mode, as we use an omni-directional antenna and simply aim to point the antenna reasonably well towards the ground for communication with the ground station.

**Control Mode (Mission):** control mode will be active during the payload experimental tests(ISL and EDT). According to the orientation requirements for conducting tests on these two payloads, both CubeSats must actively orient in a specific direction to complete the test. Additionally, during tether deployment, ADCS must also actively operate to ensure safe and proper deployment. In this mode, ADCS is mostly active, consuming more power, but the duration will be shorter compared to the normal mode. Transition to and exit from this mode will be carried out via commands from the ground station or autonomously (scheduled). In this mode, all necessary sensors and actuators will be activated.

Additionally, in critical situations (such as low power), the ADCS enters a systemic safe mode as per the OBC command. In the safe mode, the actuator is deactivated and possibly the controller set into a low power consumption mode. Figure 68 illustrates the operational modes of the ADCS subsystem along with the transitions between these modes and the system safe mode.

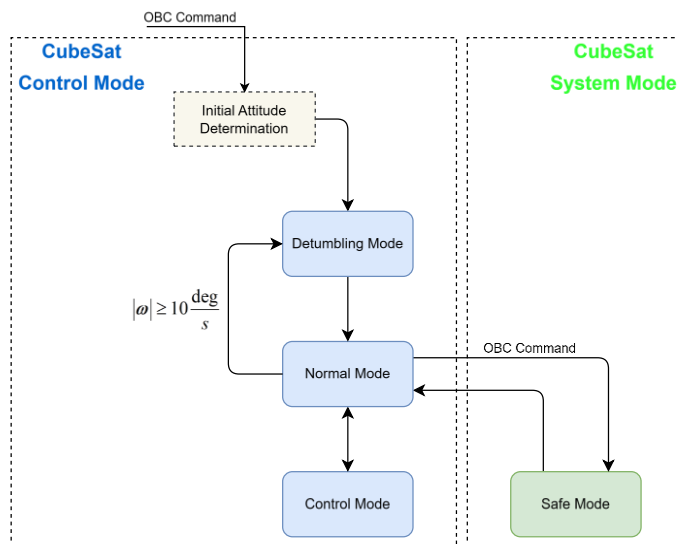


**Figure 68- ADCS Operational Modes**

## 6.5. Architecture

The following figures illustrate the physical architecture diagrams of the ADCS for SPARCS-A and SPARCS-B, respectively.

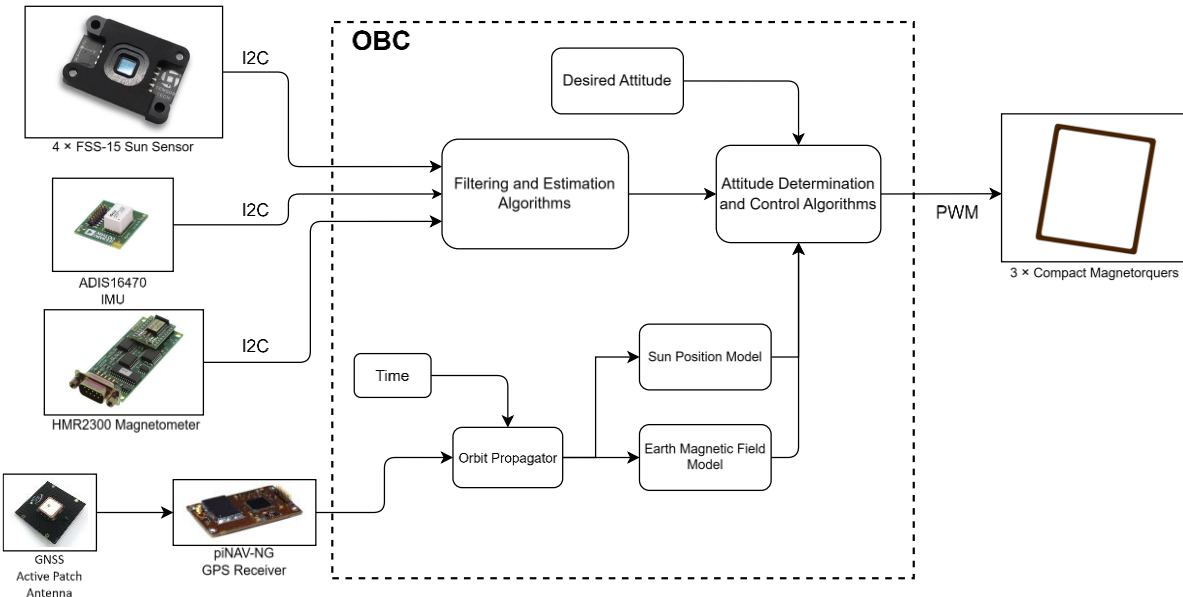


**Figure 69- Physical Architecture of SPARCS-A**

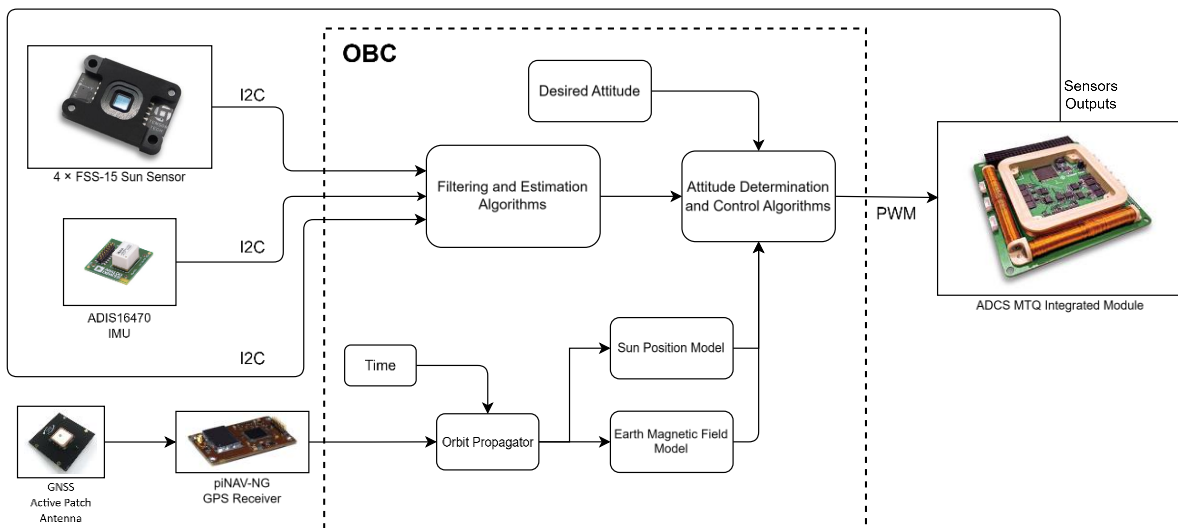


**Figure 70- Physical Architecture of SPARCS-B**



APSCO CubeSat Competition  
Conceptual and Preliminary Design Report – Ver. 1  
(IR-Sepehr)

## 6.6. Budget Estimation

**Table 28- ADCS Budgets for SPARCS-A**

Component	Product ID	Num.	Mass (g)	Dimensions (cm)	Power		Operating Temperature	Cost (USD)
					Nominal (W)	Duty Cycle (%)		
Compact Magnetorquer	-	3	20 (TBC)	7.4×7.4×0.2 (TBC)	0.25 (TBC)	50	-50°C to +100°C (TBC)	1500 (TBC)
Magnetometer	HMR2300	1	28	7.49×3.05×1.3	0.45	50	-40°C to +85°C	1670
Sun Sensor	FSS-15	4	4	2.2×1.5×0.526	0.01	50	-40°C to +85°C	1800
IMU	ADIS16470	1	10	1.1×1.5×1.1	0.14	50	-25°C to +85°C	250
GPS Receiver	PiNAV-NG	1	24	7.11×4.57×1.1	0.125	50	-40°C to +85°C	700
GNSS Active Patch Antenna	GAPA	1	20	2.5×2.5×0.97	0.05 (TBC)	50	-30°C to +70°C	300

**Table 29- ADCS Budgets for SPARCS-B**

Component	Product ID	Num.	Mass (g)	Dimensions (cm)	Power		Operating Temperature	Cost (USD)
					Nominal (W)	Duty Cycle(%)		
Integrated ADCS Module	MTQ-ADCS	1	140	10 × 10 × 1.351	1	50	-40°C to +70°C	6900
Sun Sensor	FSS-15	4	4	2.2 × 1.5 × 0.526	0.01	50	-40°C to +85°C	1800
IMU	ADIS16470	1	10	1.1 × 1.5 × 1.1	0.14	50	-25°C to +85°C	250
GPS Receiver	PiNAV-NG	1	24	7.11 × 4.57 × 1.1	0.125	50	-40°C to +85°C	700
GNSS Active Patch Antenna	GAPA	1	20	2.5 × 2.5 × 0.97	0.05 (TBC)	50	-30°C to +70°C	300



## 7. Power

The electrical power subsystem (EPS) plays a crucial role in the success of any CubeSat mission by providing the necessary power and specific voltage to all onboard systems. It ensures seamless operation in the varying environmental conditions encountered in space. Without a suitable power supply, the craft would be unable to function. The EPS must efficiently generate, store, and distribute power to support the payload and meet the mission requirements. However, the limited size and resources of CubeSats present significant challenges in designing the electrical power subsystem. In addition to being reliable, the system must also be cost-effective. To address these requirements, the use of COTS (commercial-off-the-shelf) components with a high specific power to mass ratio and redundancy of critical sub-circuits is proposed. This report aims to provide insights into our strategic approach to developing a robust and resilient power infrastructure as we navigate the complexities of conceptualizing and designing CubeSats.

The design objectives of the power system include providing sufficient power to the electrical subsystem, minimizing power drain from the batteries, ensuring efficient recharging of the batteries, and minimizing weight and volume.

Also, the health of the satellite needs to be checked regularly to make sure that there are no major problems in any sub-system during its operations in orbit. Collecting routine information from various sub-systems and sensors is also a core function of the EPS. This involves measuring various important voltages, currents, and temperatures which are called the “Housekeeping Parameters”. These are communicated back to the ground as a part of the telemetry of the satellite for operators to keep track of the overall health of their system and guard against potential faults or poor performance. The high levels of radiation in space can cause a “single event latch-up” in the semiconductor devices on the satellite. This can damage some of the components on the satellite if the power is not turned off quickly enough, so the EPS is also required to protect the satellite and its sub-systems against over-currents.

### 7.1. Requirements

There are certain electrical requirements that are recommended for the standard CubeSat form factor which EPSSs should adhere to. Component selection, the operation and other subsystem's requirements that are not mentioned in the text are exclusively listed below.

- The satellite's interior must accommodate sufficient space for both battery packs and EPS boards.



- The EPS shall operate independently from any other subsystem. Other subsystems shall not be able to make any changes to the behavior of the EPS. Excluded from these requirements the housekeeping data interface and direct Ground Command.
- No electronics may be active during launch to prevent any electrical or RF interference with the launch vehicle and primary payloads. CubeSats with rechargeable batteries must be fully deactivated during launch or launch with discharged batteries.
- Solar cells that are connected with inverted polarity, shall not interfere with the functionality of the rest of the EPS.
- The ability to remotely monitor and control power distribution and power switches via Telecommand should be available.
- To keep track of the status of the EPS, it is necessary to transmit EPS data to ground stations in the form of telemetry.
- Batteries must be activated no less than half an hour after leaving the pod.
- The selected components shall have a lifespan that is at least as long as the orbital lifespan of the satellite.
- The antennas and solar cells shall be positioned strategically to ensure that the power production remains unaffected by the shadow effect.
- The CubeSat must incorporate a “remove before flight” pin to prevent accidental activation of any of the electrical systems during any conducted ground tests.
- The EPS subsystem is responsible for ensuring that the necessary voltages and currents are provided for the payload and other subsystems.
- CubeSats will incorporate battery circuit protection for charging/discharging to avoid unbalanced cell conditions.
- The power subsystem's volume, mass, and cost budget shall not exceed 15% of the overall budget.

By meticulously delineating these requirements, we aim to establish a robust foundation for designing, implementing, and validating the power subsystem's functionality, reliability, and performance within the CubeSat platform. Through rigorous analysis, testing, and refinement, we endeavor to fulfill these requirements while fostering innovation, efficiency, and mission success in alignment with APSCO's overarching objectives and guidelines.

## 7.2. Component Configuration

Based on the tasks of the electrical power subsystem, it can be broken down into three main components.

- The first is power generation.
- The second is energy storage.
- The third is Power Control and Distribution Unit (PCDU).

However, as the project progresses to subsequent stages, the payload specifications may necessitate modifications and enhancements to the subsystems and components.

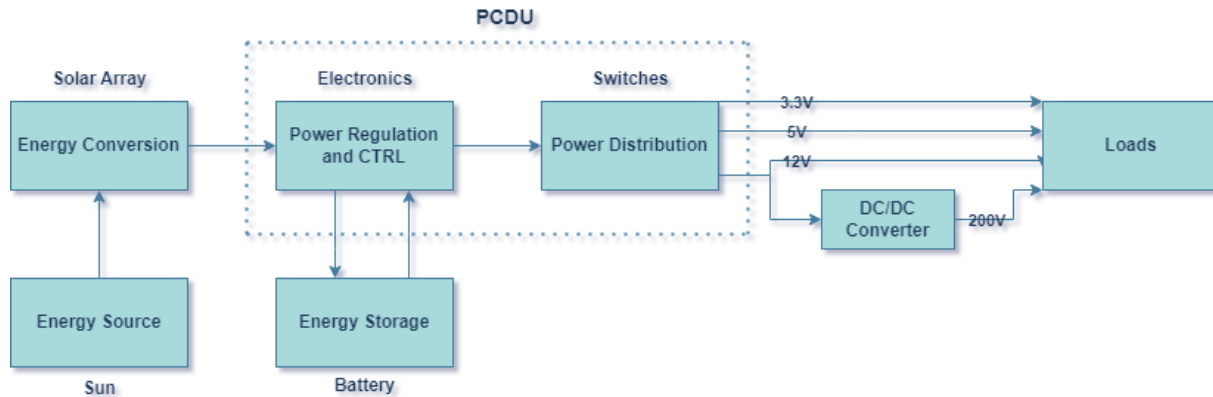


**Figure 71- SPARCS-B functional and component architecture  
 (Similar to SPARCS-A, however, it doesn't have a DC to DC converter)**

### 7.2.1. Solar Array Configuration

Due to weight limitations, it is extremely difficult to store enough energy to allow the CubeSat to operate in space for extended periods of time, often years, so it is necessary to generate electrical power and the source of the power is the energy collected from the solar panels which are exposed to direct solar radiation or to indirect radiation from albedo. Power generation is dependent upon energy absorbed by photovoltaic cells, which will be mounted on the body of the CubeSat. Solar panels are the primary source of power for CubeSats, converting solar energy into electrical power. The design of solar panels for nano satellites must strike a balance between efficiency, mass, and available surface area. During periods of sunlight, the satellite's sides are exposed to the sun, enabling power generation. Conversely, during eclipse, the satellite relies on stored power from batteries. So, it should generate enough power in sunlight to meet CubeSat's needs in eclipse.

Given the compact size of the satellite, it is preferable to opt for body-mounted solar cells that offer high efficiency in order to eliminate the need for a deployable solar panel, which may introduce complexities in terms of mechanisms and control. Moreover, body-mounted solar panels tend to be more durable, as they are seamlessly integrated into the spacecraft's structure and can be customized to fulfill particular thermal and radiation criteria. So, to generate electrical power from sunlight, we will use some pieces of space qualified Gallium Arsenide, triple-junction solar cells. And then the electrical power shall be harvested by a corresponding circuit. Triple-junction cells are commonly used due to their ideal efficiency to cost ratio. Also, GaAs solar cells have a higher efficiency compared to silicon solar cells, which is crucial for maximizing the power output in small spacecraft with limited surface area and it leads to smaller and lighter solar panels, which is beneficial for CubeSats with limited mass and volume constraints.



### 7.2.2. Battery Configuration

Energy storage devices, known as secondary (rechargeable) batteries, play a crucial role in providing power during periods of eclipse when solar panels are unable to generate electricity or are too distant to supply direct power. These batteries undergo a process where electrical energy is converted to chemical energy during charging, and then reversed during discharge, depending on the application requirements.

The selection of a specific type of battery is determined by various criteria such as energy density, life cycle, reliability, and cost, all of which must be carefully evaluated. The reliability of a battery is primarily influenced by the electrochemical system it is based on. Among the available options, lithium-polymer and lithium-ion batteries stand out due to their longer lifespan, high power and energy density, as well as superior efficiency. Noteworthy characteristics of these batteries include a wide range of operating temperatures and a significant working cycle, allowing them to deliver short, high-energy peaks without compromising the cell. Moreover, these batteries do not possess a memory effect, meaning they are less impacted by their charge and discharge history. Despite the higher price of lithium batteries compared to other options, this factor does not significantly impact the decision-making process. Lithium polymer batteries, being the most technologically advanced and expensive, are preferred for use in the power subsystem due to their unique features. The key difference between lithium-ion and lithium-polymer batteries lies in the electrolyte material, with the polymer electrolyte of a Li-Poly battery having low intrinsic conductivity, enabling the cell to be extremely thin. Therefore, based on the aforementioned reasons, the lithium polymer battery is the optimal choice for integration into the power subsystem.

### 7.2.3. PCDU configuration and selection

The Power Control and Distribution Unit (PCDU) is a crucial component of a satellite, responsible for regulating, controlling, and distributing power. It also monitors and protects the satellite's power bus. Alongside the On-Board Computer (OBC), the PCDU plays a vital role in the satellite's operations. The tasks of the PCDU begin with maximizing the power obtained from solar panels. It then converts this power into useful voltages to operate electronics and charge batteries. The PCDU ensures the safe storage of energy in the batteries and distributes power to all systems as needed. Throughout the entire mission lifetime, it autonomously safeguards against unexpected events and accidental damage.

In Low Earth Orbit (LEO), which is a common orbit for CubeSats and small satellites, the illumination conditions from the Sun can vary significantly. The solar array incidence angles and temperatures can range from -40°C to +80°C during each orbit. As the power generated by the solar arrays is influenced by temperature, the Electrical Power System (EPS) must effectively manage these varying conditions to optimize power generation and storage. To achieve this, it is important to select a component that includes a Maximum Power Point Tracker (MPPT) with a Battery Bus. This ensures that power from the solar arrays is optimized and the battery is safely charged during periods of sunlight. Additionally, it enables an efficient discharge path from the battery to the avionics and



APSCO CubeSat Competition  
Conceptual and Preliminary Design Report – Ver. 1  
(IR-Sepehr)

payload during eclipse. To enhance the efficiency of solar power conversion, MPPT algorithms are necessary. The general approach is to have one MPPT channel per solar panel. To achieve high efficiency, DC-DC converters should be utilized. Since only three surfaces can be illuminated at any given moment, the number of pulse converters can be limited to three. Each of these converters should be connected to panels on opposite sides.

The voltages planned to be provided for the components and subsystems are 3.3, 5, 12. However, payload in addition needs a 200 volts line for its emitter and collector. In order to achieve this voltage bus, it is necessary to utilize a PCDU board that provides 3.3, 5, and 12 volts voltage levels. Additionally, a DC-to-DC voltage converter capable of converting 12 volts to 200 volts is required.

The STARBUCK-NANO, a flight-proven subsystem optimized for Low Earth Orbit (LEO), has been chosen for this specific purpose. It is tailored to accommodate 1U, 2U, and 3U CubeSats equipped with body-mounted solar panels. Each power generation unit is self-sustaining and does not rely on other sections within the Electrical Power System (EPS). The redundant solid-state isolation switches enhance its reliability during launch operations. By utilizing Maximum Power Point Tracking, the STARBUCK-NANO employs an efficient battery charging mechanism that maximizes power generation from the CubeSat solar arrays. Analog components and various built-in protection methods are integrated to ensure safe operation during transportation, launch, and comprehensive EPS telemetry via the I2C network. The power systems are customized for each platform and solar panel size. The STARBUCK-NANO series can accommodate both body-mounted and deployable solar panel configurations, as well as support Lithium Polymer Battery setups.

**Table 30- PCDU General Features**

Design Life	5 years in LEO
Regulated Power Buses	3.3V, 5V, and 12V
Latching Current Limit (LCL)	10 Configurable
Interfaces	I2C
Max. Battery Voltage	8.2V
Operating Temperature	-40°C to 85°C
Storage Temperature	-50°C to 100°C
Vacuum	10^-5 torr
Radiation Tolerance	10 KRad
Vibration	To [RD-3]

**Table 31- Product Information**

Product	NANO-PICO	NANO
Integrated Battery	10 or 20Wh	No
Intended Use	1U CubeSat	2U and 3U CubeSat with body panels
Mass (typical)	86 g	86 g
Length	95.89 mm	95.89 mm
Width	90.17 mm	90.17 mm
Height	16.2 mm	16.2 mm



**Figure 72- Selected PCDU**

Based on the specifications outlined in the aforementioned table and the discussed design requirements, the Nano-Pico model has been chosen for SPARCS-A, while the Nano model has been selected for SPARCS-B.

A cost-effective DC-HV DC converter, utilizing the TL3843 Low-Power Current-Mode PWM Controller from TI, will be employed to produce a maximum of 200 volts. Input and output connections are designed to be facilitated through screw terminal connectors, with onboard LED D1 signaling the presence of input power. This design delivers a 200V DC output at 20mA from a 12V DC input source which meets the requirements of the payload.

DC to DC converter features:

- Operating Power Supply 12V DC @ 1A (Range 10V to 15V DC)
- Output 150V DC @ 50mA to 200V DC @ 20mA
- Operating Frequency 40Khz
- Over Current Protection
- D1 Power LED
- Screw Terminal Connectors for Input and Output
- PCB Dimensions 61.28 x 36.04 mm



**Figure 73- Selected DC-to-DC converter component**

### 7.3. Power consumption estimation

An essential aspect of the power subsystem design involves a thorough analysis of the power consumption patterns of individual subsystems. By evaluating the power needs of each component, engineers can optimize the power distribution strategy, ensuring efficient utilization of available resources. We must pay particular attention to power consumption trends at the beginning and end of the satellite's lifespan to ensure consistent and reliable performance throughout its mission.



APSCO CubeSat Competition  
Conceptual and Preliminary Design Report – Ver. 1  
(IR-Sepehr)

The average and maximum power consumption of individual components are provided below. By utilizing these power consumption figures, the instantaneous and average power consumption of the satellite can be determined based on the satellite's phase and mode. The momentary maximum power consumption is typically attributed to the connection of the batteries and the maximum momentary output current they can provide. Consequently, the components' duty cycle is not considered when calculating the maximum power consumption, and it is assumed that a restricted timeframe needs to be allocated.

**Table 32- power consumption of SPARCS-A**

<b>Component</b>	<b>Number</b>	<b>Supply Voltage (V)</b>	<b>Duty Cycle (%)</b>	<b>Nom Power consumption (Wh)</b>	<b>Max Power consumption (Wh)</b>
PCDU	1	-	100	0.2	0.2(TBC)
Compact Magnetorquer	3	1.25 to 7.5	50	0.25	1.75
Magnetometer	1	6.5 to 15	50	0.45	0.45(TBC)
Sun Sensor	4	3.3 to 5	50	0.01	0.01(TBC)
IMU	1	3.0 to 3.6	50	0.14	0.18
GPS Receiver	1	2.7 to 3.6	50	0.125	0.125(TBC)
GPS Antenna	1	3.3 to 5	50	0.05	0.05(TBC)
OBC board	1	3.3	100	0.4	0.4(TBC)
Dosimeter	1	3.3 or 5	100	10 $\mu$	0.01
TT&C Antenna	1	3.0 to 3.6 (3.3 Nom)	10	0.04	2W(During Deployment)
TT&C Board	1	6.5 to 20	10	0.48 (receiver) 4.0 (transmitter)	6.6
<b>SUM</b>				<b>1.86</b>	<b>15(TBC)</b>

**Table 33- power consumption of SPARCS-B**

<b>Component</b>	<b>Number</b>	<b>Supply Voltage (V)</b>	<b>Duty Cycle (%)</b>	<b>Nom Power consumption (W)</b>	<b>Max Power consumption (W)</b>
PCDU	1	-	100	0.2	0.2(TBC)
DC/DC converter	1	12	30	6(TBC)	8
ADCS-MTQ Board	1	3.3 to 5	50	1	1(TBC)
Sun Sensor	4	3.3 to 5	50	0.01	0.01(TBC)
IMU	1	3.0 to 3.6	50	0.14	0.18
GPS Receiver	1	2.7 to 3.6	50	0.125	0.125(TBC)
GPS Antenna	1	3.3 to 5	50	0.05	0.05(TBC)
OBC board	1	3.3	100	0.4	0.4(TBC)
Dosimeter	1	3.3 or 5	100	10 $\mu$	0.01
TT&C Antenna	1	3.0 to 3.6 (3.3 Nom)	10	0.04	2W(During Deployment)
TT&C Board	1	6.5 to 20	10	0.48 (receiver) 4.0 (transmitter)	6.6
Servo Motor	1	4.8 to 6	1	0.954	6.6
Camera	1	3.3	1	0.9	1.4
Emitter, Collector, Wire	6,2,2	0 to 200	30	1.6 (TBC) (summation)	4 (TBC) (summation)
Tether MCU	1	5.1	10	2.6	2.6(TBC)
<b>SUM</b>				<b>4.29 (TBC)</b>	<b>30(TBC)</b>

The power consumption profiles for various high power-consuming modes are determined by specifying the average and maximum power consumption of individual power-consuming components, along with detailing the phases and modes in which each subsystem operates and how they function within those phases and modes.

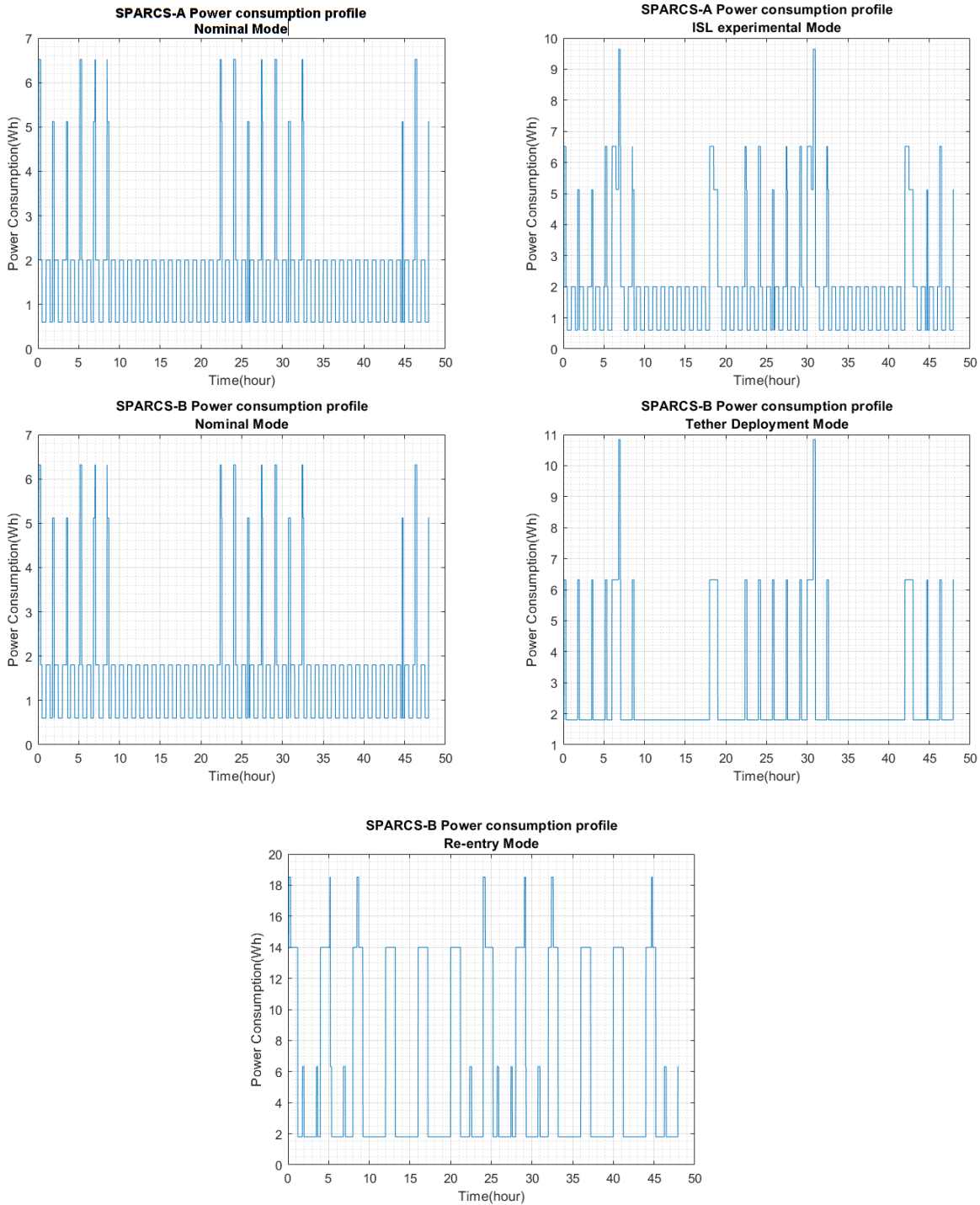


**Figure 74- Power consumption profile for some modes of SPARCS-A and SPARCS-B**

The profiles displayed indicate the energy usage across various modes, serving as crucial data for determining the appropriate sizing of solar cells and batteries.

#### 7.4. Cells selection and power generation estimation

It is imperative that the generated power consistently exceeds the consumption rate during every operational phase of the satellite. This ensures that all subsystems receive adequate power supply, thereby preventing any operational interruptions or failures. A satellite in LEO experiences a range of 5,000 – 5,500 cycles of eclipses over a year with a duration of 30 – 40 minutes each. These eclipses happen approximately every 90 minutes, as the satellites in LEO are positioned comparatively lower and complete a revolution faster. The amount of incoming light depends on the distance of the craft's orbit from the Sun as the intensity varies per the inverse square law, and the projected surface area of panel exposed to the Sun as this varies throughout orbit depending on the cosine angle of the panel with respect to the Sun's absolute position.

At this point in time, Given that the design is still in preliminary phase and the uncertainty in payload design still exists, our aim is to harness our full capacity for power generation. Subsequently, we utilize the most expansive cell area possible with optimal efficiency. To fully utilize the space available on the CubeSat body, we opt for rectangular XTE-SF SpectroLab solar cells. These GaAs cells boast a space heritage of over two decades and exhibit an efficiency of 32.2% at the start of their lifespan, decreasing to 27.9% towards the end.

**Table 34- XTE-SF general features (post 1 MeV e-Retention) For Temperature coefficients (10°C to 70°C)**

Parameters	BOL	10-yr LEO
Efficiency <sub>mp</sub>	32.2%	0.93
V <sub>oc</sub> (V)	2.750	0.92
J <sub>sc</sub> (mA/cm <sup>2</sup> )	18.6	1.00
V <sub>mp</sub> (V)	2.435	0.92
J <sub>mp</sub> (mA/cm <sup>2</sup> )	17.9	1.00
Open Circuit Voltage (mV/°C)	-5.6	-6.1
Short Circuit Current (μA/cm <sup>2</sup> °C)	11	9
Maximum Power Voltage(mV/°C)	-6.2	-6.4
Maximum Power Current(μA/cm <sup>2</sup> °C)	8	7

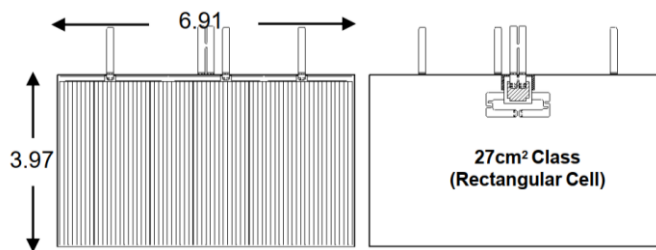


**Figure 75- Selected Solar cell general configuration**

Based on the solar cell chosen, SPARCS-A has 11 cells mounted on its body, while SPARCS-B has 21 cells, representing the maximum capacity for each of these satellites. The remaining space on the

satellites' bodies is allocated for other components. Based on the specified voltage and current input to the power board, along with design constraints such as maximum power generation, multiple solar cells are interconnected in a series configuration. Consequently, several parallel strings of cells will be formed.

The CubeSats are designed with nadir earth pointing and have less than a 10% offset. The option of pointing towards the sun to increase power generation is not being considered due to mission and control constraints, as well as the CubeSats' ability to generate sufficient power without doing so. However, if additional power is required, our design in ADCS also allows to include a sun-pointing attitude maneuver for both SPARCS-A and SPARCS-B.

The power production of each CubeSats has been calculated at the beginning and end of their life for each month, taking into account the variation in the sun's radiation angle. This calculation was performed using STK and MATLAB software packages for one orbit.

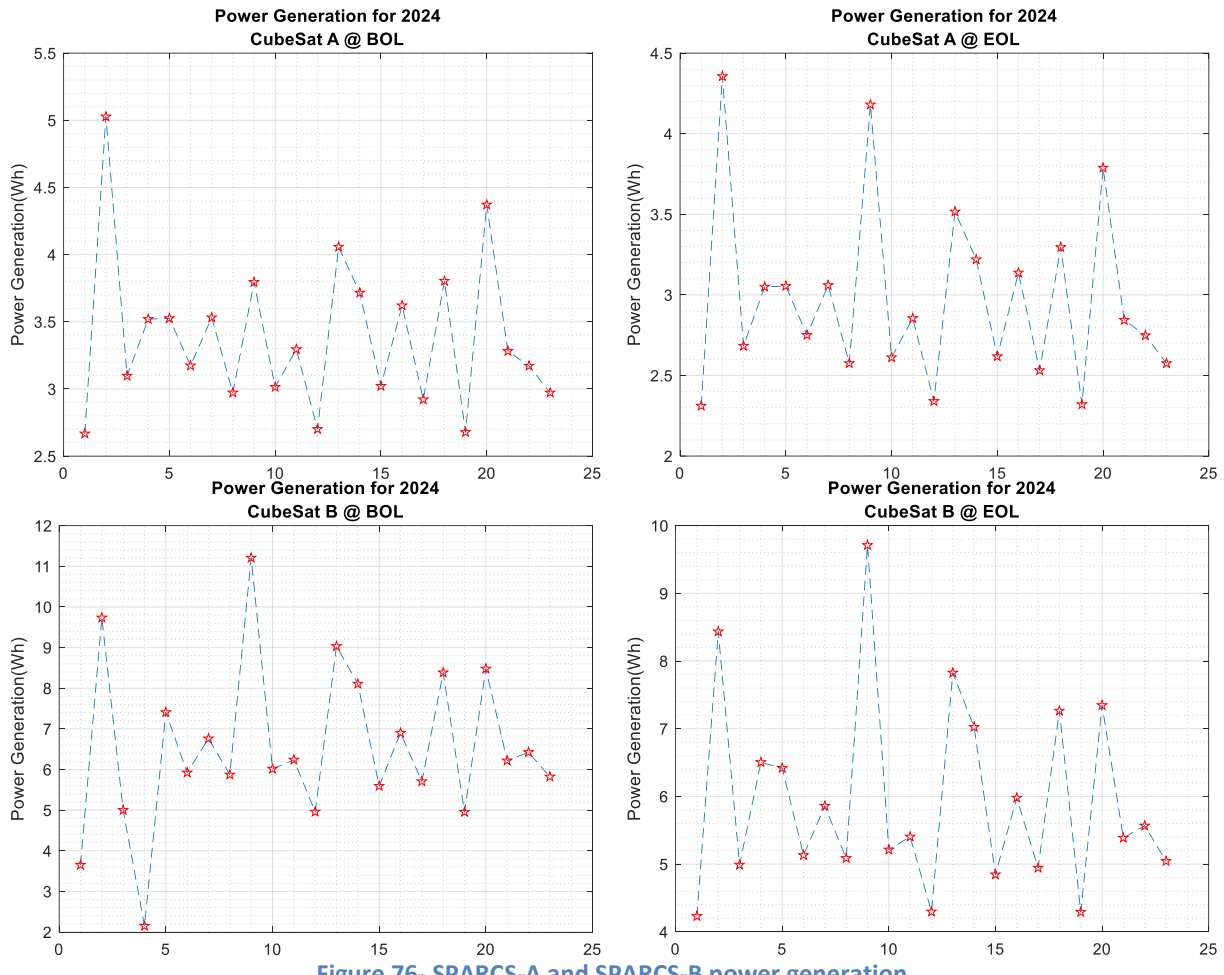


**Figure 76- SPARCS-A and SPARCS-B power generation**

The provided table presents the average, maximum, and minimum production power values based on the aforementioned graphs, in addition to the average power consumption.

**Table 35- SPARCS-A and SPARCS-B Power generation**

	Average power generation	Minimum power generation	Maximum power generation
SPARCS- A - BOL	3.3 Wh	2.6 Wh	5 Wh
SPARCS- A - EOL	2.9 Wh	2.3 Wh	4.3 Wh
SPARCS-B - BOL	6.5 Wh	2.2 Wh	11.2 Wh
SPARCS-B - EOL	5.9 Wh	4.2 Wh	9.7 Wh

It is crucial to note that not all the power generated can be effectively delivered to consumers. Factors like battery efficiency (90%) and losses in wires and connections (95%) must be taken into account, constituting approximately 85% of the overall efficiency of the power generation system. Consequently, the actual production capacities are 15% less than the figures indicated in the table provided above. On the whole, it is recommended that the average production power exceeds the average power consumption by 10% to ensure the satellites can effectively carry out their mission. Nevertheless, after factoring in the 85% efficiency of power production, the average power production values in both satellites consistently surpass the average power consumption values by over 20%. This discrepancy can be attributed to various considerations, including system reliability and uncertainties in payload design during this phase of development.

**Table 36- SPARCS-A and SPARCS-B average power generation and consumption**

	Actual Average power generation	Average power consumption
SPARCS- A	2.6 Wh	1.86 Wh
SPARCS- B	5.3 Wh	4.29 Wh

## 7.5. Battery sizing and selection

To be able to reliably use satellite batteries on-board space systems, environmental conditions become even more important to be considered in design, as it can be possible for battery systems to leak, or even explode. Some of the important parameters to consider for selecting the right set of batteries include; Depth of Discharge (DoD), shelf-life, ability to recharge, power capacity (in Ah), weight, operating temperature range, resistance to shock and vibration, power management schemes, charge cycles, specific energy, cost, and ruggedness. A common issue with satellite battery technology is overcharging. Overcharging should also be considered during the design and testing phase to avoid the risk of overheating once the maximum voltage is reached. Overheating may lead to explosion or fire, which would likely be catastrophic to a mission. Finally, other undesirable conditions for a battery would include short circuiting, an operating temperature higher or lower than the designed range, exceeding the preset limits of the DOD, a build-up of pressure inside the cell due to the chemical reactions, and excessive current developing. These form additional requirements for our EPS design.

Battery selection is an essential part of spacecraft design as spacecraft as energy storage must be sufficient to meet load demands during daylight and eclipse. The selection criteria for batteries depend on four primary figures of merit, which include specific energy, energy density, specific power and power density, and cycle life.



APSCO CubeSat Competition  
Conceptual and Preliminary Design Report – Ver. 1  
(IR-Sepehr)

Given that lithium polymer batteries typically have a voltage of 3.7 volts, it is necessary to combine multiple batteries in series and parallel to achieve the desired voltage, current, and stored energy. To determine the required capacity of this battery pack, two factors need to be taken into account: the ability to provide power to the satellite during intervals when the system operates outside its nominal design conditions, and the maximum power supply needed. The maximum power required by the satellites depends on their phase and modes, as well as the power consumed by the components. In the worst-case scenario, which includes peak power consumption during the mission (as you can see in power consumption profiles) and potential system errors leading to overloading of the power supply subsystem, the power consumption have been calculated to be 10 watts for SPARCS-A and 20 watts for SPARCS-B (in one hour). Furthermore, it is assumed that the satellites may deviate from their nominal conditions for a maximum of 2 consecutive orbits. To ensure the longevity of the batteries, a minimum acceptable depth of discharge of 30% (TBC) has been considered. Taking into account the aforementioned factors, as well as energy loss in the battery cells over time and the need for system redundancy, a battery pack with a capacity of 20-Watt hours has been determined for SPARCS-A, while SPARCS-B requires a battery pack with a capacity of 30-Watt hours. It is widely recognized that the aforementioned battery capacities align with the satellite's maximum power consumption.

A 20 Watt-hour battery is integrated in the SPARCS-A PCDU, while a 30 Watt-hour Optimus model is employed for the SPARCS-B battery pack. The OPTIMUS batteries are known for their high capacity and low mass and volume. These lithium polymer batteries are specifically designed for LEO missions with a maximum altitude of 850km and can be seamlessly integrated with the STARBUCK EPS range. To ensure optimal performance in low temperatures, all battery systems are equipped with autonomous integrated heater systems. Furthermore, multiple protection systems are implemented at the cell, battery, and system levels to automatically respond to external fault conditions and prevent irrecoverable damage to the battery and overall system.

**Table 37- Battery general specification**

Model	OPTIMUS-30
Material	Lithium Polymer
Capacity	30 Wh
Mass (typical)	268 g
Dimension	95.89 x 90.17 x 21.55 mm <sup>3</sup>
Storage Temperature	Recommended: -10°C to +10°C, 1 Year: -20°C to +20°C 3 Months: -20°C to +45°C, 1 Month: -20°C to +60°C
Vacuum	10 <sup>-5</sup> torr
Operating Temperature	-10°C to +50°C
Vibration	To [RD-2]
EoC Voltage	8.26 V (typical)
Full Discharge Voltage	6.2 V (typical)
Charge Voltage Limit	8.4 V (max)
Discharge Voltage Limit	6.2 V (min)
Charge/Discharge Current Rate	1.53 (fraction of capacity) discharge voltage limit: 3V
Quiescent Power Consumption	< 0.1 W (30 Wh & 40 Wh)
Interfaces	Standard CubeSat PC104
Power Buses	3V3 and 5V

Serial Ports	I2C
--------------	-----



Figure 77- Selected battery pack picture

## 7.6. Budget estimation

In this section, there is an estimate of the mass, volume, power, temperature and cost budgeting of the power subsystem separately for the selected components.

Table 38- Power subsystem budget estimation of SPARCS-A

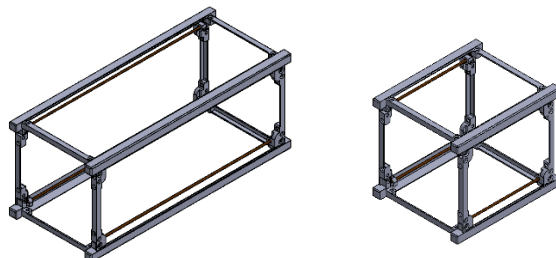
Component	Product ID	Num.	Mass (g)	Dimensions (cm)	Power		Operating Temp. (°C)	Cost (USD)
					Nominal (W)	Duty Cycle (%)		
PCDU	STARBUCK NANO-PICO	1	86	9.6×9×1.6	0.2	100	-40 to +85	TBD
Battery	Battery Integrated to PCDU	1	200	9.6×9×1.5	-	-	-10 to +50	TBD
Solar Cells	XTE-SF	11	2.7 each	3.97×6.91×0.02	-	-	-10 to +70	TBD

Table 39- Power subsystem budget estimation of SPARCS-B

Component	Product ID	Num.	Mass (g)	Dimensions (cm)	Power		Operating Temp. (°C)	Cost (USD)
					Nominal (W)	Duty Cycle (%)		
PCDU	STARBUCK NANO	1	86	9.6×9×1.6	0.2	100	-40 to +85	TBD
Battery	OPTIMUS-30	1	268	9.6×9×2.2	-	-	-10 to +50	TBD
Solar Cells	XTE-SF	21	2.7 each	3.97×6.91×0.02	-	-	-10 to +70	TBD
DC/DC converter	TL3843	1	100 (TBC)	6.13×3.6×3	6 (TBC)	30 (TBC)	TBD	TBD

## 8. Structure and mechanism

The requirements related to the outer dimensions of standard CubeSats are presented in document CDS<sup>1</sup>. The total external dimensions for both SPARCS A and SPARCS B satellites as defined by the standard are 366×100×100 mm<sup>3</sup>. The main structure of SPARCS-A, and B is designed according to the 3U CubeSat format by ISIS, where SPARCS-A is equivalent to 1U and SPARCS-B is equivalent to 2U. Nearly all structural details from ISIS, which also holds space certification, have been considered in the satellite design, making it essentially the same commercial model as that of the company. The figure below shows a solid model of the structure of SPARCS-A and SPARCS-B satellites along with the support rods for the boards.



**Figure 78- Left: 2U Bus model of SPARCS-B; Right: 1U Bus model of SPARCS-A**

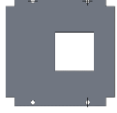
Each CubeSat's primary structure comprises top and bottom frames along with four side ribs, all covered by panels. The table below outlines the main components of the structure along with their respective materials.

**Table 40- Structure's main components for SPARCS-A and SPARCS-B**

No.	Component Name	Number		Material	Shape
		SPARCS-A	SPARCS-B		
1	Spacer	24	36	PTFE	
2	Rod	4	4	Stainless Steel 316	
3	Main Frame	2	2	Aluminum 6061-T6	
4	Rib	4	4	Aluminum 6061-T6	
5	Side plate	4	4	Aluminum 6061-T6	

<sup>1</sup> CubeSat Design Specification

---

6	End plate	1	0	Aluminum 6061-T6	
7	M2.5X6 screw	24	24	Stainless Steel 316	

---

The figure below illustrates dimensional specifications and a model of the main structure body.

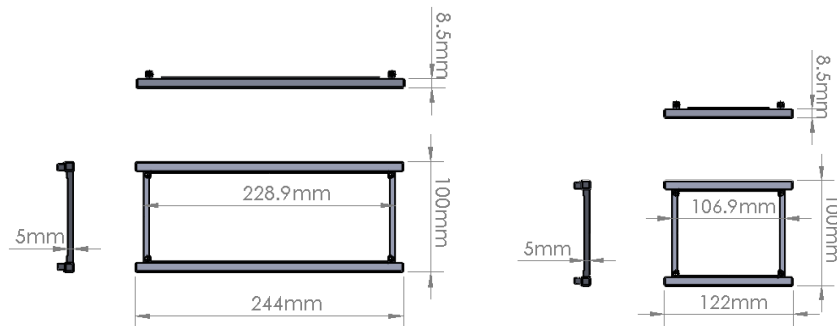


**Figure 79- Dimensions of the main structure bodies  
(Left: SPARCS-B, Right: SPARCS-A)**

In the figure below, the dimensional specifications of the ribs are also provided.

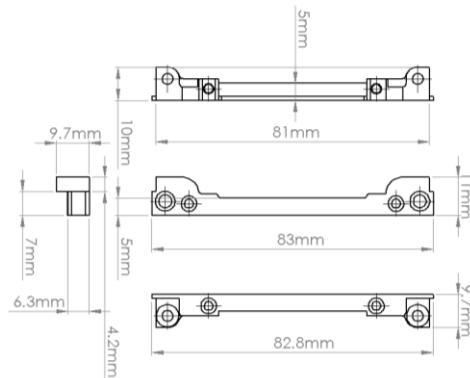


**Figure 80- Dimensions of the rib structures  
(dimensions in millimeters)**

## 8.1. Structure Materials

The primary material used in commercial models worldwide is typically aluminum 6061-T6 or 7075. We use aluminum 6061-T6 to create a more cost-effective structure. Stainless steel is used for rods, and spacers are commonly made of PTFE. The boards are also made of FR4. The mechanical properties of these materials are provided in the table below.

**Table 41- Mechanical and thermal properties of the materials used in SPARCS-A, and B**

Material Property	Aluminum 6061-T6	Stainless Steel 316	FR4-CW	PTFE
Density (kg/m <sup>3</sup> )	2690	7870	1850	2140
Yield Strength (MPa)	241	310	345	20.7
Young's Modulus (GPa)	70	205	21	0.4
Poisson's Ratio	0.33	0.27	0.12	0.45



Thermal Expansion Coefficient (1/°C)	23.4	16.5	Along x-axis: $1.4 \times 10^{-5}$ Along y-axis: $1.2 \times 10^{-5}$ Along z-axis: $7 \times 10^{-5}$	145
Thermal Conductivity (W/m°C)	161	15	Through-plane $\approx 0.3$ in-plane $\approx 0.9$	0.25
Specific Heat (J/kg°C)	934	510	$1.15 \times 10^3$	970

## 8.2. Structural Subsystem Validation Plan

It should be noted that since the structure has been designed based on a commercially validated model with space certification, we can have a very high level of confidence in its proper functioning. Additionally, SPARCS-A, and B structures are single-material, simple structures that, unlike larger microsatellites, lack complexity in the design and manufacturing process. Nevertheless, according to standards, we will implement a validation plan. According to the ECSS standard, the required documents for the structural subsystem validation plan will include the following topics.

### 8.2.1. Static loading design

Loading design<sup>1</sup> follows the requirements defined in Annex B of the ECSS-E-ST-32 standard. Loading design is a part of the Design Justification File (DJF). In loading design, necessary discussions are provided to ensure the validity of the design process and to justify the mechanical design.

This document includes a description of details and methodologies for tracking design loading models and the lifecycle used in the mechanical design of the structure. It serves as an input to the quality process and mechanical design of the structure, prepared for similar project-related documents (such as strength and stress analysis, test characteristics, etc.). In SPARCS-A, and B modeling, aluminum 6061-T6 is used for structural components, and FR4 material is considered for equipment boards.

- **Boundary conditions (BCs) and loading methods on SPARCS-A, and B**

The loads imparted from the launcher to the SPARCS-A, and B will not directly affect the both CubeSats itself but will first be transmitted to the payload. Due to the small dimensions of the payload, it will be assumed to act as a solid body that transmits the launcher's loads to the CubeSats in the same manner. Under these conditions, the loads will only be applied to the four rails at the corners of the CubeSats, which are in contact with the payload. The application of boundary conditions for the CanX-7 CubeSat within the payload is depicted in Figure 81, where the CubeSat is held in place inside the payload only by the four side rails, with no contact with other aspects of the CubeSat.

<sup>1</sup> Design loads

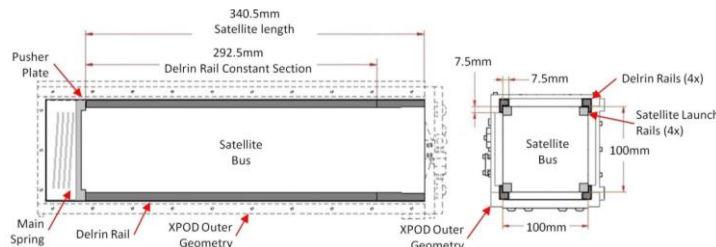


**Figure 81- The contact conditions between the CubeSat and the payload in the rails<sup>1</sup>**

In the figure below, BCs in the x and y directions and the method of applying loads in these two directions are illustrated. As observed, these two faces represent simple BCs.

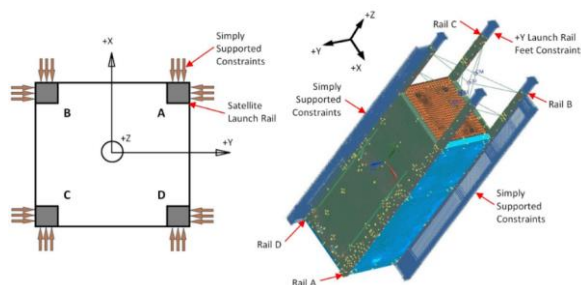


**Figure 82- Payload-to-rail loading and boundary conditions for CubeSat in x and y directions**

BCs in the z-direction will differ slightly. In the z-direction, the CubeSat is held at one end by a plate connected to a spring, and at the opposite face, the CubeSat is fully fixed by a closed payload door, ensuring complete fixation of the CubeSat. These fixed maintenance conditions result in very minimal deflection (approximately 0.5 mm in each direction) and are controlled accordingly. Therefore, it is assumed that the CubeSat inside the payload will not experience any movement. Similar boundary conditions were considered in a similar study on the SEAM CubeSat, depicted in the figure below<sup>2</sup>.

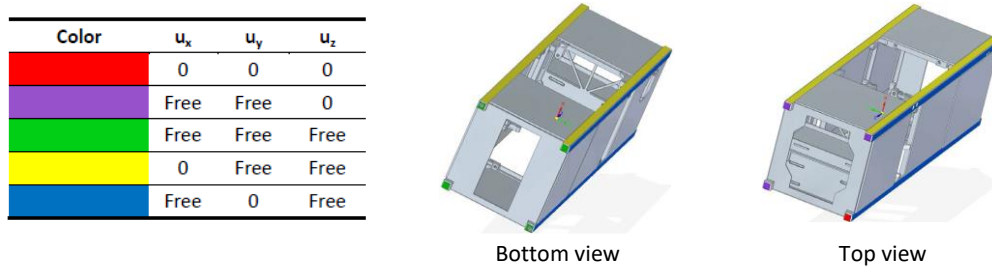


**Figure 83- Boundary conditions simulated for the SEAM CubeSat**

- Analysis results with launcher environmental loads

For the design, analysis, construction, and testing of a CubeSat, detailed information and specifications of the launcher must be available. For each launcher, considering its velocity and acceleration at different stages of launch and the time of CubeSat release from the launcher, all

<sup>1</sup> Chung, J.C.-J., Mechanical Subsystem Development for the CanX-7 Nanosatellite, the NEMO-HD Microsatellite, and the XPOD Mass Dummy. 2014, University of Toronto (Canada).

<sup>2</sup> Military Handbook - MIL-HDBK-5H: Metallic Materials and Elements for Aerospace Vehicle Structures (Knovel Interactive Edition). U.S. Department of Defense.

necessary parameters in the design including accelerations, natural frequencies of the launcher in longitudinal and lateral directions, and all dynamic environments that the CubeSat will encounter during launch are provided in separate tables or diagrams in the Launch Vehicle Manual User's Guide<sup>1</sup>. These details enable the designer to perform their design and analyses, ensuring that the design parameters align theoretically with the specified values in the provided tables.

Given the unspecified launcher, environmental loads for the Soyuz launcher have been applied based on the satellite compatibility manual. Assuming a safety factor of 1.25, the values of quasi-static accelerations will be as follows.

**Table 42- Quasi-static acceleration values**

Acceleration Component	Acceleration considering a safety factor of 1.25 (g)	Maximum accelerations according to the compatibility manual (g)
Longitudinal acceleration	6.25	5
Lateral accelerations	2.25	1.8

The analysis conducted in the finite element software has considered the values from the above table. An example of the finite element mesh is shown in Figure 84.

The first step in a finite element analysis is selecting the appropriate elements. For modeling the satellite, solid elements and standard solving techniques in ANSYS Workbench software have been used. For defining materials, aluminum 6061-T6 has been used for structural components. For equipment boards, FR4 material (crosswise model with a lower Young's modulus) has been considered. The connection between the two equipment pieces has been constrained as "Bonded" in the software, ensuring they are fixed together. The effect of mesh refinement on the accuracy of results has also been investigated, and efforts have been made to refine the mesh to achieve a more precise analysis.

Based on the simulation results and the application of launcher environmental loads mentioned, the maximum von Mises stress in SPARCS-A is 4.96MPa at the connection of the sun sensor to the outer panel, and in SPARCS-B, it is 25.5MPa at the connection of the board supporting rods to the side ribs.

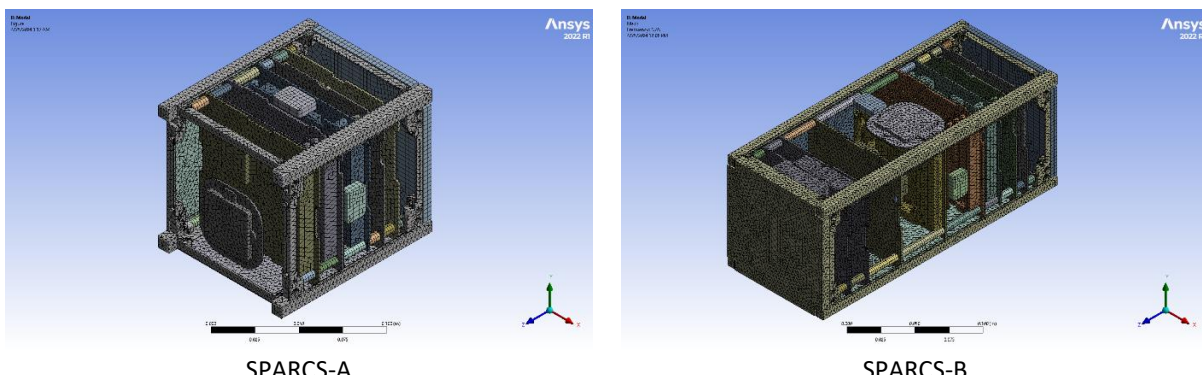


**Figure 84- Sample mesh**

<sup>1</sup> [Soyuz-Users-Manual-March-2012](#)

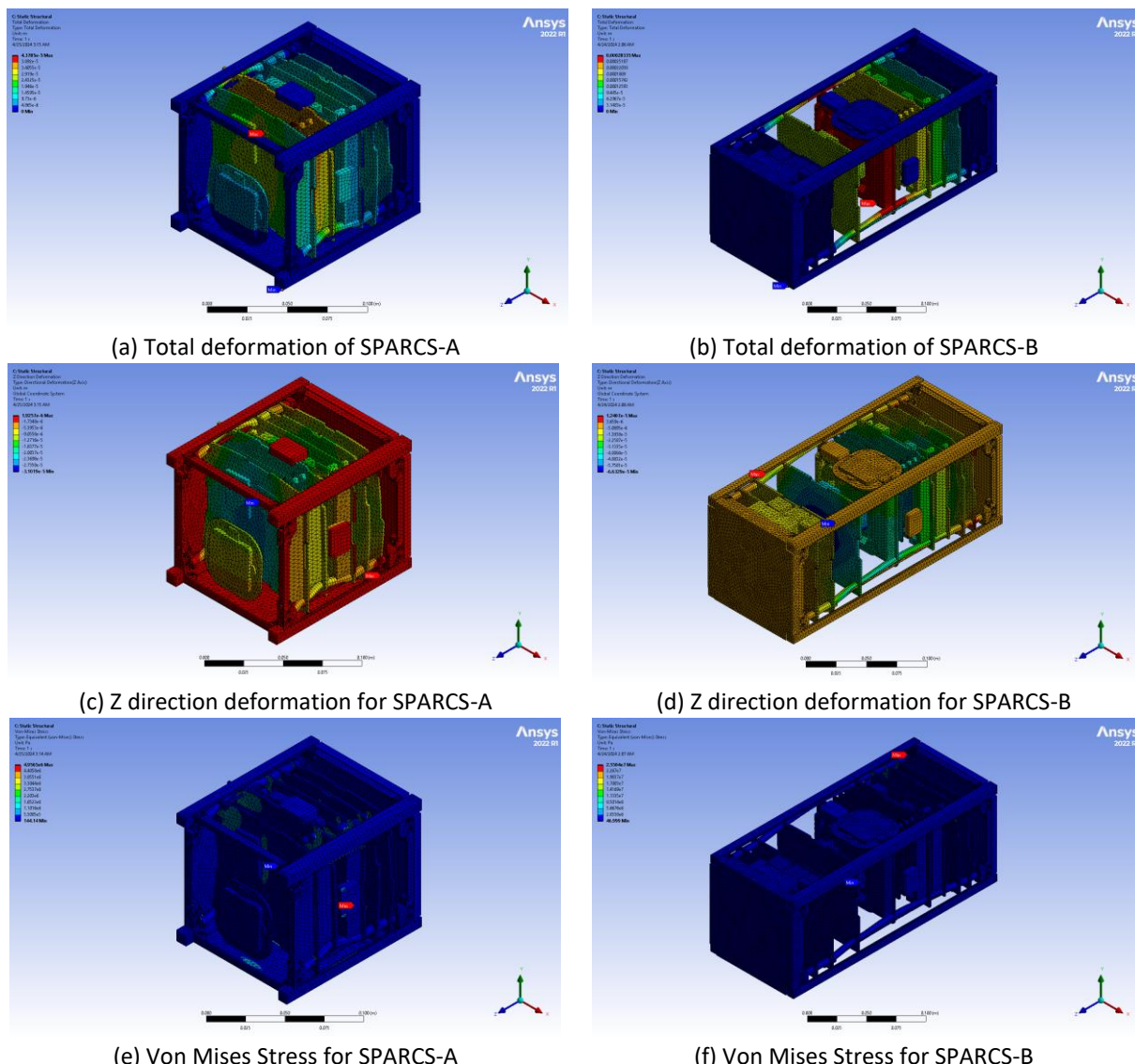


**Figure 85- Static analysis results**

Despite the obtained stress values, they are significantly lower than the yield stress of aluminum 6061-T6. Therefore, in all parts including the main structure, the resulting stress values are below the yield stress of aluminum 6061-T6. Consequently, the designed structure has a sufficient safety margin in terms of stress. The maximum displacement of the SPARCS-A structure is 0.0044 mm at the center of the 20W battery end plate, and the maximum displacement of the SPARCS B structure is 0.2834 mm at the connection of the ADCS-MTQ board to the rods. Based on the obtained values and the safety margin relationship provided below, these values can also be calculated.

$$MoS_{SPARCS-A} = \frac{\text{Allowable Stress}}{\text{FoS} \times \text{Actual Stress}} - 1 = \frac{240}{1.25 \times 4.96} = 37.71 \geq 1.5 \quad (8-1)$$

$$MoS_{SPARCS-B} = \frac{\text{Allowable Stress}}{\text{FoS} \times \text{Actual Stress}} - 1 = \frac{240}{1.25 \times 25.5} = 6.53 \geq 1.5 \quad (8-2)$$

The sum of the obtained results confirms the proposed design with high reliability for use in both satellites. More detailed analyses, including stress concentrations at screw holes, other loadings such as random vibrations, etc., will be further investigated in the detailed design phase.

### 8.2.2. Modal analysis

According to the handbook related to the frequencies of the Soyuz launcher, both satellites must meet minimum requirements for their natural frequencies based on the longitudinal and lateral launch vehicle frequencies, as depicted in the figure below.

**Table 43- Constraints on natural frequencies of Soyuz launch vehicle**

Direction	The fundamental (primary) frequency (Hz)
Lateral	$\geq 15$
Longitudinal Frequency	$\geq 35$

Accordingly, the lateral frequency of both satellites must be greater than 15 Hz, and the longitudinal frequency of both satellites must be greater than 35 Hz.

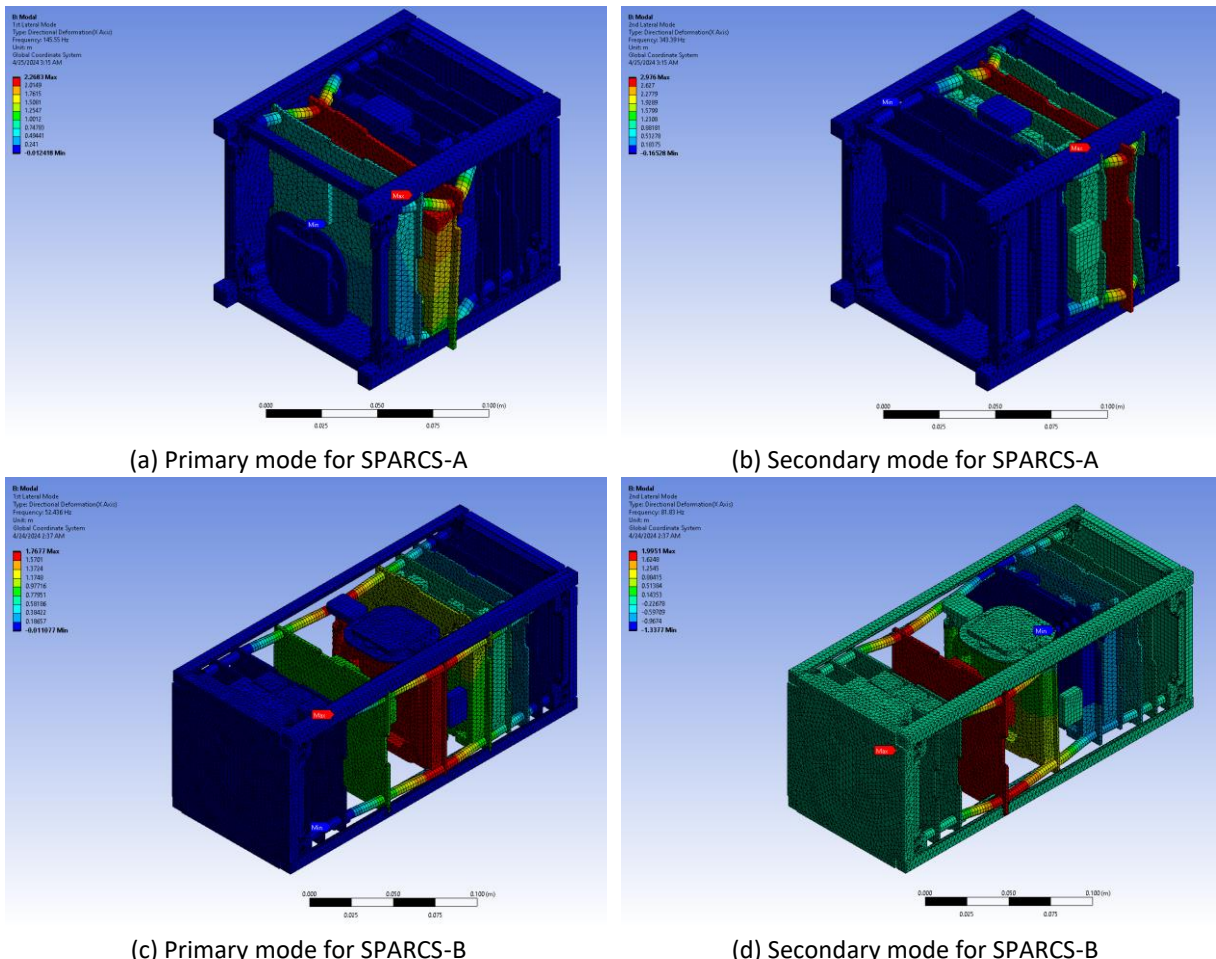


**Figure 86- Lateral modes**

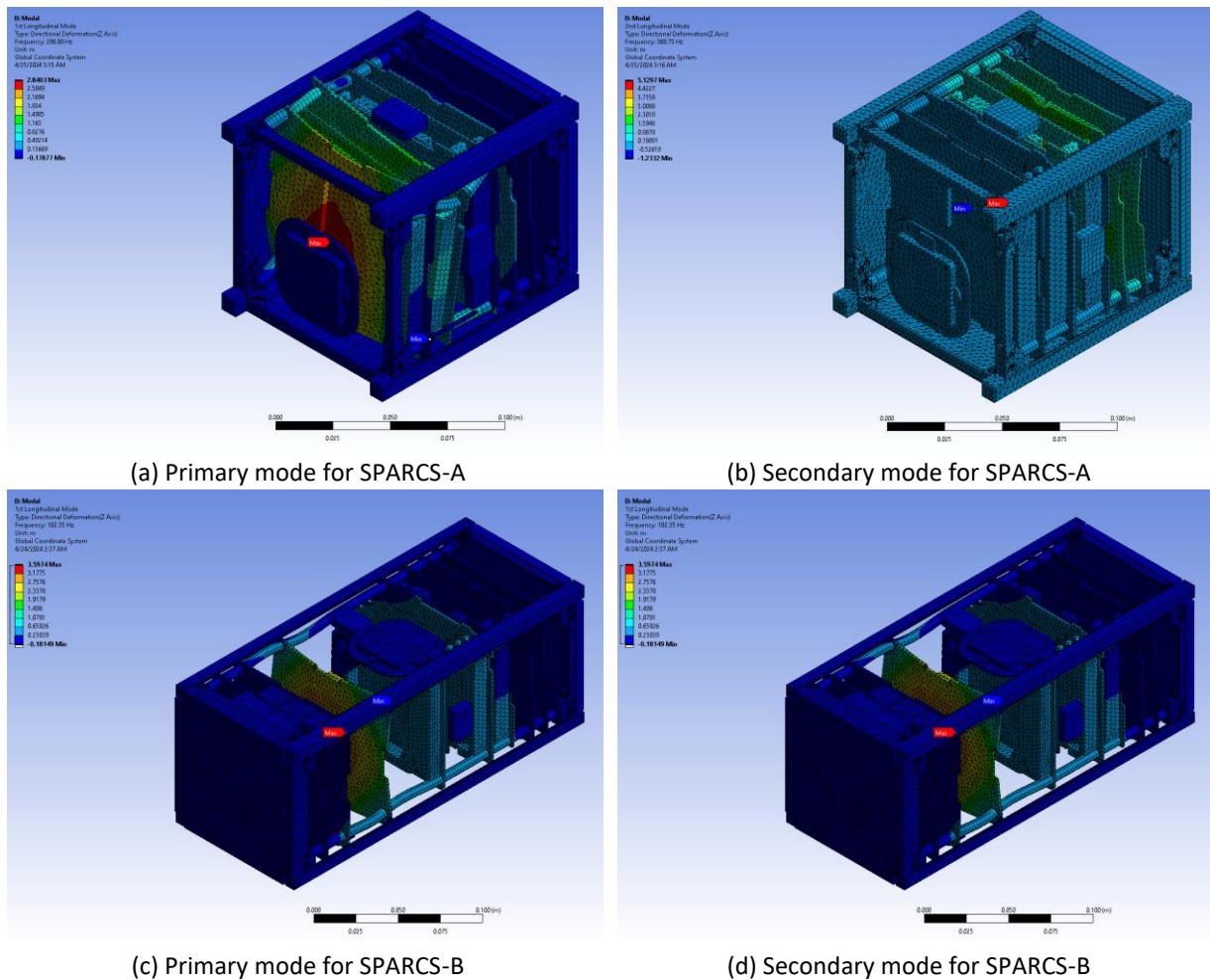


**Figure 87- Longitudinal modes**

Based on the results, the first and second lateral frequencies for SPARCS-A are 145.55 Hz and 343.39 Hz, respectively. For SPARCS-B, the first and second lateral frequencies are 52.436 Hz and 81.83 Hz, respectively. Additionally, the first and second longitudinal frequencies for SPARCS-A are 286.88 Hz and 368.73 Hz, and for SPARCS-B, they are 182.35 Hz and 222.02 Hz. Therefore, both satellites meet the frequency requirements. Note that in this modal analysis, similar to the previous section, we have used the same mesh and boundary conditions.

### 8.3. Budget Estimation

Mass and dimensions budget is provided in table below.

**Table 44- Structure mass and dimensions budget**

No.	Component Name	Number		Dimensions (cm)		Mass (g)	
		SPARCS-A	SPARCS-B	SPARCS-A	SPARCS-B	SPARCS-A	SPARCS-B
1	Spacer	24	36	0.6 x 0.6 x (0.5-5) (avg: 0.6 x 0.6 x 2.8)		0.2-2 (avg: 1.1)	
2	Rod	4	4	0.2 x 0.2 x 8.35	0.2 x 0.2 x 20.55	2.1	5.1
3	Main Frame	2	2	10 x 12.2 x 1.54	10 x 24.4 x 1.54	29	42



APSCO CubeSat Competition  
Conceptual and Preliminary Design Report – Ver. 1  
(IR-Sepehr)

4	Rib	4	4	0.97 x 1.12 x 8.28		5.4
5	Side plate	4	4	10.69 x 8.26 x 0.06	22.8 x 8.26 x 0.06	14
6	End plate	1	0	9.8 x 9.8 x 0.06		13.1
7	M2.5X6 screw	24	24	0.5 x 0.5 x 0.6		0.3

- Cost budget.

The cost of the structure was provided in the cost breakdown section. As explained, the model supplied by ISIS costs about \$5,000.

- Power budgeting (if applicable).

The structure itself does not consume power, and the only related consumption can be attributed to the microswitch for turning the satellite on and off, as well as the power needed to release the strings used to deploy antennas and mechanisms (if applicable), all of which occur only once at the start of CubeSat injection into orbit.



## 9. Thermal control

The thermal control system of the CubeSat is responsible for regulating the temperature conditions of all subsystems within the CubeSat within appropriate ranges to ensure proper and efficient operation, as well as preventing damage throughout the CubeSat's lifetime. Achieving TCS objectives requires compliance with requirements and implementation of various actions during design, procurement, equipment manufacturing, maintenance, CubeSat assembly, integration, and testing until successful mission placement in orbit with high reliability. This section provides an overview of satellite thermal modeling and analysis based on the ECSS-E-ST-31C standard.

The thermal control system must fulfill the following common objectives for the CubeSat:

1. 1. Control the temperature of CubeSat components and equipment within the permissible temperature range.
2. 2. Control the temperature gradient in sensitive CubeSat equipment (K/length).
3. 3. Control the rate of temperature change and temperature stability within the permissible range (K/time).
4. Control the heat flow (conductive/radiative) within the satellite (W).

### 9.1. CubeSat Control Scenarios and Operational Modes

CubeSat operational scenarios have a significant impact on the thermal environmental conditions of the CubeSat. CubeSat scenarios, including its orientation relative to the sun and Earth, the flux incident on each facet of the CubeSat and its duration, as well as internal heat dissipation of the CubeSat equipment per mission, are all influential. On the other hand, the beta angle parameter also plays a crucial role in visualizing the thermal environment of the orbit, especially for LEO orbits. The CubeSat's orientation is such that it always has an antenna facet directed towards the Earth.

### 9.2. CubeSat Orbital Conditions and Beta Angle

Various parameters in a CubeSat's orbit are used to investigate thermal control, but the beta angle parameter is particularly significant in visualizing the thermal environment of the orbit, especially for LEO orbits. The beta angle of the orbit is the minimum angle between the CubeSat's orbital plane around the Earth and the solar vector and can vary from 90+ to 90- degrees (Figure 88). The CubeSat in this project has a beta angle ranging from zero to 55 degrees. Beta angles are often expressed as positive or negative. If the CubeSat rotates in its orbit in a counterclockwise direction relative to the sun's perspective, the orbit's beta angle is positive; otherwise, it will be negative.

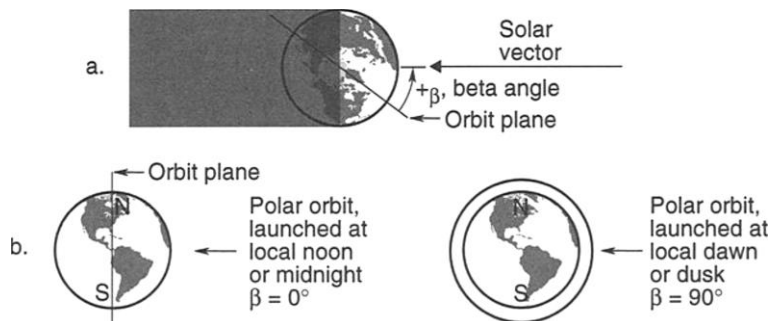


**Figure 88- Orbit beta angle**

### 9.3. Geometric Mathematical Modeling in Thermal Desktop Software

The Geometric Mathematical Model (GMM) has been implemented in the Thermal Desktop software and is presented below.

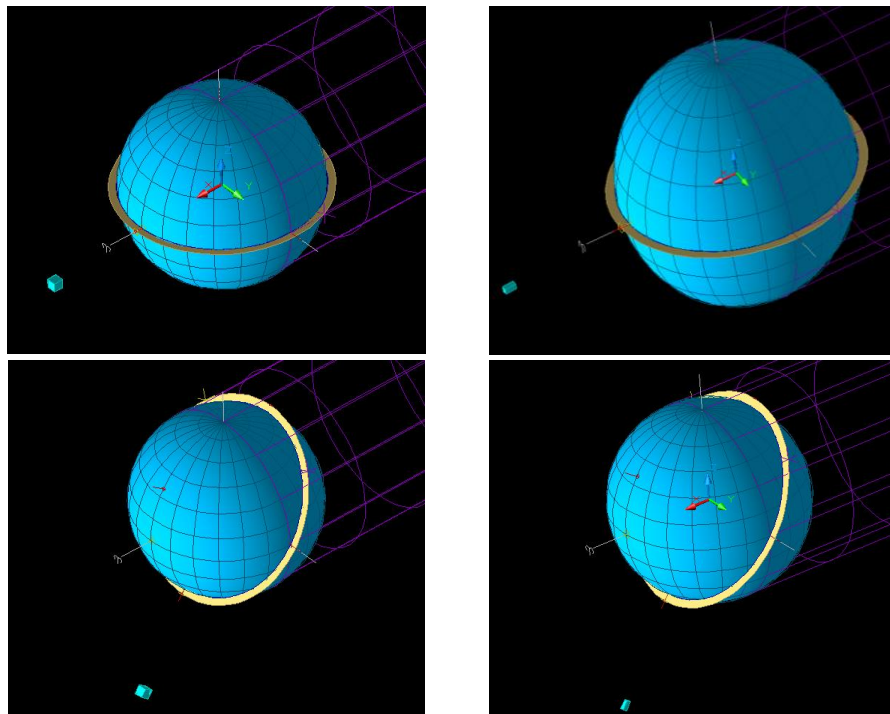


**Figure 89- CubeSat schematic in Thermal Desktop software for beta angles of 0 and 55 degrees.**

### 9.4. Values of Parameters Used in Worst Case Hot and Cold Calculations

Thermal analysis of the satellite is typically conducted based on two worst-case scenarios: Worst Case Cold (WCC) and Worst Case Hot (WCH). The worst-case cold scenario occurs when the CubeSat experiences the maximum duration in shadow, resulting in the minimum heat generation within the CubeSat. In the worst-case Hot scenario, the CubeSat experiences the minimum duration in shadow, leading to the maximum heat generation. When the launch time and other necessary parameters are determined, by plotting the changes in beta angle (the angle between the sunlight and the

orbital plane), the maximum and minimum values can be identified, and they can be used in calculations related to maximum and minimum temperatures.

In the calculations related to the worst-case scenarios, the values mentioned in Table below have been used. The values for the albedo coefficient and IR flux are extracted from the Gilmore<sup>1</sup> book, considering the values of beta angle, orbit inclination angle, and orbit period duration.

**Table 45- Values of parameters used in worst-case hot and cold calculations**

Parameter	Magnitude		Unit
	Hottest	Coldest	
Altitude (h)	550		km
Time period (T)	5739		s
Orbit beta angle	0-55		Degree
Suns direct solar flux ( $Q_s$ )	1367(at spring or fall)		W/m <sup>2</sup>
Albedo (a)	0.26	0.19	-
Earth IR flux ( $Q_{IR}$ )	257	218	W/m <sup>2</sup>
Earth radius ( $R_e$ )	63.78.14		km
Boltzmann coefficient ( $\sigma$ )	$5.67 \times 10^{-8}$		W/m <sup>2</sup> K

#### 9.4.1. Surface Heat Fluxes:

The following results obtained from Thermal Desktop software for the heat fluxes to each panel of the CubeSat are presented. These values are shown for beta zero and 55 degrees and in the solar incidence state as an example.

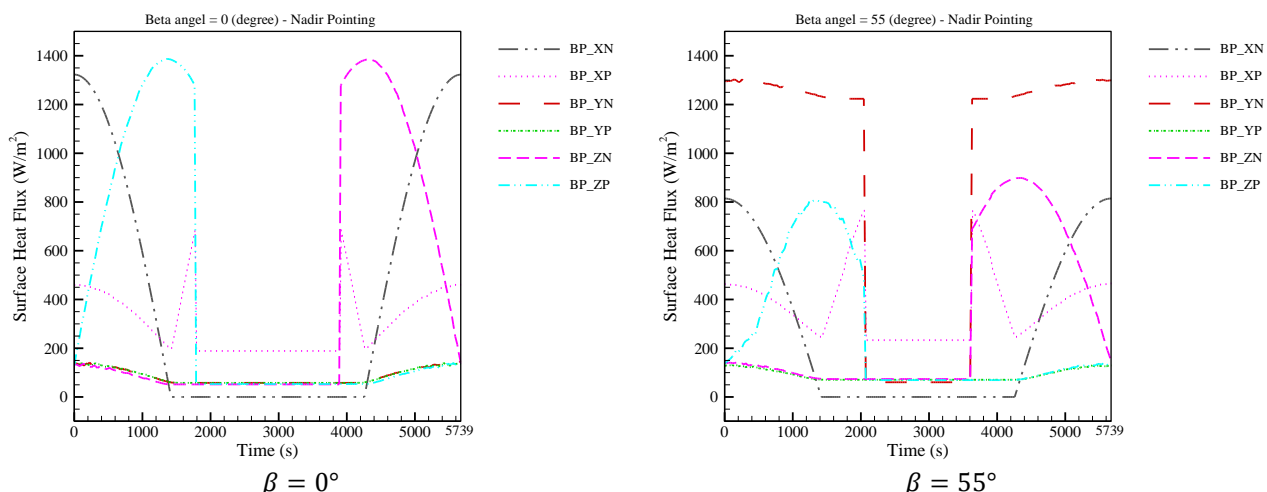


**Figure 90- Heat fluxes on CubeSat faces at**

#### 9.5. Thermal Mathematical Model:

The aim of CubeSat thermal modeling and analysis in finite element software is to investigate the capability, durability, and desired performance of satellite components under thermal loading. By using the obtained results, it is possible to modify and optimize the design and ultimately achieve

<sup>1</sup> Gilmor, D., Spacecraft thermal control handbook. Fundamental Technologies. Vol. 1. 2002: El Segundo, California, Aerospace Press.

the appropriate final design. Additionally, during CubeSat testing, the analysis results can be utilized. The first step in the analysis is to create a suitable thermal model of the structure that possesses the physical and structural characteristics and limitations of the actual model.

Solar Absorption and Thermal Emissivity Coefficients of the materials used in the satellite are crucial parameters in determining and controlling the satellite's temperature. Since factors such as thickness, surface preparation, coating formulation, manufacturing techniques, etc., affect these parameters, it is usually necessary to measure the absorption and emissivity coefficients of materials before their application. Additionally, because most materials undergo degradation and partial damage due to factors such as exposure to space vacuum<sup>1</sup>, ultraviolet radiation, and micrometeoroid impacts, laboratory tests related to these materials need to be conducted before obtaining approval for use in space. The thermal-optical coefficients applied in the analysis are provided below based on values presented in relevant aerospace references.

**Table 46- The applied thermal-optical coefficients used in the analysis<sup>2</sup>**

	$\alpha$	$\epsilon$
	Absorption	Emissivity
White color	0.35	0.85
Black color	0.89	0.9
Matte black anodize	0.88	0.88
Alodine aluminum	0.4	0.5
Aluminum surface	0.15	0.3
MLI	0.15	0.05
Radiator	0.15	0.8
Solar cell	0.92	0.85
Communications patch antenna	0.65	0.85

## 9.6. CubeSat Model Meshing

The meshing of the CubeSat thermal model is illustrated in figure below.

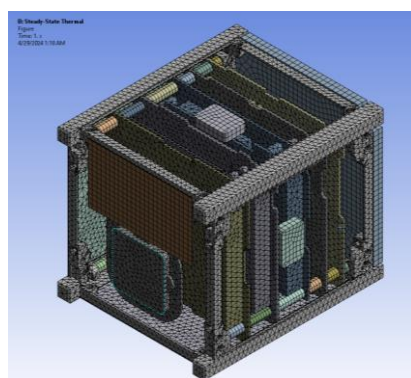


**Figure 91- CubeSat Meshing and Grid Pattern**

<sup>1</sup> outgassing

<sup>2</sup> Gilmore, D.G., Spacecraft Thermal Control Handbook Second Edition Ed. Vol. Volume I: Fundamental Technologies American Institute of Aeronautics and Astronautics, Inc.

The most important parameters influencing the selection of the CubeSat mesh element count are the accuracy of results and reasonable analysis time. It is necessary to strike a suitable balance between these two parameters in each model. Due to the long solving time, exhaustive mesh studies are not feasible. The required number of elements is determined based on experience from other projects and comparison with other similar satellites. Therefore, there is confidence in the independence of the solution from the number of elements.

### **9.7. Applying Radiative Conditions to CubeSat Components:**

In general, radiation in a CubeSat can be divided into three categories:

1. Interchange Radiation between Various CubeSat Components: Based on surface emissivity coefficients and view factors between them.
2. Radiation Emitted from CubeSat Surfaces to Outer Space: Considering a temperature of 2.7 Kelvin and surface emissivity coefficients.
3. Radiative Heat Flux Entering and Exiting Satellite Surfaces: Based on surface absorption coefficients.

Radiative heat flux entering CubeSat surfaces is analyzed according to the results obtained from thermal analysis performed in Thermal Desktop software, considering the coldest and hottest states mentioned.

### **9.8. Results and Discussion:**

The results for Worst Hot Case (WCH) at Beta 55 degrees and Worst Cold Case (WCC) at Beta zero degrees are depicted in the below figures:

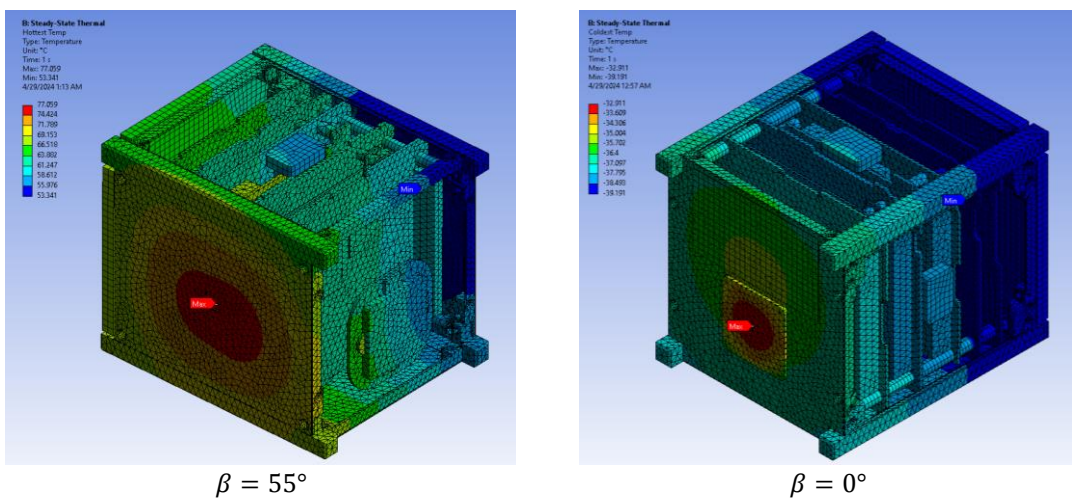


**Figure 92- Temperature contour of equipment in WCH State**

## 9.9. Summary:

The general results arising from the thermal analysis of the CubeSat are presented as follows:

- The significant variation in the orbital beta angle (the angle between the solar rays and the orbital plane) complicates the thermal design of this CubeSat to some extent. The beta angle varies from zero to 55 degrees in this orbit.
- To achieve better heat transfer within the CubeSat, the use of thermal conductors or thermal fillers appears necessary. Thermal adhesives reduce the thermal resistance between surfaces in contact with each other.
- Due to the negative temperatures occurring in some areas of the structure, the use of electric heaters for controlling the allowable temperature range of sensitive equipment such as payloads and batteries seems necessary in these areas.
- In order to enhance radiative interaction between the structural panels and internal equipment, an emissivity coefficient of 0.8 is considered for the internal surface coatings, with a black color.
- For thermal monitoring of various points and controlling electric heaters, the use of temperature sensors in different areas of the structure and sensitive thermal equipment should be considered.

The heat control hardware needed has provided in table below.

**Table 47- Summary of the specifications of the thermal control subsystem considered**

System		Use
Insulators	Black anodizing	CubeSat internal faces
	Gold anodizing	CubeSat outside faces
	Other faces	Bare Aluminum Solar cell's faces
Semi-active member	Electrical Heater	Payload Battery
Adhesive	Heat conductor	At the connection point to increase thermal conductivity
Temperature Sensor	Digital	On every electrical board
	Analogue	On equipment bodies

As previously mentioned, comparing the overall results of simulations using ANSYS software and examining the logic of behavior in the responses and the temperature ranges obtained, it can be stated that the results are logical and reliable. However, according to the simulation standards, validation and accuracy verification should be performed through thermal tests, and simulation parameters should be updated based on the test results.

## 10. Ground station

### 10.1. Requirements

- The ground station's communication system must be able to link the team to the satellite system with minimum effort.
- The design must correspond to the parameters of the purchased boards.
- Different budget estimations (including mass, cost, and power) must be less than 15% of the total budget of the whole system.
- The designed boards must fit in the communication system and link perfectly with the purchased boards.
- The system must be able to transmit and receive more than the maximum data rate in the receiving mode of our system.
- For reliability purposes, the antennas must be able to transmit the required output power to ensure a safe margin.
- The system must be able to link with each satellite to ensure further reliability.

### 10.2. Communication Architecture

#### 10.2.1. Block Diagram and System Components

The main ground station for the satellite is located in Iran. The block diagram below outlines the key components:

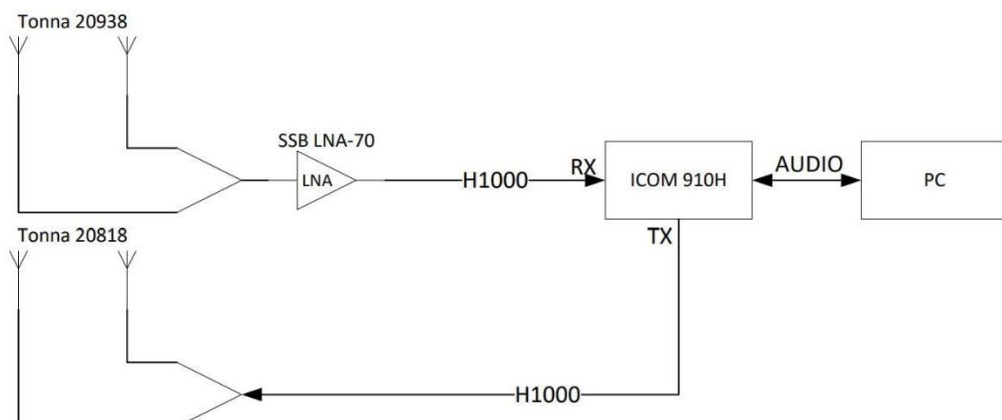


**Figure 93- Ground Station Communication Schematic (source: PW-SAT)**

- Transceiver: ICOM IC-910H, which facilitates both transmission and reception.



- B) Antenna System: Cross Yagi-Uda antennas (Tonna 20818 for VHF and Tonna 20938 for UHF) equipped with symmetrical splitters to minimize signal rotation losses.
- C) LNA: Specifically, the SSB LNA-70 to boost the weak signals received from the satellite.
- D) Computer System: Used for decoding and data processing.

#### **10.2.2. Product Tree Breakdown**

- Communication Equipment
  - o Transceiver: ICOM IC-910H
    - Antennas
      - VHF Antenna: Tonna 20818
      - UHF Antenna: Tonna 20938
    - Amplifiers
      - LNA: SSB LNA-70
  - o Control and Processing Unit
    - Computer
    - Rotator for Antennas
    - Terminal Node Controller (TNC) for Digi Modes

#### **10.2.3. Detailed Equipment Specifications**

- Frequency Range: The system operates with a frequency of 435.020 MHz for reception and 145.900 MHz for transmission.
- Antenna Gain: The VHF antenna provides a gain of 14.8 dBi, and the UHF antenna system can deliver gains of up to 16 dBi.
- LNA Gain: The low-noise amplifier boosts the signal by 21 dB.
- Expected System Losses: These include atmospheric losses, polarization losses, and other systemic attenuations, approximating around 20 dB.

#### **10.2.4. Expected Performance Parameters**

- Receiver Sensitivity: -98 dBm for the VHF receiver at a bit error rate of 1e-5.
- Transmitter Power: Maximum output power of 27 dBm for the UHF transmitter.
- Operational Margins: Detailed link budgets estimate an uplink margin of 9 dB and a downlink margin of 12 dB, ensuring robust communication capabilities under nominal conditions.

### **10.3. Operating features and parameters**

#### **10.3.1. Frequencies**

- Uplink Frequency: 145.900 MHz. This frequency is used to transmit signals from the ground station to the satellite.



- Downlink Frequency: 435.020 MHz. This frequency is used for the satellite to send data back to the ground station.

#### **10.3.2. Antenna Types**

- VHF Antenna: Tonna 20818, which is a cross Yagi-Uda antenna configuration. This antenna type is known for its high gain and directivity, which is crucial for VHF operations.
- UHF Antenna: Tonna 20938, also a cross Yagi-Uda configuration but optimized for UHF frequency operations. Like the VHF antenna, it provides high gain and directivity which are essential for reliable UHF communications.

#### **10.3.3. Antenna Gain**

- VHF Antenna Gain: 14.8 dBi. This gain level enhances the VHF uplink capabilities by concentrating the signal power in a specific direction, thereby increasing the effective transmission range.
- UHF Antenna Gain: 16 dBi. Similar to the VHF antenna, this gain helps in focusing the downlink signals towards the ground station, improving the reception quality of signals from the satellite.

#### **10.3.4. Radiation Patterns**

- The radiation patterns of the antennas are a crucial aspect as they define how signals are distributed by the antennas in different directions. This has significant implications for the coverage area and the efficiency of signal transmission and reception.
- VHF Antenna Radiation Pattern: The radiation pattern for the VHF antenna typically shows a narrow beam-width that focuses energy in a specific direction, which is optimal for reaching the satellite in its specific orbital path. The pattern generally exhibits a main lobe directed skyward with minimal side lobes, reducing interference from terrestrial sources.
- UHF Antenna Radiation Pattern: Similarly, the UHF antenna radiation pattern is designed to concentrate the signal power in a narrow beam directed towards the satellite. This pattern ensures that the maximum power is radiated in the direction of the satellite while minimizing losses due to side and back lobes.

#### **10.3.5. General Radiation Characteristics**

- Effective Range and Directionality: Both antenna types are designed to maximize the line-of-sight communication with the satellite. Their high directional gains ensure that the antennas can communicate effectively over the vast distances involved in space communications.
- Polarization and Losses: The antennas are typically polarized to match the satellite's transmission and reception characteristics, which helps in minimizing polarization



APSCO CubeSat Competition  
Conceptual and Preliminary Design Report – Ver. 1  
(IR-Sepehr)

losses. Additionally, the ground station uses symmetrical splitters and low-noise amplifiers to further mitigate signal losses and enhance the received signal strength.



Figure 94- Tonna 20818 Yagi antenna



Figure 95- ICOM IC-910H Transceiver



APSCO CubeSat Competition  
Conceptual and Preliminary Design Report – Ver. 1  
(IR-Sepehr)

## REFERENCES

1. Young, S. *How Many Satellites Are in Space? The Spike in Numbers Continues*. Available from: <https://blog.ucsusa.org/syoung/how-many-satellites-are-in-space-the-spike-in-numbers-continues/>.
2. *How Many Satellites are in Space?*
3. *Payloads and rocket bodies in space, by orbit*. Available from: <https://ourworldindata.org/grapher/space-objects-by-orbit>.
4. *FCC to set five-year deadline for deorbiting LEO satellites*. Available from: <https://spacenews.com/fcc-to-set-five-year-deadline-for-deorbiting-leo-satellites/>.
5. PACK, E., *Electrodynamic tether technology for passive consumable-less deorbit kit*. 2019.
6. Cosmo, M.L. and E.C. Lorenzini, *Tethers in space handbook*. 1997.
7. Misra, A., M. Nixon, and V. Modi, *Nonlinear dynamics of two-body tethered satellite systems: Constant length case*. The Journal of the astronautical sciences, 2001. **49**: p. 219-236.
8. Lutgens, F.K., E.J. Tarbuck, and D. Tusa, *The atmosphere*. 6th ed. 1995: Prentice-Hall Englewood Cliffs, NJ, USA.
9. Misra, A. and V. Modi, *Extensional oscillations of tethered satellite systems*. Journal of Guidance, Control, and Dynamics, 1988. **11**(6): p. 594-597.
10. Lorenzini, E., M. Grossi, and M. Cosmo, *Low altitude tethered Mars probe*. Acta Astronautica, 1990. **21**(1): p. 1-12.
11. Kalaghan, P.M., Arnold, D.A., Colombo, G., Grossi, M.D., Kirschner, L.R., and Ominger, O., *Study of the Dynamics of a Tethered Satellite System (Skyhook)*. 1978.
12. Mehdi, K. and K. Misra Arun, *Effects of aerodynamic lift on the stability of tethered subsatellite system*. ISSN 0065-3438, 1993: p. 1263-1281.
13. Biswell, B.L. and J. Puig-Suari, *Lifting body effects on the equilibrium orientation of tethers in the atmosphere*. Acta astronautica, 1998. **43**(9-10): p. 521-529.
14. Hughes, P.C., *Spacecraft attitude dynamics*. 2012: Courier Corporation.
15. Lanoix, E.L., *A mathematical model for the long-term dynamics of tethered spacecraft*. 1999.
16. Alpatov, A.P., et al., *Dynamics of Tethered Space Systems*. 2010: CRC Press, Taylor & Francis Group.